2024

Adaptation to Hypoxia and Nitrate/Nitrite Assimilation Require Species-Specific Regulation by DosR and NnaR in Mycobacterium abscessus

Breven S. Simcox
University of Central Florida

ADAPTATION TO HYPOXIA AND NITRATE/NITRITE ASSIMILATION REQUIRE SPECIES-SPECIFIC REGULATION BY DosR AND NnaR IN *MYCOBACTERIUM ABSCESSUS*

by

BREVEN S. SIMCOX
B.S. University of Florida, 2001

A dissertation submitted in partial fulfillment of the requirements
for the degree of Doctor of Philosophy
in the Department of Burnett School of Biomedical Sciences
in the College of Medicine
at the University of Central Florida
Orlando, Florida

Spring Term
2024
Major Professor: Kyle Rohde

ABSTRACT

Mycobacterium abscessus (*Mab*) is an opportunistic pathogen afflicting immunocompromised patients and individuals with underlying comordibities such as Cystic Fibrosis (CF). Treatment strategies are limited due to inherent antibiotic resistance and restricted accessibility of *Mab* to antibiotics within macrophage phagosomes, granuloma lesions, and the mucus laden CF airways. Transcriptional adaptation to stresses encountered in these niches such as hypoxia, reactive nitrogen intermediates (RNI) and elevated nitrate and nitrite are not well-understood. In *Mycobacterium tuberculosis* (*Mtb*) hypoxia adaptation and nitrate metabolism are linked via induction of the two-component system (TCS) DosRS and nitrate metabolism genes. $DosRS_{Mtb}$ induces a 50-gene regulon necessary for hypoxia adaptation including the NarK2 transporter facilitating nitrate use as a terminal electron acceptor via a respiratory nitrate reductase. The role of the *Mab* DosRS ortholog in hypoxia adaptation and nitrate metabolism is not-well defined. To address this knowledge gap, we developed an *in vitro* hypoxia model to examine differential gene expression and phenotype of a *Mab dosRS* mutant. RNAseq revealed hypoxic induction of >1000 genes including 127 DosR-dependent genes many of which are species-specific. Absence of $DosRS_{Mab}$ led to attenuated growth in hypoxia highlighting the necessity of $DosRS_{Mab}$ for hypoxic adaptation. Nitrate metabolism genes including a putative nitrate/nitrite regulator (*nnaR*) were downregulated in hypoxia suggesting a novel interplay between hypoxia and nitrate metabolism in *Mab*. To assess the role of NnaR in the regulation of nitrogen metabolism, we constructed a *Mab nnaR* knockout mutant. qRT-PCR revealed NnaR is necessary for regulating nitrate and nitrite reductases along with a nitrate transporter, a role distinct from other mycobacteria. Loss of NnaR compromised the ability of *Mab* to assimilate nitrate or nitrite as sole nitrogen sources highlighting its necessity. This work provides a first look at species-specific transcriptional adaptations to hypoxia and nitrate metabolism driven by DosRS and NnaR in *Mab*.

I would like to dedicate this body of work to my beloved husband and my parents. Without their love and support I would not have accomplished my goal of earning a PhD. To my husband, the sacrifices you made for me to pursue my dream were immeasurable and the most selfless acts I have ever witnessed. THANK YOU for believing in me and loving me. I love you endlessly. To my parents, your emotional support and support you provided for our dog Clyde so I could work late at the lab was crucial to my success and Clyde's well-being. You are loved by us all.

ACKNOWLEDGEMENT

I would like to first thank the University of Central Florida for the opportunity to pursue a PhD in Biomedical Sciences. I'm so proud to be a Knight and to have shared my experience through this journey with fellow Knights including students and faculty. A very special acknowledgement goes to my mentor Dr. Kyle Rohde who welcomed me into his lab as a post baccalaureate student after taking his rigorous course Infectious Processes which I later became a teaching assistant for the same course. Dr. Rohde, thank you for taking a chance on me and believing in me when I had very little experience in microbiology and molecular biology. Without your patience, guidance, and flexibility with my schedule I would not be writing this acknowledgement page. Enduring a PhD program as a parent was not an easy feat and your understanding of my commitment to my family was crucial to my success. The Rohde lab became my second family and I'm so grateful to all my lab mates (past and present) that encouraged me when times were tough and for their friendships which I know will last a lifetime.

My committee members also played a crucial part in my journey, their critiques and support helped my development as a scientist. Dr. Mollie Jewett, thank you for always having an open door and open heart. Your kindness and willingness to guide me and help me troubleshoot will stay with me the rest of my life. I'm so grateful to you! My fellow Giants fan, Dr. Teter, thank you for your guidance throughout my PhD. I appreciate all your thoughtful comments and questions during my annual committee meetings and during my time as a student in your Host-Pathogen Interactions course. You are truly one of the most amazing professors I have ever had. If I ever become a professor or teach at an institution your teaching style will be adopted. Dr. Roy, you were there for me from the beginning. Thank you for giving me my first opportunity in a lab at UCF when I had no clue what I was doing. All I knew was I wanted to explore the field of molecular biology

so without you none of this would have been possible. You gave me my first opportunity as a scientist, and I never looked back.

Other professors I would be remiss to not thank for their contributions in helping me develop as a scientist include Dr. Travis Jewett, Dr. Robert Borgon, Professor Verity, Dr. Tara Strutt, Dr. McKinstry, and Dr. King. I'm in awe of all of you and so appreciative of all the lessons you have taught me from scientific education to helping me overcome my fear of public speaking. Dr. Travis Jewett, I consider you an honorary committee member. Your generosity with time and resources will never be forgotten. There is one teacher not associated with UCF that I would like to thank. Mr. Cattel, I truly believe I would never have gone to college if it wasn't for you. You were the best and most thoughtful teacher I had in high school. I'm so fortunate to have had you for every high school math class grade 10-12. You believed in me like nobody ever had and held me accountable for my work and my actions. Your tough love has stayed with me my entire adult life. It took a special teacher to call me over the phone every night to help me with homework when I was home sick with the chicken pox. You are truly one of a kind.

Finally, I would like to thank all faculty and staff in the Burnett School of Biomedical Sciences. Everyone in this department from administration to housekeeping makes it possible for all students to pursue their dream of becoming a scientist. Everyone's contribution matters in our success and I'm forever grateful to those behind the scenes. I am unable to thank everyone individually but it's so important for me to acknowledge Lisa Vaughn. Lisa, I can't thank you enough for your support with all things administrative and for your encouragement from the start. You have been there for me every step of the way and without you the program would not be the same.

TABLE OF CONTENTS

LIST OF FIGURES xi

LIST OF TABLES xiii

CHAPTER ONE: INTRODUCTION 1

Nontuberculous Mycobacteria 1

History Of *Mycobacterium Abscessus* 2

Mycobacterium Abscessus Infections 4

Mycobacterium Abscessus Morphotype And Relationship To Virulence And Drug Susceptibility 7

Environment Of The Cystic Fibrosis Lung 9

Transcriptional Regulation And Two-component Signaling 10

Two-component Systems Of Mycobacteria 12

Mycobacterium Tuberculosis DosRS Two-component Signaling 14

Mycobacterium Abscessus DosRS Two-component Signaling Role in Hypoxic Adaptation 16

Nitrogen Assimilation 18

CHAPTER TWO: MYCOBACTERIUM ABSCESSUS DosRS TWO-COMPONENT SYSTEM CONTROLS A SPECIES-SPECIFIC REGULON REQUIRED FOR ADAPTATION TO HYPOXIA 22

Abstract 22

Introduction 23

Methods 26
Mycobacterium Abscessus Cloning....26
Hypoxic And Re-aeration Culture Models....27
RNA Experiments 27
Lux Reporter Assays....28
Results 29
Growth And Transcriptome Remodeling Of Mab In A Defined Hypoxia Model 29
Construction And Validation of $Mab_{\Delta dosRS}$ And $Mab_{\Delta dosRS+C}$ 37
$DosRS_{Mab}$ Is Required For Maximal Growth In Hypoxia 39
Identification Of A Large And Unique Gene Set Regulated By $DosRS_{Mab}$....44
Discussion....51
CHAPTER THREE: NNAR REGULATES NITROGEN ASSIMILATION GENES IN *MYCOBACTERIUM ABSCESSUS*....57
Abstract....57
Introduction 58
Methods 63
Plasmid And Mycobacterium Abscessus Strain Construction....63
Bacterial Growth Conditions And Nitrogen Supplementation....64
RNA Extraction And QRT-PCR And Operon Validation....64
Mycobacterial Protein Fragment Complementation Assays (M-PFC) 65

Nitrogen Utilization Assay 65
Results 67
Identification And Bioinformatic Analysis Of Mab Orphan Response Regulator NnaR 67
The Genomic And Transcriptional Organization Of The NnaR Regulon In Mab 69
NnaR-Dependent Expression Of The NarK3-SirB Operon And NasN 75
NnaR Is Required For Survival On Nitrate Or Nitrite 78
NnaR and DosS Do Not Display Interaction In An M-PFC Assay 81
Discussion 83
CHAPTER FOUR: UNPUBLISHED ANIMAL EXPERIMENTS 88
Abstract 88
Introduction 89
Methods 92
βENaC Breeding 92
Mab Culture Preparation For Infection 92
Animal Infection 92
Cyclophosphamide Administration 93
Results 93
Pilot Study Utilizing C57BL/6N Mice 93
βENaC Multi-dose Infection 95
Smooth, Rough And Clinical Isolate Infection Model 98

Neutropenic Mouse Model 102
Discussion 105
CHAPTER FIVE: UNPUBLISHED PROTEIN WORK 109
Methods 109
Cloning Of DosR Into pET28b 109
Protein Purification 110
Electromobility Shift Assay 110
DosR Phosphorylation 111
Results 111
DosR Protein Resides In The Insoluble Fraction 111
Phosphorylated DosR Interacts With Predicted Promoter Sites 113
CHAPTER SIX: DISCUSSION 117
APPENDIX PRIMER, PLASMID AND STRAIN TABLES 133
REFERENCES 142

LIST OF FIGURES

FIGURE 1: BRITISH THORACIC SOCIETY RECOMMENDED TREATMENT STRATEGY 6

FIGURE 2: TWO COMPONENT SIGNALING MECHANISM 11

FIGURE 3: TWO-COMPONENT SYSTEMS OF MYCOBACTERIUM TUBERCULOSIS 13

FIGURE 4: GROWTH KINETIC COMPARISONS OF MAB390S 30

FIGURE 5:TRANSCRIPTOME ANALYSIS OF MAB390S IN DEFINED HYPOXIA MODEL 36

FIGURE 6: VALIDATION OF $MAB_{\Delta DOSRS}$ AND $MAB_{\Delta DOSRS+C}$ 38

FIGURE 7: $MAB_{\Delta DOSRS}$ IS ATTENUATED IN HYPOXIA 41

FIGURE 8: HYPOXIA-INDUCED MORPHOLOGICAL CHANGES IN $MAB_{\Delta DOSRS}$ 42

FIGURE 9: DOSRS IS REQUIRED FOR RESUSCITATION AFTER HYPOXIA. 43

FIGURE 10: MAB DOSR DEPENDENT DIFFERENTIAL GENE EXPRESSION AT 1% O_2. 48

FIGURE 11: QRT-PCR VALIDATION OF MAB DOSR REGULATED GENES IN 1% O_2 49

FIGURE 12: LUX REPORTER ACTIVITY IN 1% O_2 50

FIGURE 13: BIOINFORMATIC ANALYSIS OF NNAR DOMAIN STRUCTURE AND SEQUENCE ALIGNMENT 68

FIGURE 14: NASN SEQUENCE ALIGNMENT 71

FIGURE 15: THE NNAR REGULON IS INDUCED WHEN NITRATE OR NITRITE ARE THE SOLE SOURCES OF NITROGEN 72

FIGURE 16: NITRATE ASSIMILATION GENE ORGANIZATION IN MTB AND MSM 73

FIGURE 17: GROWTH ANALYSIS OF MAB390S AT DIFFERENT CONCENTRATIONS OF INORGANIC NITROGEN SOURCES. 74

FIGURE 18: NNAR-DEPENDENT EXPRESSION OF THE NARK3-SIRB OPERON AND NASN 77

FIGURE 19: NNAR IS RESPONSIBLE FOR NITRITE UTILIZATION AND GROWTH WHEN NITRATE AND NITRITE ARE SOLE SOURCES OF NITROGEN 80

FIGURE 20: M-PFC ASSAY DISPLAYS LACK OF INTERACTION BETWEEN NNAR AND DOSS 82

FIGURE 21: MULTI-DOSE INFECTION YIELDS SUSTAINED INFECTION OVER TIME IN C57BL/6N MICE 95

FIGURE 22: βENAC MULTI-DOSE INFECTION MODEL 97

FIGURE 23: βENAC SMOOTH AND ROUGH STRAIN INFECTION 99

FIGURE 24: CLINICAL ISOLATE INFECTION OF βENAC MICE 101

FIGURE 25: CYCLOPHOSPHAMIDE TREATED MICE 104

FIGURE 26: PROTEIN WORKFLOW 112

FIGURE 27: UNPHOSPHORYLATED DOSR EMSA ASSAY 115

FIGURE 28 PHOSPHORYLATED DOSR DISPLAYS BINDING INTERACTION WITH PROMOTERS 116

LIST OF TABLES

TABLE 1; STRAINS USED IN CHAPTER 2 134

TABLE 2; PLASMIDS USED IN CHAPTER 2 134

TABLE 3; PRIMERS USED TO CONSTRUCT DOSRS MUTANT 135

TABLE 4; PRIMERS USED TO CONSTRUCT DOSRS COMPLEMENT 135

TABLE 5; PRIMERS USED TO CONSTRUCT LUX REPORTERS 135

TABLE 6; PRIMERS USED FOR QRT-PCR IN CHAPTER 2 136

TABLE 7; RRNA DEPLETION PROBES USED IN CHAPTER 2 137

TABLE 8; PRIMERS USED TO GENERATE NNAR KNOCKOUT AND COMPLEMENT IN CHAPTER 3 139

TABLE 9; OPERON PRIMERS USED IN CHAPTER 3 139

TABLE 10; QRT-PCR PRIMERS USED IN CHAPTER 3 140

TABLE 11; PRIMERS USED FOR GENOTYPING βENAC MICE 140

TABLE 12; PRIMERS USED FOR PET28B CLONING IN CHAPTER 5 140

TABLE 13; PRIMERS USED TO AMPLIFY PROMOTER SEQUENCES USED IN CHAPTER 5 141

CHAPTER ONE: INTRODUCTION

Nontuberculous Mycobacteria

Mycobacteria are categorized into two distinct groups*: Mycobacterium tuberculosis complex (MTC)* and nontuberculous mycobacteria (NTM). *MTC* consists of a group of genetically similar bacteria *(M. tuberculosis, M. bovis, M. africanum, M. microti, M. caprae, M. pinnipedii*, M. orgyis, M. mungi, *M. suricattae* and *M. canettii)* capable of causing tuberculosis in a variety of hosts whereas, NTM consists of a group of bacteria incapable of causing tuberculosis or leprosy (1-5). NTM species are classified as either rapidly growing mycobacteria (RGM) with colonies appearing in less than a week or slow growing mycobacteria (SGM) with colonies appearing in more than a week (2,6,7). NTM species exist within the environment and are found in soil and water with a small number of species categorized as opportunistic pathogens. Three groups of NTM comprise the most common infections found in humans: *M. abscessus*, *M. fortuitum* and *M. avium complex* (5). Disease caused by these opportunistic pathogens range from skin and soft tissue infections to pulmonary infections with pulmonary infections accounting for ~90% of infections (8,9). Infections caused by NTM are a growing concern in developed countries due to a higher prevalence than *Mtb*. A two-year study in Oregon published by Winthrop *et al*., in 2010 predicted 26.7/100,000 were infected with NTM verse 2.5/100,000 with *Mycobacterium tuberculosis* (*Mtb*) in persons over 50 (10). Due to the lack of resources, reporting standards and inability to test for all NTM species the prevalence of NTM infections may be higher than suspected (11). Since the 2 -year study was published the British Thoracic Society (BTS) has endorsed testing standards to facilitate more accurate testing and reporting. The BTS recommends a positive test for identical NTM species acquired from 2 or more sputum samples, radiological testing and the presence of characteristic symptoms (12). Additional recommendations include microscopy and culturing of

isolated pathogen for diagnosis, and antibiotic susceptibility testing to aid in treatment after diagnosis (12). The two most common NTM species identified in this study were the SGM *M. avium* and the RGM *M. abscessus* (10).

History Of *Mycobacterium Abscessus*

The RGM *Mab* was first documented in 1952 by Moore and Frerichs in a publication describing an unusual knee infection with characteristics resembling the acid-fast bacilli *Mycobacterium tuberculosis* (*Mtb*). At the time of this study, mycobacteria infections in humans other than tuberculosis and leprosy were unappreciated therefore the infection was initially diagnosed as *Mtb* because of a positive acid-fast test of bacterial isolates taken from the knee and the absence of skin lesions (a common symptom of leprosy). Due to spreading of the infection (resulting in gluteal abscesses after specimens were taken for identification) which had been self-limited for nearly 50 years prior, further tests were performed to identify the infection. Bacteria obtained from the new infection site grew quickly ruling out *Mtb* as the culprit and spurred an interest in testing for Nocardia. Soon after testing, *Nocardia* was ruled out and extensive *in vitro* and *in vivo* phenotypic tests were performed to identify the acid-fast bacteria causing the soft-tissue infection. Utilizing mycobacteria classification systems identified by Thomson (1932) and Gordon (1937), Moore and Frerichs found no commonalities between previously identified mycobacteria species. Their research determined the mycobacteria causing the knee infection had not been previously documented and named the newly identified bacteria as *Mycobacterium abscessus* due to the formation of abscesses during active infection (13).

Since the discovery of *Mab*, numerous taxonomic changes have occurred (14). The first taxonomic change occurred in 1972 when *Mab* was classified as a subspecies of *Mycobacterium*

chelonei (*M.chelonei*) and hence, referred to as *M. chelonei subsp*. *abscessus.* This redesignation of *Mab* was part of a larger effort to accurately identify and consistently name rapidly growing mycobacteria (RGM) according to Runyon's IV class system-a classification system dependent upon rate of growth and pigmentation. At the time the classification study was initiated little consistency existed in nomenclature and classification of RGM. This study consisted of the classification of 50 RGM cultures that underwent 195 test characters to build a matrix resulting in the identification of 9 clusters of RGM species. Cluster 9 belonging to *M. chelonei* consisted of two groups 9a and 9b representing *M. chelonei subsp. abscessus* and *borstelense,* respectively (15). Due to advancements in molecular biology, 20 years later *M. chelonei subsp. abscessus* was re-classified as *Mab* once again. DNA hybridization confirmed differences in genetic make-up between *M. chelonei* and *M. abscessus* granting the re-classification and "elevated" *Mab* as its own species (16). In the 14 years that followed, 2 *Mab* subspecies (*massiliense* and *bolettii*) were identified through phenotypic assays and partial PCR amplification sequencing of 16S rRNA, *rpoB*, and *recA*, (17,18). Although many of the biochemical features were similar to *Mab,* differences occurred in a handful of phenotypic tests and susceptibility to antibiotics prompting further analysis via genetic comparisons. A greater than 99.6% sequence identity of 16S rRNA determined *M*. *abscessus* and *M. massiliense* belong to the same species however, differences in *rpoB* and *recA* classify *M*. *massiliense* as a subspecies of *Mab* (17). Previously, 16S rRNA was determined to be an inadequate marker for distinguishing rapidly growing mycobacteria species as many shared >99 % identity and in most cases RGM carry two different 16S rRNA genes (*Mab* carries only one) making species differentiation almost impossible without sequencing other genes or performing phenotypic studies (18,19). Interestingly, the number of 16S rRNA copies are responsible for differences in growth rates with slow growers containing a single copy whereas rapid growers contain 2 copies apart from *Mab* (20,21). The same group to identify *M*. *massiliense*

also identified *M*. *bollettii* as a subspecies of *Mab* in a follow up study utilizing the same standards previously used relying upon phenotypic tests and sequence identity of *rpoB* (18). In 2013, Bryant et. al., confirmed the subspecies status of *M. abscessus*, *M*. *bollettii*, and *M*. *massiliense* via whole genome sequencing allowing these subspecies to be classified as the *MABS* complex. Although the *MABS* complex is genetically and phenotypically similar, identification of *Mab* subspecies is an important determinant for treating infection due to differences in antibiotic susceptibility e.g., both *M. abscessus* and *M. bollettii* have inducible macrolide resistance due to a functional erm gene whereas the gene is present in *M*. *massiliense* but non-functional (22). In addition to inducible macrolide resistance in subspecies *M*. *bollettii* and *M. abscessus* all three subspecies display intrinsic and acquired antibiotic resistance such as antibiotic targeting enzymes, target modifying enzymes, efflux pumps, transcriptional regulator induction, and genotypic changes complicating treatment for those infected (14,23,24).

Mycobacterium Abscessus Infections

Although *Mab* is commonly found in soil and water, it is considered an emerging opportunistic pathogen with potentially detrimental consequences. Infections caused by *Mab* are a growing area of concern due to increased prevalence, vulnerability of the immunocompromised population and individuals with pre-existing lung conditions, and limited treatment options due to antibiotic resistance. *Mab* is capable of causing a wide array of infections such as skin, soft tissue, ocular, wound and pulmonary infections in immunocompromised individuals and individuals with pre-existing lung infections such as bronchiectasis and cystic fibrosis (CF) (8,25-27). *Mab* is the most common rapidly growing NTM recovered from the CF lung resulting in lung function decline, extended hospitalization and in some cases exclusion from lung transplants (14,27,28). Due to *Mab's* intrinsic and acquired antibiotic resistance treatment options are limited, and cure rates are

extremely low with less than 50% efficacy further complicating the treatment of CF (14,24,29,30). The current British Thoracic Society endorsed intervention strategy relies upon a multi-drug cocktail over a pro-longed time course often resulting in side effects in already sick individuals (12,14). This multi-drug long term treatment strategy consists of intravenous, oral and nebulized drug administration over two phases, an initial phase lasting 1 month and continuation phase lasting > 12 months (Figure 1) (14). Despite the long-term administration of multi-drug cocktails *Mab* is still refractory to treatment highlighting the need for the development of new therapeutic strategies and discovery of new drug targets. Further complications in treatment stem from the presence of heterogenous sub-populations of *Mab* within the lung which have varying antibiotic susceptibilities due to genetic diversity and SNPs (31). In addition to these genetically diverse sub-populations within the lung during infection is the presence of 2 distinct *Mab* morphotypes which have different impacts on drug susceptibility and host immune response (29,32-34).

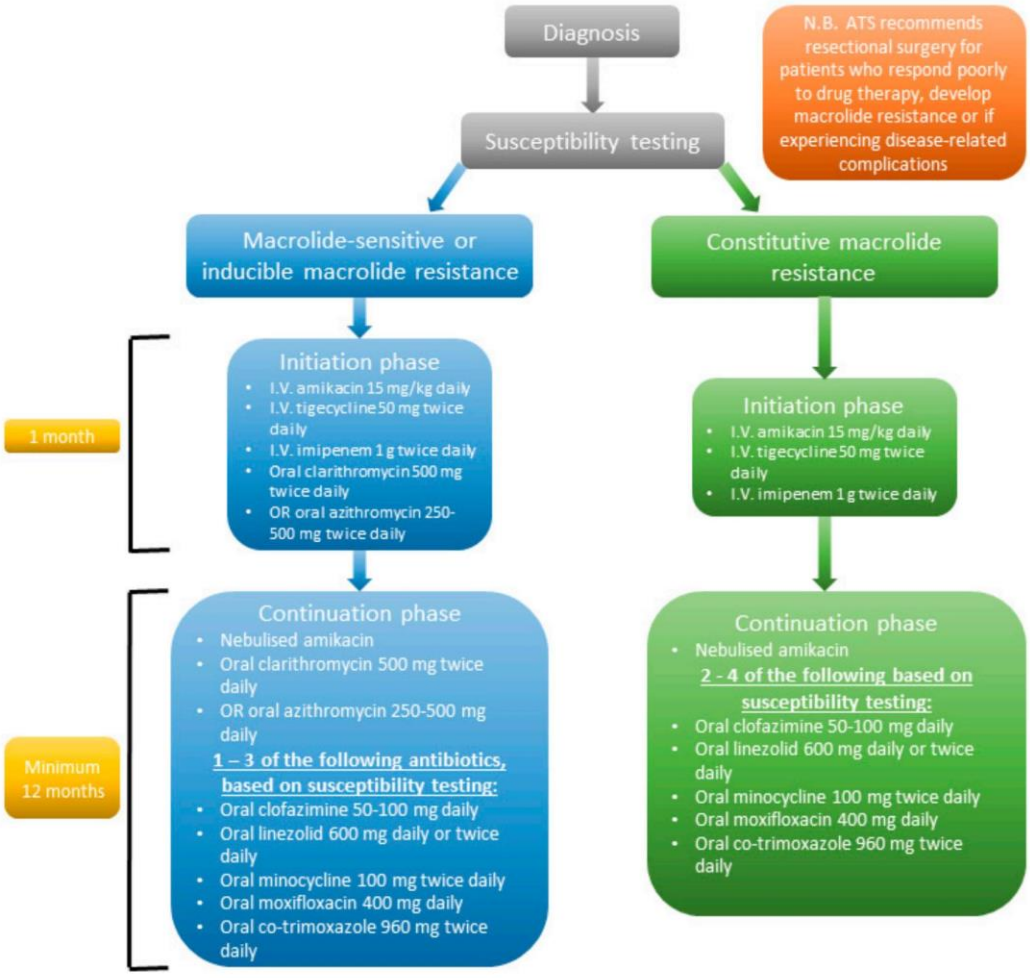

Figure 1: British Thoracic Society recommended treatment strategy

Adapted from: Lopeman, R. C., Harrison, J., Desai, M., and Cox, J. A. G. (2019) Mycobacterium abscessus: Environmental Bacterium Turned Clinical Nightmare. *Microorganisms* **7**

Mycobacterium Abscessus Morphotype And Relationship To Virulence And Drug Susceptibility

Mab exists as a smooth (S) or rough (R) morphotype with glycopeptidolipids (GPLs) existing in the cell envelope or the absence of GPLs in the cell envelope, respectively (35,36). The presence of GPL is associated with motility, biofilm formation and the absence of cording (aggregates of cells in a defined order that form serpentine like structures (37)) whereas the absence of GPL is associated with cord formation and lacks motility and biofilm formation (38). These distinct morphological traits are responsible for host mediated immune responses and disease progression. The R morphotype lacking GPLs is correlated with hypervirulence and inflammatory response whereas the S morphotype is linked to colonization and biofilm formation (33,35,38-41). Absence of GPLs exposes the surface associated molecules phosphatidyl-myo-inositiol-dimannnoside and lipoproteins which stimulate TLR-2 signaling resulting in inflammation via TNF (tumor necrosis factor) induction (42-44). An *in vivo* murine study performed by Catherinot *et al*., discovered clinical and laboratory strains of the R morphotype resulted in fatal infections and increased TNF-α production compared to the S morphotype providing evidence of distinct pathophysiology between the two morphotypes (39). Not only do the S and R morphotype differ in their ability to cause inflammation via TLR-2 but also differ in engulfment by macrophages and ability to reside within the phagosomes. Roux *et al*. demonstrated differences in engulfment and residence within macrophages due to the presence or absence of cording further affirming distinctions in virulence (38). Cording is a feature observed in the R morphotype limiting phagocytic uptake by macrophages compared to the smooth morphotype. Furthermore, the phagosomes consisting of S and R morphotypes display different characteristics such as single bacteria and the absence of acidification for the S morphotype but multiple bacteria and the

presence of phagosomal acidification for the R strain (38). Despite R infected macrophages undergoing apoptosis due to phagolysosome fusion this does not result in the killing of R *Mab.* After apoptosis R *Mab* is able to live in the extracellular environment causing more inflammation via TLR-2 signaling or spread from cell to cell resulting in more apoptosis (36). Although a correlation exists between the absence of GPLs, hypervirulence, and inflammation the mechanism for transition from smooth to rough is not fully understood.

The first comprehensive study investigating the molecular mechanism of S to R transition identified SNPs, indels, and replication errors within the *gpl* locus between S and R isogenic pairs through genomic comparisons. This study also observed differential gene expression outside the of the *gpl* locus via microarray and RNAseq between these isogenic pairs however it remains unclear whether this is a cause or effect of the presence of absence of GPL (45). A subsequent study by Daher et al., examined the genes within *gpl* locus responsible for glycosylation of the outer membrane and found the absence of Gtf1 and Gtf2 resulted in a rough morphotype with increased virulence (46). Additionally, a study assessing the effects of aminoglycosides found sub-inhibitory concentrations of amikacin led to a shift from smooth to rough morphology (47). This change in morphology is attributed to the upregulation of the transcription factor whiB7 in response to sub-inhibitory concentrations of amikacin (*MAB_3508c*). Overexpression of *MAB*_3508c resulted in a rough colony morphology suggesting morphological changes are a result of gene induction rather than amikacin directly acting upon cell wall components (46). Evidence gathered from morphological studies points to multiple mechanisms responsible for the transition from smooth to rough colonies highlighting *Mab's* intricate ability to remodel its cell wall. R *Mab* is particularly burdensome to CF patients as this morphotype is a commonly recovered

isolate from the CF lung and is associated with hypervirulence and low drug susceptibility (33,48,49).

Environment Of The Cystic Fibrosis Lung

CF patients are particularly vulnerable to bacterial infections due to the inability to clear pathogens from the lungs as a consequence of the viscous mucus and impaired innate immune defenses of lungs impacted by CFTR mutations (50,51). *Mab* infections account for 56% of recovered RGM species from the lungs of CF patients and may continue to increase due to the possibility of person to person spread (28,52). Infections caused by *Mab* are a major cause of concern within the CF population due to the association with lung function decline, prolonged hospital stays, an increase in hospital visits and in some cases exclusion from lung transplants (14,27,28). Further complicating clearance of *Mab* within the CF lung is the ability for this opportunistic pathogen to survive within the hypoxic environments of granulomas and alveolar macrophages which impedes antibiotic accessibility (53-56). In addition to residence within granulomas and alveolar macrophages, *Mab* is also able to withstand the mucus laden airway of the CF lung. The thick viscous mucus that accumulates within the CF airway is documented to have a pO_2 of ~1% and increased levels of nitrate, nitrite and nitric oxide requiring adaptation by *Mab* to survive in these harsh environments (57-59). Transcriptional responses to host-derived stresses has only recently been examined (60,61). Studies identifying key regulators implicated in adaptation to host derived stresses are extremely limited warranting further investigation to understand *Mab* persistence within the host (60-62).

Transcriptional Regulation And Two-component Signaling

Understanding the genetic strategies *Mab* employs to withstand host-pressures such as hypoxia and for utilization inorganic nitrogen sources with the host milieu will give us insights into how *Mab* is able to cause persistent infections in the harsh environment of the CF lung. One mechanism commonly used by prokaryotes to regulate gene expression in response to stimuli/cues and host pressures is two-component signaling (TCS) (63-67).This is a highly conserved signal transducing system allowing dynamic changes in gene expression in response to environmental changes (63,67,68). TCS allows adaptations to a multitude of stresses occurring within the environment and in response to host derived stresses to allow for cell-wall remodeling, locomotion via chemotaxis, shifts in metabolism due to replete or deplete nutrients, dormancy, and virulence (63,64,67,69-75). A typical TCS is comprised of 2 proteins, a sensor histidine kinase (HK) and a cognate response regulator (RR) (63,69) responsible for signal recognition and promoter binding, respectively (Figure 2). HKs detect signals via sensor domains causing a change in conformation leading to auto-phosphorylation of a conserved histidine residue in the transmitter domain (63,76,77). Phosphorylated HKs activate cognate (genetically linked and often co-transcribed) RR via phosphorylation of conserved aspartate residues allowing homo-dimerization (63,76). RR dimers bind to DNA through DNA recognition domains leading to changes in gene expression for adaptation in response to signaling cues received from SK (63,76). Although SKs and RRs are typically paired responses, RRs can be phosphorylated by non-cognate SKs or serine/threonine kinases, some RR's lack a cognate SK and are known as orphan response regulators (ORR), orphan SKs (OSK) lack a cognate RR, heterodimers can form between different RRs, and RR binding to DNA is not always confined to a specific DNA recognition site (68-70,78,79). Cross talk can occur between TCS allowing dynamic and flexible genetic regulation via converging pathways for adaptation (69,70,78-80).

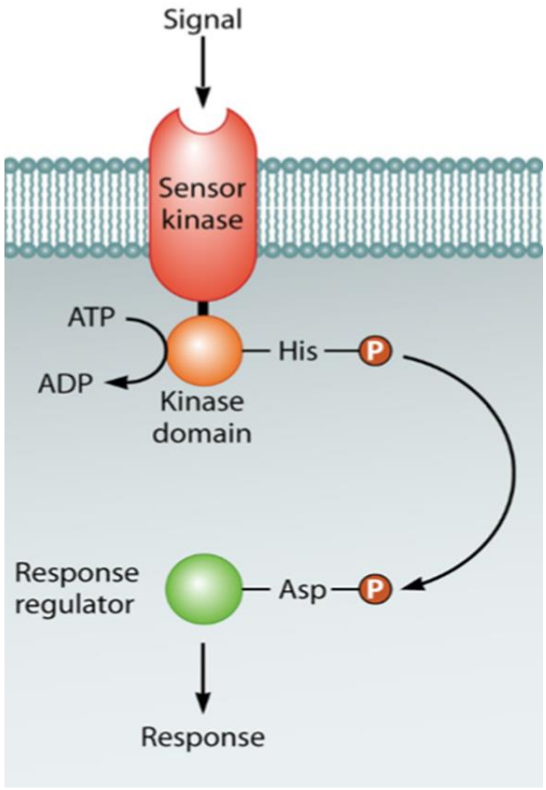

Figure 2: Two Component signaling mechanism

Adapted from: Bretl, D. J., Demetriadou, C., and Zahrt, T. C. (2011) Adaptation to environmental stimuli within the host: two-component signal transduction systems of Mycobacterium tuberculosis. *Microbiol Mol Biol Rev* **75**, 566-582

Two-component Systems Of Mycobacteria

The number of TCS encoded within the genomes of prokaryotes relates to its lifestyle and size of genome ranging from over 100 in *Myxococcus xanthus* to only 4 in *Mycobacterium leprae* (67,81). The average number of TCS across prokaryotes is around 30 however, *Mab* contains 11 of the 12 TCS orthologous to *Mtb* (the *Mab* ortholog of Rv0060-0061-*tcrA* is absent) (67,82,83). The roles of TCS in *Mtb* include but are not limited to cell replication, cell wall biogenesis, adaptation to intracellular environments such as survival within alveolar macrophages, secretion of virulence factors, nitrate metabolism and hypoxic adaptation (Figure 3) (67,82). Our understanding of the roles of the *Mab* TCS orthologs is rudimentary at best and prior to the initiation of this study there were no studies published examining the functions of the *Mab* TCS orthologs (60,84).

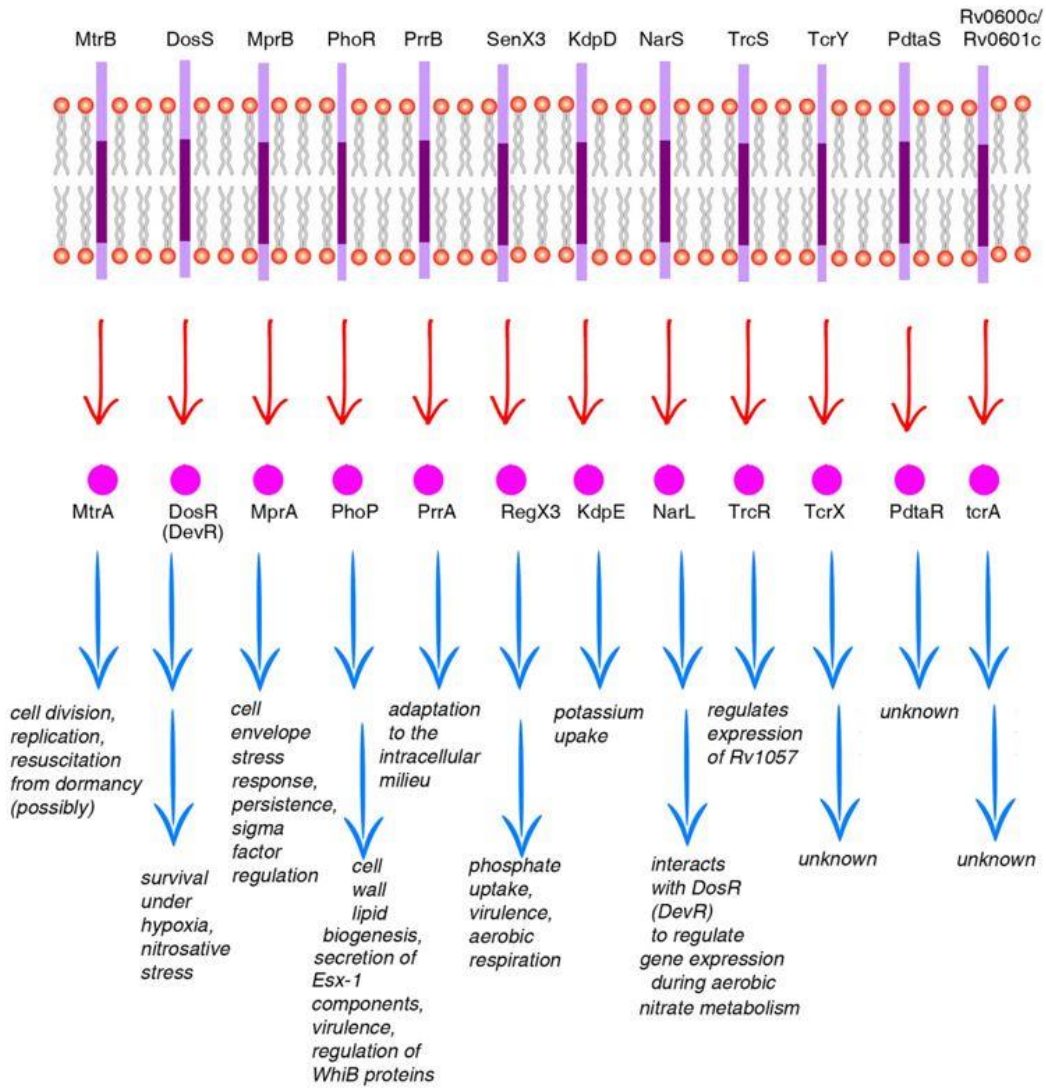

Figure 3: Two-component systems of Mycobacterium tuberculosis

Adapted from: Kundu, M. (2018) The role of two-component systems in the physiology of Mycobacterium tuberculosis. *IUBMB Life* **70**, 710-717

Mycobacterium Tuberculosis DosRS Two-component Signaling

Mab and *Mtb* share similar niches within the human host such as the aforementioned alveolar macrophages and granulomas. *Mtb* survival within host niches requires elaborate gene regulation to combat the hypoxic environments associated with macrophages and granulomas (a hallmark feature of *Mtb* infections) (85-89). *Mtb* infected macrophages and granulomas have a pO_2 ~1% (55,89), thus limiting the availability of oxygen as a terminal electron acceptor in the respiratory chain. Adaptation to this lower pO_2 requires transcriptomic alterations to allow for alternate respiration and survival. *Mtb* utilizes the well-documented atypical two-component system DosRS/T (comprised of DosS (HK) genetically linked to DosR (RR) and DosT (SK) that isn't genetically linked to either DosS or DosR) , to combat hypoxia, nitric oxide, and carbon monoxide stress (76,90-93). *Mtb* DosRS is implicated in the transition from a replicative to non-replicative state known as dormancy/latency in response to these gaseous stresses via regulation of a ~50 gene regulon (75,92-95). Within this regulon are genes expressing, heat shock proteins, triacylglycerol synthase, ferredoxins, universal stress proteins, diacylglycerol acyltransferases, nitroreductases, *narX* (putative nitrate reductase), *nark2* (nitrate symporter), DosS and DosR among others which are necessary for entry into dormancy (54,93,95,96). This dormant state induced by hypoxia is characterized by non-replicative persistence, phenotypic drug tolerance, increased lipid droplet formation and increased nitrate reduction signifying a transition to nitrate respiration all of which requires intricate gene regulation by DosR (75,85,97-99). Absence of the components of *Mtb* DosRS/T results in growth attenuation in *in vitro* hypoxia models using the Wayne Model of hypoxia (cultures grown in sealed tubes with minimal culture to headspace ratio to allow gradual depletion of oxygen) and *in vivo* in animal models capable of forming hypoxic granulomas (75,89,94,100,101). *Mtb* DosRS plays a pivotal role in gene regulation allowing the necessary adaptation for survival in the hypoxic environments associated with the host. This

system is critical for host-related dormancy and is a distinguishing factor in discriminating between active and latent *Mtb* infections (102-104).

Mtb DosR has also been documented to co-regulate gene expression via heterodimer interactions with the RRs NarL and PhoP for aerobic nitrate metabolism and metabolic transitioning for hypoxia adaptation, respectively (78,105,106). Both heterodimer interactions mediate expression of nitrate assimilation genes highlighting the link between DosR and nitrate metabolism for both respiration and assimilation (78,105,106). Microarray analysis determined an overlap of 16 genes between *dosR* and *narL Mtb* mutants subjected to hypoxia and exposed to nitrate as the only nitrogen source, respectively suggesting these genes may be co-regulated (105). Among these genes was *narK*2, a nitrate symporter, which plays an important role in transporting extracellular nitrate into *Mtb* during hypoxia for use as a terminal electron accepter in lieu of oxygen (107-109). *narK*2 not only acts as a transporter of nitrate during hypoxia but also transports nitrate during nitrogen depletion for use as an inorganic nitrogen source (109). Further analysis revealed NarL and DosR interact to cooperatively regulate gene expression only during aerobic conditions with the addition of nitrate implying the importance of DosR and NarL for the intricate balance between nitrate respiration and assimilation (105).

PhoP has also been shown to regulate a subset of DosR regulated genes in aerobic conditions and interact with DosR via protein-protein interaction (PPI) to regulate gene expression during hypoxia (78,106,110). Most notably, in the absence of *phoP* down-regulation of *dosR, hspX* and *narK2* occurs in aerobic conditions but not in hypoxia implying basal levels of *dosR* may be dependent upon *phoP* (95,106). Common to aerobic and hypoxic conditions in the *phoP* mutant is the marked down-regulation of nitrate metabolism genes *narG* (a dual functioning

respiratory/assimilatory nitrate reductase) belonging to the *narGHIJ* operon and *nirB* (nitrite reductase) (106). As mentioned previously, genes involved in nitrate metabolism provide a means of respiration during hypoxia, inorganic sources of nitrogen for biomolecule formation, or defense against RNI so it is not surprising multiple response regulators modulate gene expression for fine tuning of transcriptional responses. Protein-protein interactions between non-cognate RR *e.g.,* NarL-DosR and PhoP-DosR, affirm DosR regulon genes require fine tuning and integration of multiple host derived cues for transcriptional alterations both in aerobic and anaerobic conditions to allow transcriptional remodeling for adaptation (78,105,106).

Mycobacterium Abscessus DosRS Two-component Signaling Role in Hypoxic Adaptation

Despite extensive studies of the *Mtb* TCS particularly DosRS, this topic of study is virtually untouched for *Mab*. *Mab* harbors 11/12 TCS orthologous to TCS of *Mtb* however, prior to the initiation of this dissertation work none of the roles of these orthologs had been determined (67) . Our lab was particularly interested in uncovering the role of *Mab* DosRS due to the similar lifestyle of *Mtb* and the additional hypoxic and nitrosative stresses encountered in the CF lung (53,54,57-59,91). The mucus laden airway, intracellular environment of infected macrophages and granulomas are all hypoxic with an oxygen concentration approximating 1% requiring *Mab* adaptation through genetic alterations for survival (55,59,89). *Mab* persistence within these environments requires intricate gene regulation that has not been studied highlighting the need for investigation if we hope to gain an understanding of *Mab's* ability to persist within the harsh milieu of the CF lung.

Mab DosS and DosR orthologs share 50% and 72% identity with *Mtb* DosS *and* DosR implying similar roles may exist between orthologs. At the time this study was undertaken in 2017 work in this area was rudimentary with only 2 publications making mention of *Mab* DosRS (61,111). A bioinformatics study performed by Gerasimova et al., from 2011 identified a 6 gene *Mab* DosR regulon via comparison of *Mtb* promoter motifs to predict *Mab* DosR binding sites. This data was interpreted to mean the *Mab* DosR regulon is much smaller than *Mtb* despite a larger genome and the ability to live within a host and in the environment (112). The predicted *Mab* DosR regulon consists of *MAB*_3890c (*Mab dosS*), *MAB*_3891c (*Mab dosR*), *MAB*_2489, *MAB*_3902, *MAB*_3903, and *MAB*_3904. A second study to make mention of *Mab* DosRS reported differential gene expression in 56 genes with a log change of +/- 1 in NO (which this group deemed as hypoxia) including *dosR* and the 5 other predicted genes by Gerasimova et al., however it should be noted their hypoxia model consisted of NO exposure rather than true hypoxia (61). This study affirmed induction of the predicted DosR regulon in a hypoxia like-model however regulation via *Mab* DosRS was not determined. Due to *Mab* containing a larger genome consisting of ~800 species specific genes we predict the *Mab* DosR regulon is much larger than previously reported (112,113). The previous *Mab* DosR studies failed to directly evaluate the role of DosR leaving unanswered questions such as is DosRS required for hypoxic adaptation, is DosRS responsible for signal recognition, and if DosR regulates the predicted regulon and if the DosR regulon consists of more genes than predicted. Addressing these knowledge gaps will give a better understanding of the role of *Mab* DosR. To bridge this gap in knowledge, biochemical assays must be performed that include identifying genes induced in true hypoxia, identifying DosR regulated genes, determining a DosRS phenotype, and determining whether hypoxia and nitrate metabolism are linked.

To answer these questions, we developed a hypoxia model mimicking the oxygen concentration *Mab* experiences within the CF airway, within macrophages and granulomas utilizing a hypoxic incubator set to ~1% O_2 (114). This hypoxic model enabled us to determine the necessary role of *Mab* DosRS in hypoxic adaptation. The *Mab dosRS* mutant strain ($Mab_{\Delta dosRS}$) displayed a growth defect and switched from an S to R morphotype in hypoxia compared to WT *Mab* and *Mab dosRS* complement strain ($Mab_{\Delta dosRS+C}$) (114). To identify *Mab* genes involved in hypoxic adaptation transcriptomic analysis was utilized. RNAseq was used to investigate differential gene expression (DGE) of *Mab* grown at 1% O_2 verses 20% O_2 to identify genes involved in adaptation to hypoxia. Hypoxic cultures displayed induction of 1,190 genes compared to cultures grown at 20% O_2 (114). Not surprisingly, the genes encoding *Mab dosRS* displayed the greatest fold induction of all the TCS within the *Mab* genome. The only other noteworthy TCS genes displaying DGE were *narS* and the ORR *MAB_3520c* (orthologous to the nitrate/nitrite regulator known as *nnaR* in *S. coelicolor*, *Msm* and *Mtb*). Of the 1,190 genes induced in hypoxia 127 were downregulated in the *Mab dosRS* mutant strain ($Mab_{\Delta dosRS}$) implying the *Mab* DosR regulon is larger than previously predicted. Many of the DosR regulated genes are species-specific to *Mab* suggesting hypoxic adaptation by *Mab* and *Mtb* requires different strategies. These observations affirm the importance of *Mab* DosRS for hypoxic adaptation and highlight species specific mechanisms for survival.

Nitrogen Assimilation

Further distinguishing *Mab* adaptation to hypoxia from *Mtb,* is the observed down-regulation of the ORR NnaR and nitrate/nitrite assimilation genes suggesting the interplay of hypoxic adaptation and nitrate metabolism between the two species is different. Corroborating the

distinction between hypoxia adaptation and nitrate metabolism in *Mab* is the absence of a known respiratory nitrate reductase such as the *narGHIJ* operon found in *Mtb* suggesting *Mab* is unable to use nitrate as a terminal electron acceptor (115). However, it is reasonable to suspect *Mab* is capable of assimilating nitrate due to the presence of a putative nitrate/nitrite transporter (*narK3*), nitrite reductase (*nirBD*), ferrochetalase (*sirB*-responsible for the last step in siroheme synthesis an important cofactor for nitrite and sulfite reductases) arranged in operon with *nnaR* that was shown to be down-regulated in hypoxia in our RNAseq study (114). *In silico* analysis confirmed the presence of a putative nitrate reductase (*nasN*) in a different locus than *nnaR* which was also downregulated in our RNAseq study (114). It is clear, different adaptation strategies are utilized among these two species for hypoxic adaptation prompting further investigation of the *Mab* ORR NnaR and its role in regulating nitrate assimilation.

NnaR was first identified as a target and co-activator of GlnR, the master regulator of nitrogen metabolism, in *S. coelicolor* (116). *S. coelicolor* GlnR regulates 17 genes associated with nitrogen metabolism including *narK* (nitrate transporter), *nasA* (nitrate reductase), *nirB* (nitrite reductase) and *nnaR* (nitrate/nitrite regulator) and is indispensable for growth when nitrate is used as a sole nitrogen source (116-118). Research performed by Amin *et al*., confirmed GlnR S. coelicolor is dependent upon NnaR for co-activation of *narK* and *nirB* but not *nasA*. In the absence of NnaR, *S. coelicolor* was unable to grow on nitrate or nitrite as sole nitrogen sources however, nitrate reduction was confirmed suggesting the phenotype arose from the inability to further reduce nitrite>ammonium implying NnaR co-regulates *nirB* but not *nasA* (116). Nitrate assimilation genes are regulated similarly in *Msm* and *S.coelicolor*, with both utilizing GlnR and NnaR to regulate nitrate transport genes (*Msm* ortholog=narK3), *nirB* and nitrate reductase genes (*Msm* ortholog=*nasN* annotated as a pseudogene *Msm_4260*) (116,119-121). *Msm* GlnR and NnaR are

both necessary for growth when nitrate and nitrite are used as sole nitrogen sources but like *S. coelicolor* nitrate reduction (nitrate>nitrite) occurs in the Nnar mutant but not in the GlnR mutant implying NnaR is not essential for nitrate reduction in *Msm (116,119-121)*. A comparable role for NnaR in *Mtb* or *Mab* has not been determined, however similar roles to GlnR from *S. coelicolor* and *Msm* have been documented (62,122). Only recently has the role of *Mab* GlnR been investigated affirming regulation of narK3, nirBD, and genes involved with ammonium transport and assimilation (62). Data from the *Mab* GlnR study clearly demonstrates GlnR gene regulation of key genes involved in nitrate assimilation but there was no mention of *Mab* NnaR despite *nark3*, *nirBD*, *nnaR,* and *sirB* (there was no mention of *sirB* in any GlnR or NnaR publications we could find) arranged as a possible operon (*MAB_3523c*, *MAB_3522c*, *MAB_3521c* and *MAB_3520c*, *MAB_3519c*, respectively) (62). Due to the dramatic down-regulation of this predicted operon in hypoxia and putative NnaR promoter binding sites we found via *in silico* analysis upstream of *narK3* and *nasN* we predict NnaR plays a pivotal role in nitrate assimilation (123).

To investigate the role of *Mab* NnaR, we generated a *Mab nnaR* knockout strain ($Mab_{\Delta nnaR}$) and an episomal complement strain ($Mab_{\Delta nnaR+C}$) under constitutive control. qRT-PCR was used to analyze differential gene expression of *nark3, nirBD, nnaR, sirB* and *nasN* in $Mab_{\Delta nnaR}$ confirming Nnar regulation due to downregulation of all genes except *sirB*. Presumably due to the dysregulation of nitrogen assimilation genes in $Mab_{\Delta nnaR}$ growth defects were observed when nitrate or nitrite were used as sole nitrogen sources. We were able to determine, NnaR uniquely regulates *nark3, nirBD, nnaR, sirB* and *nasN* in a species-specific manner for utilization of nitrate and nitrite. This data outlines for the first time the significance of NnaR for *Mab's* survival when nitrogen is limited underscoring the possibility NnaR contributes to virulence within the host in when nitrogen sources are limited.

The work in this dissertation highlights the species-specific role of *Mab* DosRS and NnaR for hypoxia adaptation and nitrate/nitrite utilization, respectively. Identification of these key transcriptional regulators required for growth in *in vitro* conditions mimicking host pressures sets a foundation for future *in vivo* transcriptional studies and may help to identify new drug targets. Understanding the transcriptional responses contributing to *Mab's* persistence and pathogenesis will aid the scientific community in combatting this emerging disease.

CHAPTER TWO: MYCOBACTERIUM ABSCESSUS DosRS TWO-COMPONENT SYSTEM CONTROLS A SPECIES-SPECIFIC REGULON REQUIRED FOR ADAPTATION TO HYPOXIA

The content in this chapter is published in Frontiers of Cellular and Infection Microbiology. Simcox, B. S., Tomlinson, B. R., Shaw, L. N., and Rohde, K. H. (2023) *Mycobacterium abscessus* DosRS two-component system controls a species-specific regulon required for adaptation to hypoxia. *Frontiers in Cellular and Infection Microbiology* **13 (114)**

Abstract

Mycobacterium abscessus (*Mab*), an emerging opportunistic pathogen, predominantly infects individuals with underlying pulmonary diseases such as cystic fibrosis (CF). Current treatment outcomes for *Mab* infections are poor due to *Mab's* inherent antibiotic resistance and unique host interactions that promote phenotypic tolerance and hinder drug access. The hypoxic, mucus-laden airways in the CF lung and antimicrobial phagosome within macrophages represent hostile niches *Mab* must overcome via alterations in gene expression for survival. Regulatory mechanisms important for the adaptation and long-term persistence of *Mab* within the host are poorly understood, warranting further genetic and transcriptomics study of this emerging pathogen. DosRS$_{Mab}$, a two-component signaling system (TCS), is one proposed mechanism utilized to subvert host defenses and counteract environmental stress such as hypoxia. The homologous TCS of *Mycobacterium tuberculosis* (*Mtb*), DosRS$_{Mtb}$, is known to induce a ~50 gene regulon in response to hypoxia, carbon monoxide (CO) and nitric oxide (NO) *in vitro* and *in vivo*. Previously, a small DosR$_{Mab}$ regulon was predicted using bioinformatics based on DosR$_{Mtb}$ motifs however, the role and regulon of DosRS$_{Mab}$ in *Mab* pathogenesis have yet to be characterized in depth. To address this knowledge gap, our lab generated a *Mab dosRS* knockout strain (*Mab*$_{\Delta dosRS}$) to investigate differential gene expression, and phenotype in an *in vitro* hypoxia model of dormancy. qRT-PCR and lux reporter assays demonstrate *Mab_dosR* and 6 predicted

downstream genes are induced in hypoxia. In addition, RNAseq revealed induction of a much larger hypoxia response comprised of >1000 genes, including 127 differentially expressed genes in a *dosRS* mutant strain. Deletion of DosRS$_{Mab}$ led to attenuated growth under low oxygen conditions, a shift in morphotype from smooth to rough, and down-regulation of 216 genes. This study provides the first look at the global transcriptomic response of *Mab* to low oxygen conditions encountered in the airways of CF patients and within macrophage phagosomes. Our data also demonstrate the importance of DosRS$_{Mab}$ for adaptation of *Mab* to hypoxia, highlighting a distinct regulon (compared to *Mtb)* that is significantly larger than previously described, including both genes conserved across mycobacteria as well as *Mab*-specific genes.

Introduction

Mycobacterium abscessus (*Mab*) is an opportunistic pathogen capable of causing skin, soft tissue and pulmonary infections in immunocompromised individuals and individuals with pre-existing lung disease such as cystic fibrosis (CF) and bronchiectasis (6,8,14,26,27). Impaired innate immune defenses and viscous mucus within the CF lung contribute to reduced clearance of bacterial pathogens leading to increased rates of infections and morbidity (50,51). *Mab* is the most common rapidly-growing mycobacterial (RGM) species recovered from the lungs of CF patients (28). Within the CF population and patients with underlying lung dysfunction, infections caused by *Mab* are associated with lung function decline, increased hospital visits, prolonged hospital stays and in some cases exclusion from lung transplants (14,27,28). Due to *Mab's* inherent antibiotic resistance, treatment options are limited, resulting in extremely low cure rates of less than 50% (14,24,29,124,125) The development of effective treatment strategies for *Mab* is hindered by discrepancies between *in vitro* and *in vivo* susceptibilities associated with *Mab's* unique lifestyle (29,124,126). Akin to *Mycobacterium tuberculosis* (*Mtb*), the causative agent of

tuberculosis, *Mab* resides within pulmonary macrophages and within granulomas which limit antibiotic accessibility and promote drug tolerance, making treatment of an inherently antibiotic resistant pathogen even more difficult (53,54). The viscous mucus in the CF lung represents an additional hostile niche within the host to which *Mab* must adapt (50,51,61,127). One key host-derived stress encountered by *Mab* in all three of these microenvironments is decreased oxygen tension, with oxygen tension estimated to be ~1% O_2 within these niches (55,56,59). Thus, to successfully cause an infection, *Mab* must encode mechanisms to adapt and persist under hypoxic conditions. Transcriptional responses to host-derived cues/stresses are not well-defined in this NTM pathogen, requiring further studies to understand how *Mab* adapts its physiology and virulence factor expression to cause insidious, persistent infections.

Two-component signaling (TCS) is a mechanism commonly utilized by prokaryotes to regulate virulence gene expression in response to host-derived cues (64,70-72). A typical TCS consists of a sensor histidine kinase (HK) responsible for signal recognition and subsequent phosphorylation of a cognate response regulator (RR) which binds DNA motifs within promoter regions to drive alterations in gene expression (128-131). *Mab* encodes 11 TCS, 5 orphan RRs and 1 orphan HK each with a corresponding ortholog in *Mtb*; however, in-depth studies of *Mab* TCS have not been performed (67). The well-documented atypical TCS DosRS/T_{Mtb}, is known to control a ~50 gene regulon to counteract hypoxic and nitrosative stress encountered within macrophages and granulomas (55,75,86,93,132-135). DosRS/$T_{Mtb,}$ contains 2 HKs (DosS and DosT) rather than one which are responsible for phosphorylating the RR DosR at different stages of hypoxia (136). Although *Mtb dosT* contributes to signaling in early stages of hypoxia, it is constitutively expressed and is not part of the $DosR_{Mtb}$ regulon (91). The $DosR_{Mtb}$ regulon includes autoregulation of *dosRS* itself, as well as heat shock proteins, triacylglycerol synthases, ferrodoxins, universal stress

proteins, diacylglycerol acyltransferases, and nitroreductase which are implicated in dormancy, resuscitation, phenotypic drug tolerance and increased lipid metabolism (75,85,93,97,135). Induction of *Mtb dosR* within animal models capable of forming hypoxic granulomas (rhesus macaques, guinea pigs, and C3HeB/FeJ mice) and attenuation of mutants lacking $DosRS_{Mtb}$ highlight the importance of this TCS for *Mtb* pathogenesis (89,100,137,138).

According to whole genome sequence data, *Mab* encodes a DosR ortholog (*Mab*_3891c) with a high level of homology with $DosR_{Mtb}$ (~72% identity) adjacent to and upstream of $DosS_{Mab}$ (*Mab*_3890c) with lower similarity (~51% identify) to its counterpart in *Mtb*. *Mab* does not appear to encode a secondary orphan HK analogous to DosT, with the closest homolog to *dosT* being $dosS_{Mab}$/*Mab*_3890C (53% identity). At the time this study was initiated, only two reports made mention of $DosRS_{Mab}$. A bioinformatics study by Gerasimova et al. used *Mtb* DosR promoter motifs to predict a small $DosR_{Mab}$ regulon consisting of only 6 genes (111). A subsequent transcriptomics study by Miranda Caso-Luengo et al. demonstrated induction of the 6 predicted $DosR_{Mab}$ regulated genes plus 56 other genes upon exposure to nitric oxide (NO) (61). It remained unclear whether induction of these genes occurs through signaling of $DosRS_{Mab}$ or whether hypoxia is an induction cue.

Although there is considerable overlap in the repertoires of TCS encoded by different mycobacteria, few cross-species transcriptomic studies are available comparing TCS regulons and regulatory networks between e.g. *Mtb* and NTM pathogens. Given the diversity of conditions encountered by *Mab* as an environmental, opportunistic pathogen, and larger genome (compared to *Mtb)* comprised of ~800 species-specific genes, the potential for unique gene sets in *Mab* TCS regulons is high (112,113). A hypoxia model mimicking the physiologic conditions in the mucus

of CF airways, within granulomas and intramacrophage compartments was used to evaluate the role of DosRS$_{Mab}$ and assess transcriptional regulation mediated by this TCS. Our work demonstrates DosRS$_{Mab}$ is important for maximal growth and survival in hypoxia and regulates a potentially larger set of genes than previously predicted. RNAseq revealed upregulation of >1000 genes in hypoxia including 127 putative DosRS$_{Mab}$ regulated genes. Information gained from this study identifies the importance of the DosRS$_{Mab}$ TCS in adaptation to hypoxia for survival and provides valuable knowledge of a novel set of hypoxia-induced genes in this species for future studies.

Methods

Mycobacterium Abscessus Cloning

Mab$_{\Delta dosRS}$ was generated via recombineering as described by van Kessell and Hatfull in the strain *Mab* 390S obtained from the Thomas Byrd lab (41,139). In brief, an allelic exchange substrate (AES) was engineered containing an apramycin resistance cassette flanked by ~1000 nucleotides upstream and downstream of the *dosRS* operon via round the horn PCR and fast cloning (140,141). *Mab::*pJV53 competent cells induced with .02% acetamide for 4 hours were electroporated with 100ng AES, recovered in 7H9 OADC media for 24 hours, and plated on 7H10 agar supplemented with apramycin 50 µg/ml. Complement strain, *Mab*$_{\Delta dosRS+C}$, containing *dosRS* with its native promoter was engineered using round the horn (140) and fast cloning (141) in the integrating vector pUAB400 followed by electroporation into *Mab*$_{\Delta dosRS}$ (142). *Mab* 390S and *Mab*$_{\Delta dosRS}$ were transformed with pMV306hspG13lux (Addgene #26161) to generate the constitutive lux strains, *Mab* 390S P$_{hsp60}$-lux and *Mab*$_{\Delta dosRS}$ P$_{hsp60}$-lux. Lux reporters under the control of P$_{dosR}$ and P$_{2489}$ were constructed in the background plasmid pMV306hspG13lux to

generate Mab 390S P_{dosR}-lux, *Mab*$_{\Delta dosRS}$ P_{dosR}-lux, *Mab* 390S P_{2489}-lux, and *Mab*$_{\Delta dosRS}$ P_{2489}-lux, via replacement of P_{hsp60} (hsp60 promoter) using round the horn cloning (140,141,143). Refer to Tables 1-5 for strains, plasmids and primers used for cloning.

Hypoxic And Re-aeration Culture Models

Cultures were grown in 7H9-OADC+.05% tyloxapol from glycerol stocks at 37°C while shaking unless otherwise noted. For growth kinetics assays, strains were inoculated from mid-log phase starter cultures into 13ml of media in filter-capped T-25 flasks to an OD_{600} = 0.02. Hypoxic cultures were grown standing in a hypoxic incubator set at 1% O_2 while aerated controls were cultured at 20% O_2 while shaking at 100 rpm. Re-aeration studies were conducted after cultures were subjected to hypoxia or grown at 20 % O_2 for 30 days. Optical density readings (OD_{600nm}) were taken on days 2, 3, 5, 8 and 10.

RNA Experiments

RNA was extracted as previously described (144) in triplicate from hypoxic cultures (1% O_2) and normoxic cultures (20% O_2) for qRT-PCR and RNAseq. At designated time points, cultures were pelleted at 4300 rpm for 5 minutes, resuspended in guanidine thiocyanate buffer, pelleted again at 12,000 rpm for 5 min, and stored at -80° C until processing. Thawed pellets were resuspended in 65° C Trizol then lysed using 0.1mM silicon beads in a BeadBeater at max speed for 1minute 2x followed by cooling on ice for 1 minute between bead beating. Isolation of total RNA from Trizol lysates was performed using chloroform extraction and Qiagen RNeasy column purification. Total RNA was treated with Turbo DNase (Invitrogen) to eliminate DNA contamination. 50 ng/µl of total RNA was used to generate cDNA using iScript™ cDNA synthesis kit (Bio-Rad) for qRT-PCR reactions carried out in a QuantStudio7 thermocycler. Primers used for qRT-PCR are listed in

Table 6. RNA samples for RNAseq analysis were pooled at equal RNA concentrations from three biological experiments as previously described (145,146) prior to library preparation at a concentration of 50 ng/µl in 20 µl. Only RNA samples with RIN>6 as determined by Tapestation analysis were utilized. RNA samples were sequenced by Microbial Genome Sequencing Center (MiGs) using Illumina sequencing protocol aligning reads to the *Mab* ATCC19977 genome (accession #CU458896). RNAseq data reflects a minimum of 12M paired end reads per sample. Due to incompatibility of Ribo-zero rRNA removal kit (Illumina) with *Mab* which resulted in high levels of rRNA, MiGS designed custom depletion probes (Table 7) for rRNA depletion. Raw data was received from MiGs as fastq files followed by analysis using CLC Genomics Workbench 12 (Qiagen Bioinformatics). Illumina paired importer tool was used to eliminate failed reads using the quality score parameter option set to Illumina Pipelines 1.8. Expression browser tool (v1.1) was used to calculate gene expression with an output of transcript per million (TPM). Differential gene expression is expressed as a $\log_2$FC of $\leq$-1 or $\geq$1 and visualized as scatter plots created in GraphPad Prism 9.

Lux Reporter Assays

Bio-luminescent reporter strains were grown to mid-log phase, diluted to .02 OD in 13ml in T25 flasks and grown in either 20% O_2 or 1% O_2 for 1, 5 and 20 days. 200 ul of each culture was aliquoted in triplicate into 96 well white bottomed plate to measure luminescence via Synergy H4 reader (Biotek). Fold change of luminescence was analyzed comparing individual strains in 1% O_2 to 20% O_2 using *Mab* 390S P_{hsp60}-lux or $Mab_{\Delta dosRS}$ P_{hsp60}-lux as internal controls (1%O_2(P_{dosR} or P_{2489}/P_{hsp60}))/(20% O_2(P_{dosR} or P_{2489}/P_{hsp60})).

Results

Growth And Transcriptome Remodeling Of Mab In A Defined Hypoxia Model

Our first goal was to develop a tractable *in vitro* model to investigate the mechanisms employed by *Mab* to persist under physiologically relevant oxygen-limited conditions. To do this, *Mab* 390S was grown under standing conditions in a 1% O_2 atmosphere to mimic the pO_2 observed within the CF lung, macrophages and granulomas (55,56,59). *Mab* 390S grew steadily at 1% O_2, reaching OD_{600} ~0.7 by day 5 with continued increase to ~0.9 by day 10 (Figure 4). Somewhat unexpectedly, the intended aerobic control culture (20% O_2 atmosphere, standing) had a very similar growth profile, reaching only a slightly higher OD ~1.2 by day 10 (Figure 4). In contrast, *Mab* 390S grown in 20% O_2 with shaking (100rpm) reached a maximum density by day 5 (OD_{600}~1.6) and subsequently plateaued up to day 10 (Figure 4). This difference is likely due to the microaerobic conditions experienced by bacilli growing below the media surface, as previously seen with *Mtb* and BCG strains grown in standing conditions (147,148). To maximize the contrast between aerobic and hypoxic conditions, *Mab* cultures shaking in 20% O_2 served as references for all hypoxia experiments. Thus, *Mab* is not only able to survive but to actively replicate under *in-vivo* like hypoxia conditions. It is worth noting that exposure of *Mab* to sudden hypoxia using BD Gaspack anaerobic pouches led to rapid sterilization of the cultures (data not shown). This may indicate a lower threshold of O_2 levels needed for *Mab* viability was exceeded or that slower, adaptive responses are necessary to survive.

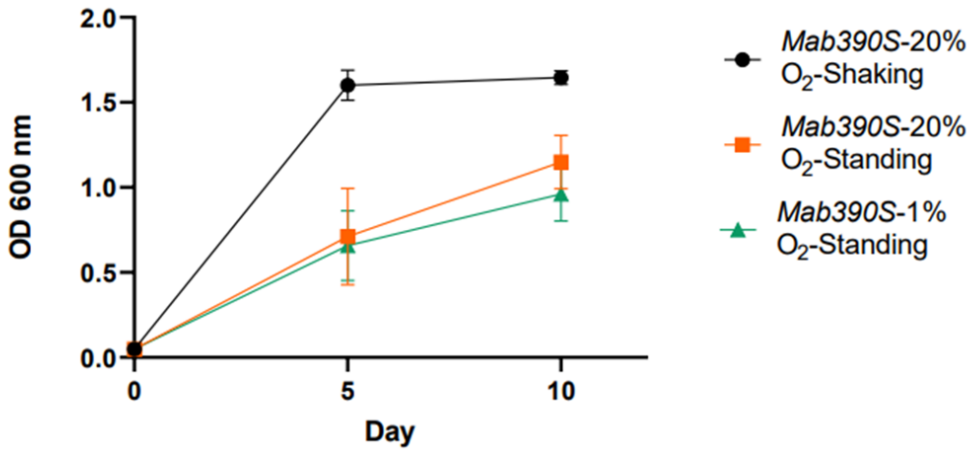

Figure 4: Growth kinetic comparisons of Mab390S

Mab390S cultures were grown in 20% O_2 while shaking (black), 20% O_2 while standing (orange) or 1% O_2 while standing (green). OD_{600nm} was taken on day 0, 5, 10.

Exploiting this model to profile *Mab* differential gene expression (DGE) in response to hypoxia, RNAseq transcriptomic analysis was conducted on wild-type *Mab* 390S cultured at 1% O_2 and 20% O_2 on day 5. This time point reflects the maximal difference in OD_{600nm} between hypoxic and aerated cultures and precedes the plateau in growth curves (Figure 4). The scatter plot in Figure 5A graphically depicts the dramatic genome-wide alterations in *Mab* 390S gene expression induced by *in vivo*-like low oxygen condition. The *Mab* hypoxia response included induction of 1,190 genes ($\geq$ 1 $\log_2$ fold change compared to 20% O_2) and downregulation of 1,062 genes ($\leq$ 1 $\log_2$ fold change compared to 20% O_2) (Table S1). This represented a larger set of hypoxia-induced genes than observed in *Mtb* in two studies under similar 1% O_2 hypoxia conditions (induction of ~400 genes detected via microarray and ~682 via RNAseq) (87,149). These data highlight the functional genomic differences between *Mab* and *Mtb,* in particular their distinct patterns of gene regulation in response to hypoxia which are discussed in detail below.

To identify putative regulators of hypoxia adaptation in *Mab,* we assessed the differential expression of TCSs and other annotated transcription factors in the 1% hypoxia model. Of the 11 TCS orthologous to *Mtb*, only *dosRS*, *mtrA*, *narS* and the orphan RRs *Mab_2133* and *Mab_3520c* displayed DGE (Figure 5A-B). *Mab_dosRS* exhibited the largest magnitude of gene induction with $\log_2$FC of 3.9 and 4.5, respectively, pointing to $DosRS_{Mab}$ as an important TCS facilitating adaptation to hypoxic stress. The other TCS components were minimally induced with a $\log_2$FC of 1.6 for *narS*, 1.2 for *mtrA* and 1.1 for the orphan RR *Mab_2133*. The roles of *narS, mtrA* and *Mab_2133* have not been determined in *Mab*. However, in the context of *Mtb*, the regulons of DosRS and NarLS TCS display partial overlap and protein-protein interactions between the RR from these two TCSs, DosR and NarL, have been detected (105). *mtrA* is essential in *Mtb* due to its role in replication, whereas in *Mab mtrA* was reported to be non-essential, pointing to potential

differences in the role of this TCS between the two species (150,151). The *Mtb* ortholog (Rv3143) of orphan RR *Mab_2133* is implicated in nitrate metabolism in the absence of oxygen, binds to *nuo* subunits required for electron transport and is within nuo operon (152). *Mab's* nuo operon displays synteny with the *Mtb nuo* operon including the orphan RR *Mab_2133*. Whereas Rv3143 was moderately induced by hypoxia in a DosR-dependent manner (65), the upregulation of *Mab_2133* in our hypoxia model was not altered in the absence of DosRS (Table S1). The only TCS gene displaying substantial downregulation was *Mab_3520c* (log_2FC = -9.7). The *Mtb* ortholog of *Mab_3520c*, Rv0260c, is known to be upregulated in hypoxia and to interact with DosS via protein-protein interaction independent of DosR; however, the function of *Rv0260c* has not been identified (149,153). The opposite pattern of regulation of Rv0260c (induced) and *Mab*_3520c (repressed) in hypoxia implies they are utilized differently for adaptation to hypoxia. Thus, our transcriptomic analyses of *Mab* under physiologic hypoxia conditions point to *Mab* DosRS as an important TCS aiding in adaptation to hypoxia.

In addition to induction of the *Mab_dosRS* TCS, we also observed upregulation of 80 single component transcription factors (TF) in hypoxia (Table S1). Due to the high number of TF, only the genes with a $log_2FC \geq 3$ are included in (Table S2) with the most highly induced genes being *Mab_4180* (lclR), *Mab_2606c* (TetR family), *Mab_4332* (TetR family) and *Mab_3018* (GntR family). The *Mtb* orthologs for *Mab_4332* (Rv0273c) and *Mab_3018* (Rv0586) have 64.14% and 45.53% identity, respectively. Rv0273c has been identified as a regulator of *inhA*, an enoyl-ACP reductase involved in mycolic acid synthesis, and Rv0586 is known to mediate lipid metabolism in *Mtb* (154-156). Both *Mab_4180* and *Mab_2606c* share less than 30% sequence homology with the *Mtb* orthologs and no known function has been identified. Although few *Mab* transcriptional

regulators have been characterized, the large number of regulators with altered expression under hypoxic stress are likely key nodes in the regulatory networks needed to adapt *in vivo* .

Due to the number of TFs and their magnitude of modulation in response to hypoxia, including upregulation of *Mab_dosRS*, the broad scope of transcriptional changes was not surprising. The list of hypoxia-induced genes included loci involved in fatty acid and cholesterol metabolism, components of the NADH-quinone oxidoreductase subunits (*nuoA-N*), 6 epoxide hydrolases (*ephD*), ATP synthase subunits, 5 mammalian cell entry operons (MCE), members of the glycopeptidolipid locus (GPL), and 520 hypothetical genes (Table S1&S2). Several pathways critical for pathogenesis of *Mtb,* such as fatty acid and cholesterol metabolism, are also induced in various hypoxia models (Wayne model, 1% O_2) and within granulomas (149,157,158). All four MCE loci in *Mtb* are differentially expressed in response to hypoxia, suggesting an important role for this family of lipid/cholesterol transporters in adaptation to this stress. While *mce2* and *mce3* were induced in a hypoxia model similar to ours (1% O_2, 5 days), *mce1* was repressed, and *mce4* expression remained unchanged (149). A separate study by Rathor *et al.* found that *mce4* was upregulated after much longer durations of hypoxia stress (159). Mce1 and Mce4 are known to play a role in the transport of fatty acids and cholesterol (158,160), whereas the function of Mce2 and Mce3 have not been determined yet. In contrast, five of the seven MCE systems encoded by *Mab* were upregulated in 1% O_2 after 5 days (Table S1&S2). Although the biological role of MCE complexes in *Mab* have not been studied, their distinct expression profile suggest they may be important for *in vivo* survival. The *Mab* hypoxia-induced gene set also included a large number of genes implicated in β-oxidation pathways - 14 *fadE* genes, 8 *fadD* genes, and one of each *fadA* and *fadH* (Table S1&S2). Upregulation of 6 *ephD* genes (an epoxide hydrolase predicted to alter the amount of epoxymycolates in the cell wall), members of the GPL locus accounting for smooth

morphology (Table S1&S2), and arabinosyltransferases A and B (Table S1) involved with arabinogalactan synthesis indicate *Mab* may undergo cell wall remodeling in response to hypoxia (44,161,162).

In addition to β-oxidation, metabolic pathway induction included *nuo* subunits *A-N*, ATPase subunits, and cytochrome P450 genes (Table S1&2). NuoA-N are subunits of the proton pumping NADH dehydrogenase type 1 responsible for transferring electrons to menaquinone in the electron transport chain (ETC) in an energy conserving manner to generate a PMF (163). Although these genes are upregulated in the RGM *Mycobacterium smegmatis* (*Msmeg)* during slowed growth and in *E.coli* in anaerobic conditions, this is not a feature observed in the hypoxic response of slow-growing mycobacteria (SGM) like *Mtb* (164,165). In contrast to *Mab*, the nuo operon and ATPase subunits are downregulated in hypoxic *Mtb*, further highlighting the distinct stress responses and energy metabolism of these two species in response to hypoxia (149,166). Of the 25 *Mab* cytochrome P450s, 14 were induced in hypoxia (Table S1&2). This data is consistent with hypoxic induction a large number of cytochrome P450s in the RGM *Msmeg* but not in the SGM *Mtb* with the exception of only 2 cytochrome P450s (134,165,167). The roles of individual *Mab* cytochrome P450s remain unknown but the functions of the *Mtb* orthologs are dependent on their ferredoxin redox partners and include cholesterol degradation, redox balance, and virulence (168). Our data supports hypoxic induction of 2 ferredoxins (*Mab_0914c* & *Mab_2049c*) and 3 ferredoxin reductases (*Mab_0930*, *Mab_2047c* and *Mab_4356c*) (Table S1). Induction of *nuo*A-N, ATPAse subunits, the large number of cytochrome P450s and ferredoxins implies *Mab* may employ different sets of genes for anaerobic respiration in its response to hypoxia and adapation.

Mab's transcriptional adaptation to hypoxia also comprised a large set of downregulated genes including but not limited to multiple TF, tRNAs, 30S and 50S ribosomal proteins, alternative sigma factors, and 431 hypothetical proteins (Table S1). Downregulation of genes involved in essential processes such as protein synthesis (e.g. tRNAs, ribosomal proteins and sigma factors) are consistent with the slowed growth observed in hypoxic *Mab* cultures. Included among the most downregulated genes in hypoxia (Table S1) is the orphan response regulator *Mab_3520c* (Figure 5B) and three adjacent upstream genes (*nirD/MAB_3521c*, *nirB/MAB_3522c*, and *narK3/MAB_3523c*) (Figure 5A) predicted to be involved in nitrite reduction and extrusion (122). *Mtb nirB* and *nirD* orthologs are reportedly induced in nutrient starvation but minimal to no DGE occurred in hypoxia at 1% O_2 (149). However, in the Wayne model of hypoxia *Mtb nirB* displayed induction and functional *nirBD* genes were required for growth in hypoxia when nitrite was used as the sole nitrogen source (169).

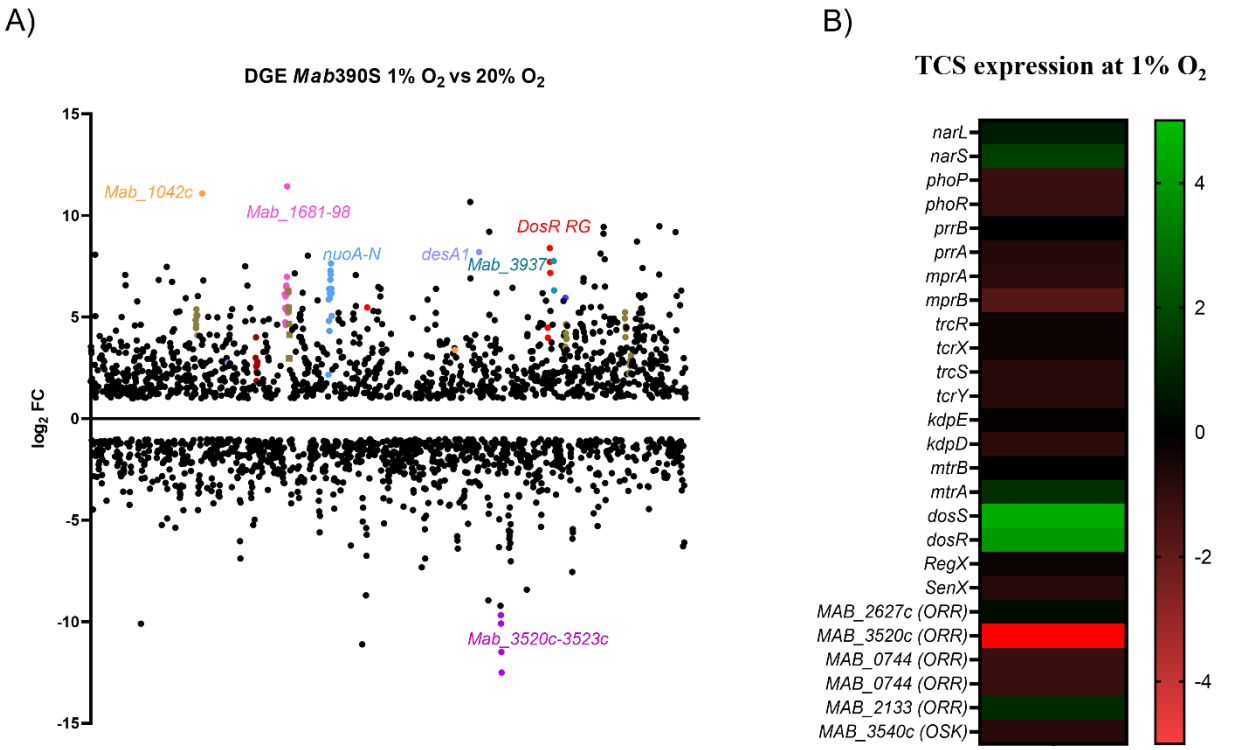

Figure 5:Transcriptome analysis of Mab390S in defined hypoxia model

DGE is visualized as **(A)** scatter plot depicting changes in gene expression reported as TPM with ≥ or ≤ log_2FC on Day 5 for *Mab* 390S 1% O_2 vs *Mab* 390S 20% O_2. Dots represent individual genes (neon green=*Mab_1042C*, pink=*Mab_1681-1698*, blue=*nuo* operon, purple= *desA1*, turquoise=*Mab_3937 & 3938*, red= predicted DosR regulated genes (RG) magenta= *Mab 3520c-3523c*). **(B)** Heat map showing DGE of TCS of *Mab* 390S in 1% O_2 vs 20% O_2. In gene names, orphan response regulators and orphan sensor kinases are denoted as ORR and OSK, respectively.

Construction And Validation of Mab$_{\Delta dosRS}$ And Mab$_{\Delta dosRS+C}$

Elucidation of the global transcriptional responses of *Mab* to hypoxia for the first time revealed the DosRS TCS is employed during hypoxic adaptation, yet much remains unknown about the role of DosRS in gene regulation and *Mab* pathogenesis. The DosR$_{Mab}$ regulon was previously predicted to consist of only 6 genes - *Mab*_3890 (*dosS*), *Mab*_3891 (*dosR*), *Mab*_2489 (universal stress protein, USP), *Mab*_3902c (ortholog of Rv2004c), *Mab*_3903 (nitroreductase) and *Mab*_3904 (USP) – based solely on bioinformatic analysis (111). However, at the time this study was initiated, the role of DosRS$_{Mab}$ signaling in gene regulation, including induction of this gene set, remained to be experimentally demonstrated. To enable determination of the DosRS$_{Mab}$ regulon and role of this TCS in *Mab* adaptation to hypoxia, we generated *Mab$_{\Delta dosRS}$* (knockout mutant) using recombineering and the corresponding complemented strain (*Mab$_{\Delta dosRS}$*$_{+C}$) expressing a single, integrated *dosRS* allele driven by its native promoter (139). In addition to confirming strain genotypes by PCR and DNA sequencing (data not shown), the absence of *dosRS* transcripts in *Mab$_{\Delta dosRS}$* and restoration to wild-type levels in *Mab$_{\Delta dosRS}$*$_{+C}$ was validated by qRT-PCR (Figure 6A). We next assessed transcript levels of 4 genes (in addition to *dosRS* operon itself) previously predicted to be DosR-dependent. Loss of a functional DosRS system resulted in down-regulation of all predicted DosR$_{Mab}$-regulated genes by >2 log (*MAB_2489, MAB_3902c, MAB_3903)* or > 1 log in the case of *MAB_3904* with restoration to wild-type levels in the complemented strain (Figure 6B), consistent with DosR-mediated induction of these genes.

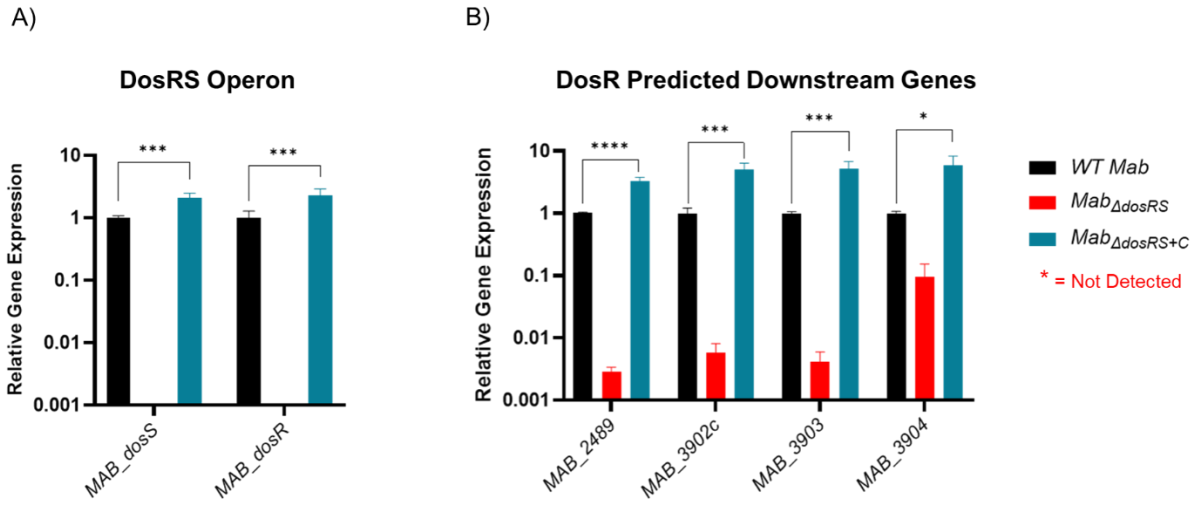

Figure 6: Validation of Mab$_{\Delta dosRS}$ and Mab$_{\Delta dosRS+C}$

qRT-PCR was performed to **(A)** confirm the deletion and restoration of *dosS* and *dosR* in *Mab*$_{\Delta dosRS}$ and *Mab*$_{\Delta dosRS+C}$, respectively, and **(B)** assess the effect on predicted downstream genes. *Mab 390S* (black), *Mab*$_{\Delta dosRS}$ (red) and *Mab*$_{\Delta dosRS+C}$ (blue). Data is representative of 3 experiments performed in triplicate. *P* values were calculated *via* one -way ANOVA using GraphPad. Red stars indicate C_t values were not detected for *Mab dosR* nor *dosS* in the mutant strain. **P*-value <.05, ****P*-value <.001 *****P*-value <.0001.

DosRS$_{Mab}$ Is Required For Maximal Growth In Hypoxia

As detailed above, to verify the role of DosRS under *in vivo* relevant conditions, we compared the growth kinetics assays of *Mab* 390S, *Mab$_{\Delta dosRS}$*, and *Mab$_{\Delta dosRS\ +C}$* in hypoxic (1% O_2, standing) versus aerobic (20% O_2, shaking) conditions. Strains were monitored over a 30-day period using CFU/ml as the readout at day 5, 20, and 30 and grown in normoxic conditions after plating. Cultures grown in 20% O_2 reached maximum growth on day 5 with no difference in growth between strains at any time point confirming fully aerated cultures are not dependent on DosRS for replication (Figure 7A). At 1% O_2 maximum growth was achieved by day 20 in *Mab* 390S with a ~2-log decrease in *Mab$_{\Delta dosRS}$* and a ~log decrease in *Mab$_{\Delta dosRS+C}$* (Figure 7B) suggesting a functional DosRS is required for maximal growth and survival during hypoxic stress. By day 30 in 1% O_2, *Mab* 390S displayed a slight decrease in CFU compared to day 20 however, this decline was also observed in fully aerated cultures indicating that hypoxic stress was not the cause (Figure 7A&B). These data support the conclusion that DosRS$_{Mab}$ is necessary for growth in hypoxic environments that mimic the physiologic environments of the CF lung, within macrophages and granulomas (55,56,59). Unexpectedly, a morphotype transition from smooth to rough occurred in *Mab$_{\Delta dosRS}$* after pro-longed exposure to 1% O_2. On day 20 and 30 an observable change in morphology occurred only in the mutant strain resulting in a heterogenous population of smooth and rough colonies (Figure 8A-D), indicating a DosR-dependent inducible alteration in cell wall composition for *Mab$_{\Delta dosRS}$*. This is corroborated by the fact that in hypoxic liquid culture assays, *Mab$_{\Delta dosRS}$* alone adopted a biofilm-like pellicle layer that was resistant to disruption, whereas other strains maintained a homogeneous composition (data not shown).

Prompted by the inability of *Mtb$_{\Delta dosR}$* to resuscitate after re-aeration from hypoxia (75,170), we investigated the ability of *Mab$_{\Delta dosRS}$* to resuscitate after 30 days in hypoxia. Day 30 cultures taken

from 20% O_2 and 1% O_2 were diluted to an OD_{600nm} of 0.02 and grown in 20% O_2 while shaking to evaluate the recovery of *Mab*$_{\Delta dosRS}$ after prolonged exposure to hypoxia. OD_{600nm} was taken over a 10-day period (Day 0, 2, 3, 5, 8, and 10) to monitor growth kinetics after re-introduction of O_2. All strains originating from aerobic conditions displayed similar growth curves after re-culturing and reached maximal OD by day 5 (Figure 9A). In contrast, after being subjected to hypoxia for 30 days, *Mab*$_{\Delta dosRS}$ displayed reduced growth compared to *Mab* 390S and *Mab*$_{\Delta dosRS+C}$ taken from 1% O_2 (Figure 9B). Attenuated growth in 1% O_2 and the inability to resuscitate after re-aeration for *Mab*$_{\Delta dosRS}$ supports a critical role for DosRS$_{Mab}$ in mediating adaptation to changing oxygen levels encountered within the host during both dormancy and reactivation.

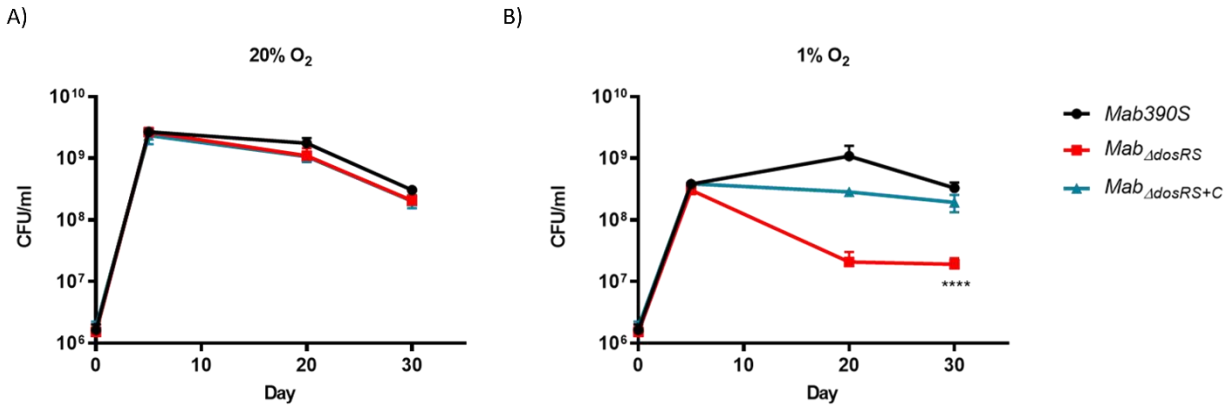

Figure 7: Mab$_{\Delta dosRS}$ is attenuated in hypoxia

Growth kinetics in hypoxia were assessed *via* serial dilutions, spot plating and enumeration of CFU/ml on day 5, 20 and 30. **(A)** Growth kinetics at 20% O_2 **(B)** Growth kinetics at 1% O_2. *Mab 390S* (black), *Mab*$_{\Delta dosRS}$ (red) and *Mab*$_{\Delta dosRS+C}$ (blue). Data reflects 3 independent experiments performed in triplicate. *P*-values were calculated *via* one-way ANOVA using GraphPad, ****P-value <.0001.

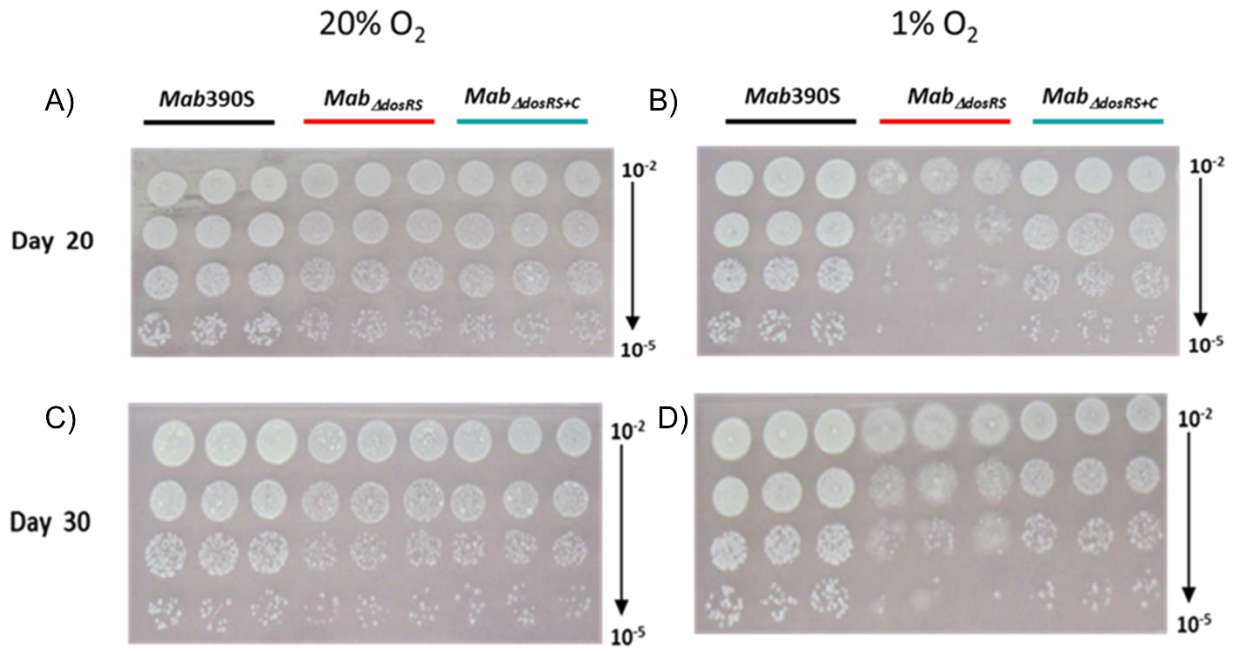

Figure 8: Hypoxia-induced morphological changes in Mab$_{\Delta dosRS}$

Cultures grown at 20% or 1% O_2 were spot plated on Day 20 and Day 30 and incubated under normoxic conditions. **(A)** Day 20 at 20% O_2 **(B)** Day 20 at 1% O_2 **(C)** Day 30 at 20% O_2 **(D)** Day 30 at 1% O_2.

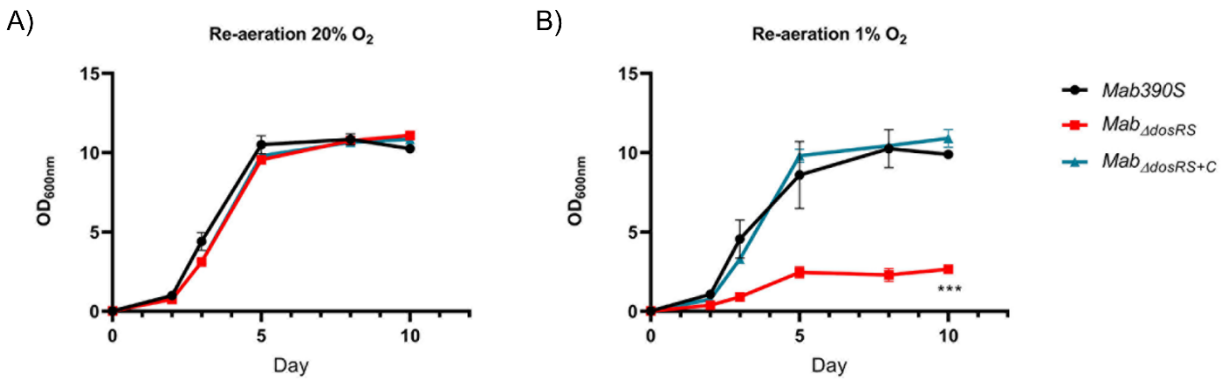

Figure 9: DosRS is required for resuscitation after hypoxia.

OD_{600nm} was taken over a 10-day period of re-aerated cultures after 30 days of growth in either **(A)** 20% O_2 or **(B)** 1% O_2. *Mab390S* (black), $Mab_{\Delta dosRS}$ (red) and $Mab_{\Delta dosRS+C}$ (blue). Data reflects 2 independent experiments performed in triplicate. *P*-values were calculated *via* one-way ANOVA using GraphPad, ****P*-value <.001.

Identification Of A Large And Unique Gene Set Regulated By DosRS$_{Mab}$

We next analyzed DGE between *Mab*390S and *Mab$_{\Delta dosRS}$* in hypoxia via RNAseq to experimentally identify DosRS regulated genes (Figure 10). Cultures of *Mab* 390S and *Mab$_{\Delta dosRS}$* were grown at 1% O_2 for 5 days at which point RNA was extracted from three independent experiments for analysis. In the absence of DosRS, 216 genes were expressed at lower levels relative to *Mab* 390S after exposure to 1% O_2 (Figure 10), of which 127 genes were also induced in *Mab* 390S by hypoxia (Table S1). This pattern is consistent with DosRS-dependent hypoxia induction, suggesting that *Mab* DosR may control a much larger regulon than previously predicted. In subsequent analyses, we defined putative DosRS-dependent hypoxia induced genes as those whose transcript levels were decreased by $\log_2FC \geq 1$ in the *Mab$_{\Delta dosRS}$* in 1% O_2 and were induced by $\log_2FC \geq 1$ in *Mab* 390S 1% O_2 (Table S2). The top 20 putative DosRS-dependent genes induced most highly by hypoxia (Table S2) include 4 of the genes previously predicted *in silico* to be members of the DosRS$_{Mab}$ regulon. Notably, two of the most highly upregulated genes, *Mab_3937* and *Mab_3354* (*desA1*), appear to be *Mab*-specific members of this regulon. *Mab_3937*, a hypothetical protein with no known ortholog, is predicted to be in an operon with *Mab_3938* and *Mab_3939*, encoding a Clp protease subunit (ClpC2) with orthologous counterparts in *Mtb* and *Msmeg* which are essential genes. (61,171,172). Both *desA1* (*Mab_3354*) and *desA2* (*Mab_1237*), desaturase enzymes with predicted roles in the biosynthesis of the mycolic acid component of mycobacterial cell walls, exhibited hypoxic DGE in the *dosRS* mutant (173,174). Recently *desA2* but not *desA1* was predicted to be an essential gene in *Mab*, *Mtb* and *Msmeg* suggesting even slight downregulation could lead to detrimental alterations in the cell wall (150,173). Although *Mtb* has orthologs of these genes (ClpC2, *desA1*, and *desA2)*, there is no evidence of regulation by DosR$_{Mtb}$, illustrating the potential for conserved TCS to interact with conserved target genes in distinct ways. Additionally, no known DosR$_{Mtb}$-regulated

genes have been deemed essential, further highlighting the unique nature of DosRS$_{Mab}$-mediated hypoxia response. Among the 127 hypoxia-induced putative DosR$_{Mab}$-dependent genes is a large gene cluster (*Mab_1681-1698)* containing hypothetical proteins, daunorubicin resistance efflux pump subunit (*drrA)*, and a putative *mce* operon (Table S1&S2). Whereas some putative *Mab* MCE gene clusters have clear orthologs in *Mtb* (e.g. MAB_4146c-4155c with Mce4, Rv3492c-3501c), the predicted *Mab* MCE proteins encoded by MAB_*1681-1698* do not directly correspond to a specific MCE loci in *Mtb.* Rather, they share low homology with components of different *Mtb* MCE complexes, necessitating further research to fully assess the role of this *Mab*-specific MCE during hypoxia.

Comparing the ~ 50 genes of the DosR$_{Mtb}$ regulon with the putative DosR$_{Mab}$ regulated genes identified in this study (Table S1), we only discovered 6 shared orthologs including 4 conserved hypothetical proteins (CHPs) plus DosR (*Mab_3891c*) and DosS (*Mab_3890c)*. In addition to the transcriptional regulator *Mab_3891c*, we found nine other transcriptional regulators to be induced by hypoxia in a putative DosR-dependent manner (Table S1& S2) with none of their *Mtb* orthologs regulated by DosR$_{Mtb}$. The transcriptional response of *Mab* to hypoxia is further differentiated from *Mtb* by the lack of regulation of any of the 7 putative triacylglycerol synthases (*tgs*) by hypoxia or DosR, a characteristic of *in vitro* dormancy and hypoxia for *Mtb* (Table S1) (95,175). Hypoxic *Mtb* positively regulates *tgs1* via DosR for synthesis of triacylglycerol (TAG) for energy storage and utilization. The absence of DosR$_{Mab}$-mediated induction of any Tgs enzymes under hypoxic stress points to a different mechanism for energy storage and utilization in *Mab* vs *Mtb* (98,135). The scope of the *Mab* DosR regulon precludes a comprehensive discussion of every downstream gene, many of which encode uncharacterized conserved hypothetical proteins. However, this

RNAseq dataset is evidence for a species-specific regulon larger than predicted bioinformatically that likely contains novel mechanisms of hypoxia adaptation and pathogenesis.

Comparative transcriptomics also revealed upregulation of 200 genes in *Mab*$_{\Delta dosRS}$ compared to *Mab* 390S (Figure 10, Table S1), however the magnitude of induction was low ranging between log_2FC of 1-3.6. Among the upregulated genes are 81 hypothetical proteins, 5 transcription factors, 30S and 50S ribosomal proteins. Included in the top 20 most highly induced genes in *Mab*$_{\Delta dosRS}$ are *Mab_3521c* (nitrite reductase) and *Mab_3523c* (nitrite extrusion protein) which were observed to be highly downregulated in hypoxic *Mab* 390S (Table S1). These data suggests that DosRS may act as a repressor of a subset of genes in hypoxic conditions, a hypothesis that remains to be experimentally validated. The low-level induction of other genes in the knockout strain may also result from indirect effects of DosRS on mycobacterial physiology under hypoxic stress.

To validate RNAseq results, two of the putative *Mab* DosR-dependent genes most differentially expressed in the mutant strain (*Mab_3354* and *Mab_3937*) were assessed via qRT-PCR along with 5 of the predicted *Mab* DosR genes (Figure 11A&B). Similar to RNAseq studies, the effect of hypoxia on gene expression was assessed in *Mab* 390S (1% vs 20% O_2) (Figure 11A) and the requirement for DosRS for DGE in response to hypoxia by comparing *Mab* 390S, *Mab*$_{\Delta dosRS}$ and *Mab*$_{\Delta dosRS\ +C}$ (Figure 11B). All genes assessed via qRT-PCR were induced by ≥ 10-fold in 1% O_2 compared to 20% O_2 for *Mab* 390S with *Mab_3937*, *Mab_3902c*, and *Mab_3354* having the highest gene induction consistent with RNAseq results (Figure 11B). These same genes displayed loss of induction in *Mab*$_{\Delta dosRS}$ by ≥ 10-fold similar to RNAseq results with restoration by *Mab*$_{\Delta dosRS+C}$ in hypoxia (Figure 11B). The most dramatic change in gene expression in *Mab*$_{\Delta dosRS}$

was *Mab_3902c* and *Mab_3937* with > 100-fold reduction compared to *Mab* 390S. Results from qRT-PCR corroborate RNAseq results and accentuate the magnitude of differential gene expression of predicted and newly discovered hypoxia-induced DosRS$_{Mab}$ regulated genes.

In addition to qRT-PCR, bacterial luciferase (Lux) reporter strains were used to evaluate the kinetics of hypoxia-dependent changes in gene expression across a broader time course. The integrating shuttle plasmid pMV306luxG13 optimized for mycobacteria consists of the constitutive P_{hsp60} and P_{G13} promoters driving expression of *luxAB* and *luxCDE*, respectively (143). Lux reporter constructs in which the constitutive P_{hsp60} promoter was replaced with promoters from two hypoxia inducible genes, DosR and *Mab*_2489 (P_{DosR} and P_{2489}) were introduced into *Mab* 390S and *Mab*$_{\Delta dosRS}$. Reporter assays performed on Days 1, 5, 20 identified temporal changes in gene expression with both promoters for *Mab* 390S but not in *Mab*$_{\Delta dosRS}$ (Figure 12A-C). The lux reporter under the control of P_{dosR} shows sustained induction over time, indicating that *dosR* is expressed throughout early and late stages of hypoxia, a trait not observed in *Mtb* (176). Although the *Mab* 390S P_{2489}-lux reporter displays modest induction of ~ 3-fold change on day 1, there is not a significant difference compared to *Mab*$_{\Delta dosRS}$ P_{2489} (Figure 12A). However, on days 5 and 20 *Mab* 390S P_{2489}-lux was highly induced compared to *Mab*$_{\Delta dosRS}$ P_{2489}-lux with fold changes of 61 and 433, respectively (Figure 12B-C). It should be noted that *Mab*$_{\Delta dosRS}$ P_{2489}-lux did exhibit low-level induction on Day 20, which may be attributable to the activity of other transcription factors. However, as noted previously, there was a significant difference compared to the expression of P_{2489} in wild-type *Mab* 390S. Lux reporters facilitated dynamic monitoring of DosRS activation by hypoxia and provide a valuable tool to explore DosR-mediated gene regulation *in vitro* and *in vivo* in response to various stresses (e.g. NO, CO, antibiotics) or host microenvironments (e.g intramacrophage, granuloma, airway mucus).

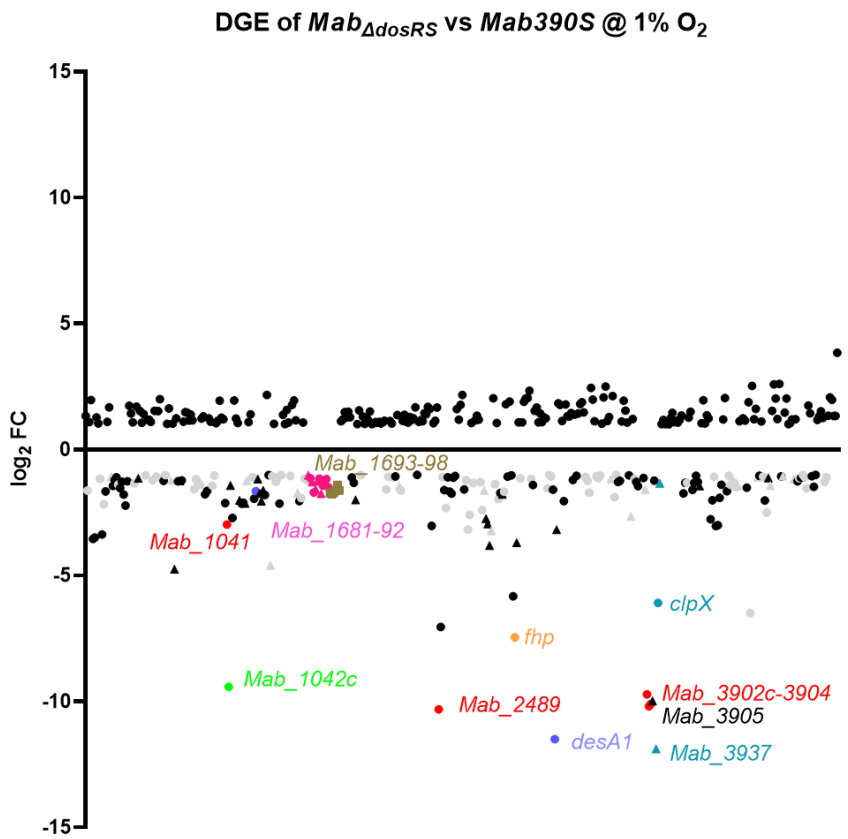

Figure 10: Mab DosR dependent differential gene expression at 1% O_2.

Scatter plot of RNAseq analysis of *Mab*$_{\Delta dosRS}$ vs *Mab* 390S after 5 days in 1% O_2. Figure shows genes with log_2FC ≤ -1 and ≥ 1. Gray circles are conserved hypothetical genes and gray triangles are *Mab* genes with no ortholog in *Mtb.* Names of select genes of interest are labeled (neon green=*Mab_1042C*, pink=*Mab_1681-1698*, purple= *desA1*, turquoise (triangle denotes no known ortholog in *Mtb) =Mab_3937 & 3938*, red= predicted DosR regulated genes (RG).

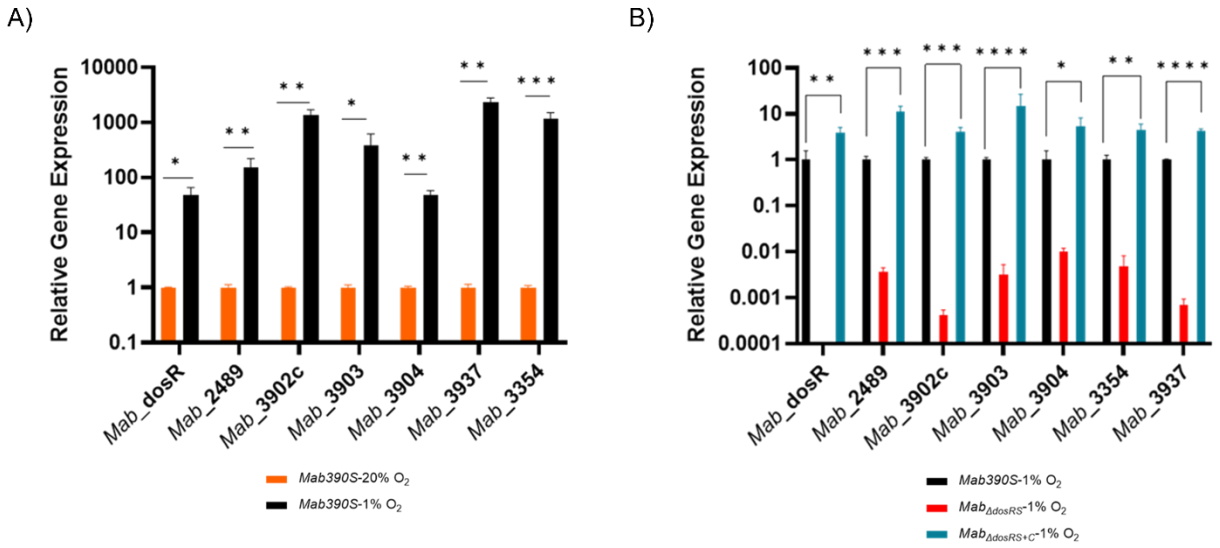

Figure 11: qRT-PCR validation of Mab DosR regulated genes in 1% O_2

qRT-PCR assessment of select DosR-dependent genes. Gene expression was calculated as relative quantitation *via* the $2^{-\Delta\Delta Ct}$ method using *sigA* as the reference gene. **(A)** Hypoxia induced gene expression. Transcript levels of select genes in *Mab* 390S 20% O_2 (orange bars) and *Mab* 390S 1% O_2 (black bars). **(B)** DosR dependent gene expression. Transcript levels of select genes in $Mab_{\Delta dosRS}$ (red bars) and $Mab_{\Delta dosRS+C}$(blue bars) were compared to *Mab* 390S (black bars) in 1% O_2 on Day 5. *P*-values were calculated using t-test **(A)** and one-way ANOVA **(B)**. **P*-value <.05, ** *P*-value <.01, ****P*-value <.001, *****P*-value < .0001. Not significant is denoted as ns.

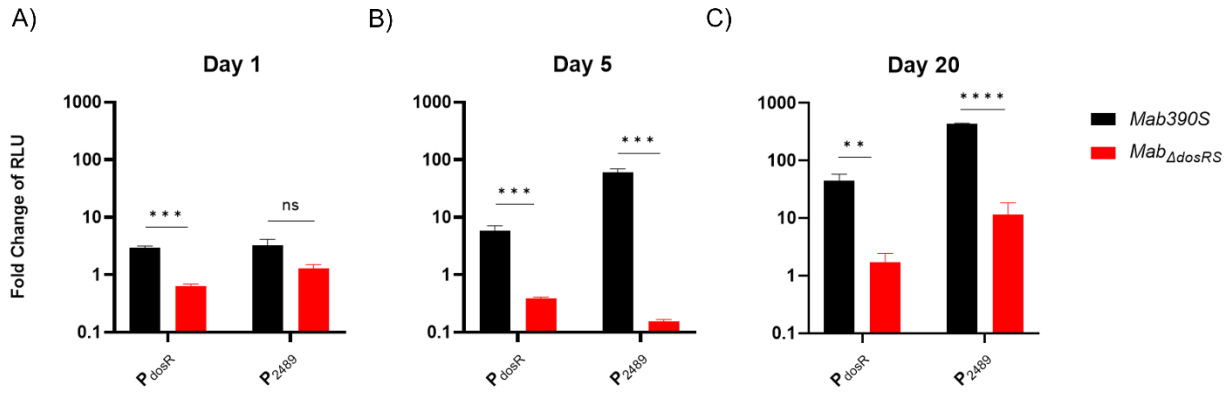

Figure 12: Lux reporter activity in 1% O_2

Kinetics of DosR-dependent gene induction measured luciferase reporter assays. Promoter activity in 1% O_2 was quantified by measuring luminescence compared to 20% O_2 cultures and normalized to lux-hsp60 constitutive promoter as a reference signal, (1%O_2(P_{dosR} or P_{2489}/P_{hsp60}))/(20% O_2(P_{dosR} or P_{2489}/P_{hsp60})) and expressed as fold change of relative light units (RLU) **(A)** 24hours, **(B)** Day 5, and **(C)** Day 20. *Mab* 390S (black bars) and $Mab_{\Delta dosRS}$ (red bars). qRT-PCR and luciferase assay data are representative of 3 independent assays performed in triplicate. *P*-values were calculated using t-test. **P*-value <.05, ** *P*-value <.01, ***P*-value <.001, ****P*-value < .0001. Not significant is denoted as ns.

Discussion

Infections caused by *Mab,* particularly within the CF population, are a major cause of concern due to the lack of efficacious antibiotics and the resulting inability to clear the infections from the airways. The poor correlation between *in vitro* drug susceptibility profiles and *in vivo* efficacy when treating *Mab* infections suggest that host-driven adaptations of *Mab* may contribute to treatment failures (23). Host-derived cues encountered by *Mab* within the viscous mucus layer of CF airways, phagosomal compartments of macrophages, and during residence within granulomas may trigger upregulation of antimicrobial resistance mechanisms (50,55,56,59). Extrapolating from studies on *Mtb* (177-179)*, in vivo* stresses such as hypoxia may also promote the development of phenotypically drug-tolerant persisters. Thus, a better understanding of *Mab's* physiological states and stress responses required for long-term persistence within the human host may lead to more effective treatment strategies.

Successful bacterial pathogens like *Mtb* and *Mab* employ extensive repertoires of transcription factors, including TCS, for coordinating gene expression to counteract host antimicrobial factors and immune pressure. The transcriptional regulatory networks and role of TCS of *Mtb* have been extensively characterized in multiple *in vitro* and *in vivo* models of infection (86,149,180-182) . In contrast, few transcriptomic studies defining *Mab* stress responses, or the role of specific transcription factors have been reported (61,127). Given the well-documented relevance of hypoxia during *Mab*-host interactions (e.g. mucus of CF airway, macrophage phagosome, granuloma) (50,55,56,59), we sought to identify molecular mechanisms that enable *Mab* to adapt to these low-oxygen niches. In the better characterized pathogen *Mtb,* the master regulator of hypoxia adaptation is the atypical TCS DosRS/T, which regulates a ~50 gene regulon upon induction by hypoxia and NO stress (93,135). *Mab* encodes orthologs of eleven of the twelve TCS

found in *Mtb,* including DosRS (*dosT* homolog missing). However, as detailed in this study, the scope and content of *Mab* regulons controlled by these TCS may be less conserved. Prior to initiation of our study, only two reports had mentioned *Mab* DosRS: i) a bioinformatics study predicting a 6 gene regulon based on previously known *Mtb* DosR binding motifs (111) and ii) transcriptomic study assessing the affect of NO exposure on the predicted genes (61). These studies, however, did not directly demonstrate DosRS-mediated regulation of the predicted genes, define the transcriptional response of *Mab* to hypoxia nor the full extent of the DosR regulon, or identify a DosRS phenotype. To begin to address these knowledge gaps we developed a hypoxic model of 1% O_2 to mimic physiologically relevant oxygen tensions *Mab* encounters *in vivo* (55,56,59) to assess transcriptomics and growth kinetics of *Mab* in the presence or absence of $DosRS_{Mab}$.

Genome wide transcriptomics identified DosRS as the main TCS activated during hypoxia and analysis of a defined mutant lacking DosRS revealed a potentially larger regulon than previously predicted. We identified 216 genes to be downregulated in $Mab_{\Delta dosRS}$ versus *Mab* 390S, 127 of which were upregulated in hypoxia. This gene set was deemed the putative hypoxia-induced DosR regulon-*Mab_3902c, Mab_3903* and Mab_*3904*), 2 novel genes displaying the highest DGE (MAB_3937 and *desA1*), 9 transcription factors, and 57 hypothetical genes among others. 22 of the 57 hypothetical genes are species-specific, further illustrating the unique nature of the regulons controlled by orthologous TCS. Not only is the *Mab* DosRS regulon likely larger than previously predicted, but it also appears to be notably larger than the well-studied *Mtb* DosR regulon. Surprisingly, the only orthologs in common between the *Mtb* DosR and *Mab* DosR regulons were the 6 genes originally predicted from the bioinformatics study and *Mab_1040,* an ortholog of the hypothetical protein *Rv3129* which is documented as an antigen in tuberculosis

patients with latent infections (135,183,184). One of the hallmarks of *Mtb* hypoxia adaptations *in vivo* and *in vitro* is the marked upregulation of *tgs1* for energy storage and utilization (175,185). The induction of *Mab_3551c*, the primary TAG synthase gene in *Mab* (186) *,* is not observed in our *Mab in vitro* hypoxia model, suggesting *Mab* mechanisms of hypoxia adaptation or cues for regulation of lipid storage are distinctive from *Mtb.*-Studies are underway to discriminate between genes whose expression is altered directly by DosR (DosR binding to promoter) versus indirectly (promoter regulated by secondary TF).

During the course of our study, Belardinelli *et al.* also reported on characterization of the *Mab* DosR regulon as part of efforts to repurpose antimalarial drugs that inhibit *Mtb* DosR as therapeutics for *Mab* (60)*.* Their transcriptomic comparison of *Mab* ATCC 19977 and $Mab_{\Delta dosRS}$ in microaerobic conditions identified 180 genes downregulated in a DosRS-dependent manner. Of these 180 genes, only 45 overlapped with our list of 216 genes downregulated in the *dosRS* mutant at 1 % O_2. Both studies included the 6 previously predicted genes and the 2 genes most highly differentially expressed on our list (*Mab_3937*, *desA1*) plus 37 other genes. Of the 45 genes in common between these 2 studies, Belardinelli *et al*., reported 38 DosR binding motifs supporting the assertion that *Mab* DosR regulon is larger than previously predicted. Discrepant findings between this report and our study could be attributable to differences in strains (ATCC 19977 vs 390S), hypoxic models (20% O_2 standing vs 1% O_2 standing), time points (24hr vs 5 days), or media (Dubos-Tween albumin vs 7H9-OADC+.05% tyloxapol). Regardless, both clearly highlight the broad scope and unique nature of the $DosRS_{Mab}$ regulon and provide a framework for future studies to fully elucidate the role of this important two-component system.

The importance of DosR-regulated genes for hypoxia adaptation was evident from growth deficits seen on day 20 and 30 and impaired resuscitation after reaeration in *Mab*$_{\Delta dosRS}$ compared to *Mab* 390S (Figure 7&9). *Mab*$_{\Delta dosRS}$ differentially expressed genes in hypoxia contain 7 genes predicted to be essential in a recent TnSeq study under aerobic conditions (150), possibly accounting for these phenotypes. Included in this list is *desA2*, a desaturase enzyme that is responsible for mycolic acid biosynthesis and is essential for growth in the RGM *Msmeg* (173). Strong induction of *desA1* in hypoxia suggests that it, along with *desA2*, may play role in cell wall modification in response to this stress. It is worth noting that, despite exclusion from the list of *Mab* predicted essential genes, the orthologous desaturase in *Msmeg* was deemed essential (187). Additionally, the MCE operon *Mab*_1693-*Mab*_1698 was differentially expressed in the mutant strain and may contribute to decreased importation of mycolic acids further disrupting cell wall integrity. The 6 other predicted essential genes possibly contributing to the *Mab*$_{\Delta dosRS}$ growth phenotype are 2 conserved hypothetical proteins (*Mab_3268c-Mab_3269c*), a DNA helicase (*Mab_3511c*), a protoporphyrinogen oxidase, a prephenate dehydratase (*Mab_0132*), and phosphoribosylformylglycinamidine synthase (*Mab_0698*).

In addition to growth/survival deficits and the inability to resuscitate, we also observed DosRS-dependent hypoxia-induced morphological changes. After 20 days in hypoxia, *Mab*$_{\Delta dosRS}$ displayed heterogeneous morphology consisting of smooth and rough colonies (Figure 8). This phenotype was not present in strains expressing DosRS or in fully aerated cultures, evidence that this TCS mediates dramatic remodeling of the cell wall in response hypoxia. The smooth and rough morphotypes of *Mab*, reflective of different compositions of the outer cell wall, have been shown to impact interactions with macrophages, immune stimulation and inflammation, antibiotic susceptibility, and virulence (33,38,40,49,188). Rough strains are able to trigger apoptosis of

macrophages and grow extracellularly as aggregates known as cords, and are associated with worse clinical outcomes (49). Mechanisms involved in smooth to rough transitions have not been fully elucidated. However, genomic comparisons between the two morphotypes revealed SNPs and indels in the *gpl* locus and in *mmpl4b* and *mps1* genes (45). In addition to total or partial loss of GPL due to mutations affecting its biosynthesis or transport, recent studies including identification of GPL+ rough clinical isolates suggest other mechanisms may also govern S→R morphotype switching (32). For example, Daher *et al.* reported that glycosylation patterns of GPL can alter *Mab* surface properties (46). An inducible transition from smooth to rough was also observed following exposure to subinhibitory doses of aminoglycoside antibiotics providing evidence for transcriptional modulation of morphotype in response to stress (47). Belardinelli et al. reported no differences in GPL content between *Mab* ATCC 19977 and isogenic *ΔdosRS* mutant after microaerobic culture for 24 hours (60). Our observation of a switch to rough morphotype in a *ΔdosRS* mutant after extended culture at 1% O_2 may reflect either adaptive cell wall remodeling triggered by lower O_2 levels or longer duration of stress in our model. Alternatively, rather than affecting GPL levels per se, inactivation of the DosRS regulon may impact GPL modifications or biosynthesis of unique cell wall constituents. Intriguingly, Pawlik *et al*. reported that expression of *dosR* was elevated in an R versus S strain (45). This seems to contrast with our data suggesting that DosRS positively regulates GPLs, or at least the smooth phenotype (e.g. loss of DosRS→rough phenotype in hypoxia). Whether this is a direct correlation or stress induced side-effect stemming from the loss of GPL remains to be determined. It is clear that much remains to be learned regarding how *Mab* regulates the composition of its complex cell wall during infection and the roles of TCS like DosRS in host-pathogen interactions.

In addition to determination of the DosRS-dependent component of *Mab* hypoxia adaptation, this is the first transcriptomics study designed to identify genome-wide changes in *Mab* gene expression in a defined, physiologically relevant model of hypoxia. RNAseq analysis of wild-type *Mab*390S in 1% O_2 versus 20% O_2 identified an additional 1,063 DosRS-independent hypoxia-induced genes with putative roles in *Mab* adaptation in hypoxia. Differential gene expression of such a large group of genes in hypoxia outside of the DosR regulon points to a sophisticated mechanism of regulation for adaptation beyond TCS. This gene set included 80 TF, lipid metabolism and transport, energetics, secondary metabolism, cell wall synthesis plus induction of 540 hypothetical proteins, (Table S3). Our data highlights the necessity of adaptation to hypoxia via a large repertoire of genes including but not limited to the TCS DosRS. Further investigation of unique *Mab* DosR regulated genes and species-specific *Mab* genes employed for hypoxic adaptation will provide beneficial insights into *Mab* pathogenesis.

CHAPTER THREE: NNAR REGULATES NITROGEN ASSIMILATION GENES IN *MYCOBACTERIUM ABSCESSUS*

Abstract

Mycobacterium abscessus (*Mab*) is an opportunistic pathogen afflicting individuals with underlying lung disease such as Cystic Fibrosis (CF) or immunodeficiencies. Current treatment strategies for *Mab* infections are limited by its inherent antibiotic resistance and restricted drug accessibility due to *Mab's* ability to reside within macrophages, granulomas and the mucus laden airways of the CF lung resulting in poor cure rates of 30-50%. *Mab's* ability to survive within the CF lung requires adaptation via transcriptional remodeling to counteract stresses like hypoxia, increased levels of nitrate, nitrite, and reactive nitrogen intermediates. *Mycobacterium tuberculosis* (*Mtb*) is known to coordinate hypoxic adaptation via induction of respiratory nitrate assimilation through the nitrate reductase *narGHIJ*. *Mab,* on the other hand, does not encode a respiratory nitrate reductase. In addition, our recent study of the transcriptional responses of *Mab* to hypoxia revealed marked down-regulation of a locus containing putative nitrate assimilation genes, including the orphan response regulator NnaR (nitrate/nitrite assimilation regulator). These putative nitrate assimilation genes, *narK3* (nitrate/nitrite transporter), *nirBD* (nitrite reductase), *nnaR,* and *sirB* (ferrochelatase) are arranged contiguously with *nasN* (assimilatory nitrate reductase identified in this work) is encoded in a different locus. Absence of a respiratory nitrate reductase in *Mab* and down-regulation of nitrogen metabolism genes in hypoxia suggest interplay between hypoxia adaptation and nitrate assimilation are different from what is documented in *Mtb*. The mechanisms used by *Mab* to fine-tune the transcriptional regulation of nitrogen metabolism in the context of stresses e.g. hypoxia, particularly the role of NnaR remain poorly understood. To evaluate the role of NnaR in nitrate metabolism we constructed a *Mab nnaR*

knockout strain (*Mab*$_{\Delta nnaR}$) and complement (*Mab*$_{\Delta nnaR+C}$) to investigate transcriptional regulation and phenotypes. qRT-PCR revealed NnaR is necessary for regulating nitrate and nitrite reductases along with a nitrate transporter. Loss of NnaR compromised the ability of *Mab* to assimilate nitrate or nitrite as sole nitrogen sources highlighting its necessity. This work provides the first insights into the role of *Mab* NnaR setting a foundation for future work investigating NnaR's contribution to pathogenesis.

Introduction

The nontuberculous mycobacteria *Mycobacterium abscessus* (*Mab*) is an opportunistic pathogen afflicting the immunocompromised and individuals with pre-existing lung disorders such as cystic fibrosis (CF) (6,8,27). CF patients are particularly vulnerable to bacterial infections due to reduced clearance of pathogens caused by viscous mucus build up in the airways of the lungs and impaired innate immune responses leading to high rates of infections and morbidity (50,51). *Mab* is the most prevalent rapidly growing mycobacteria recovered from the lungs of CF patients, often causing deleterious effects such as lung function decline, resulting in extended hospitalization and in some cases exclusion from lung transplants (14,27,28). Treatment options for *Mab* infections are limited due to inherent antibiotic resistance, resulting in cure rates of less than 50% (14,24,124,125). Like *M. tuberculosis* (*Mtb*), *Mab's* ability to reside within macrophages and granulomas physically limits exposure to antibiotics and also promotes drug tolerance by driving metabolic and transcriptional remodeling, further complicating the treatment of these infections. (53,54,124). *Mab* is also able to survive within the mucus that accumulates in the CF airway. In addition to creating a hypoxic microenvironment with a pO2 of 1%, this mucus layer is characterized by increased levels of nitrite, nitrate and nitric oxide (57-59). Adaptation to these conditions along with other host-derived stressors will require extensive alterations in gene

expression to allow *Mab* to establish persistent pulmonary infections. In *Mtb,* it is apparent that hypoxia survival strategies are inextricably linked to nitrogen metabolism via a shift to nitrate respiration as a way for bacilli to cope with low-oxygen microenvironments (99,107,108). Our current understanding of how *Mab* adapts to these stresses *in vitro* or *in vivo* remains rudimentary at best. Several recent reports, including one from our group, highlighted the role of the *Mab* DosRS two-component system in the induction of a species-specific regulon in response to hypoxia (60,114). On the other hand, research examining the regulation of nitrogen metabolism in *Mab* is lacking. Prompted by our recent analysis of the hypoxia-induced transcriptional responses in *Mab* (114), the current study provides additional evidence that *Mab* relies on strategies of nitrogen metabolism distinct from *Mtb* in response to *in vivo* relevant stresses.

The mechanisms for assimilation of nitrogen from nitrate and nitrite, which are readily accessible to mycobacteria during infection (109), have been well characterized in *Mtb* and *M. smegmatis* (*Msm*) however little is known about this facet of *Mab* host-pathogen interactions. Nitrate assimilation not only provides inorganic sources of nitrogen for the production of biomolecules but can also protect microbes against host iNOS (inducible nitric oxide synthase) derived nitric oxide (NO) an important factor used by the host to control infection (55,109,189,190). Host derived NO, after conversion to nitrate through auto-oxidation, can be exploited by *Mycobacterium* via the nitrate assimilation pathway resulting in the production of ammonium which can be stored as glutamate (109). *Mtb* constitutively expresses NarGHJI which serves as both an assimilatory nitrate reductase (NR), which converts nitrate to nitrite, and a respiratory NR allowing utilization of nitrate as a terminal electron acceptor (107,191,192). The transcriptional and post-translational activation of NarK2, a putative H^+/nitrate symporter (193) under conditions that induced DosR (hypoxia, NO, CO), serves to induce nitrogen assimilation and respiration under hypoxic conditions (93,192). The excess, potentially toxic nitrite generated by NarGHJI is either extruded

or further reduced to ammonium by the NirBD nitrite reductase (NiR) (108,109,192). *Msm* also encodes a constitutively expressed NarGHJI respiratory NR, however, unlike *Mtb,* it was shown to be non-functional for assimilation of nitrogen from nitrate (108,122,194). Instead, *Msm* relies on an unusual NADPH-dependent, diflavin-containing NR called NasN which is essential for nitrate utilization in aerobic conditions (121,194) as well as a NirBD ortholog to catalyze reduction of nitrite (169,195). Each of these components – *narGHJI, nirBD,* and *nasN* – along with a putative NarK nitrate/nitrite antiporter (MSMEG_0433) represent distinct operons or transcripts (119,120). In contrast to *Mtb* and *Msm, Mab* does not encode a respiratory NarGHJI suggesting an inability to utilize nitrate as an alternative electron acceptor in low oxygen conditions. However, the *Mab* genome does include orthologs of other key components of nitrate/nitrite metabolism, including *narK3* (*Mab_3523c*), *nirBD* (*Mab_3522c-3521c*), *nnaR* (transcriptional regulator *Mab_3520c*) and *sirB* (siroheme ferrochetalase *Mab_3519c*). These five genes are arranged as a predicted operon that we found to be dramatically repressed in response to hypoxia in a DosR-independent manner (114). Missing from this locus was a candidate NasN-type assimilatory NR. As detailed herein, we have identified a putative NasN ortholog (*Mab_2438)* that was co-regulated with the *narK3-sirB* operon (*Mab_3523c-3519c)* we predict catalyzes the reduction of nitrate to nitrite.

Both *Mycobacteria* and related *Streptomyces* rely upon an intricate network of regulators including two-component systems (TCS), serine-threonine protein kinases (STPKs), and orphan response regulators (ORR) to coordinate the integration of multiple cues to control nitrogen metabolism. GlnR, an ORR that can be activated by phosphorylation of Ser/Thr residues (196,197), is known as the master regulator of nitrogen metabolism in actinobacteria such as *Mycobacteria* and *Streptomyces*. (116,120,198). *Mtb* GlnR is required for growth on nitrate and nitrite when these are the only nitrogen sources available and was shown to be a positive regulator of *nirBD* (122). Additionally, GlnR has been shown to crosstalk with the response regulators PhoP and MtrA which

act as repressors of nitrogen metabolism through competition with GlnR for binding sites under nitrogen replete conditions (195,199-201). As discussed in more detail below, an additional ORR, NnaR, with an unusual domain structure comprised of a HemD (uroporphyrinogen-III synthase) domain fused to a DNA-binding domain, is also implicated in nitrate and nitrite assimilation (116). Despite extensive studies examining *Mtb* and *Msm* transcriptional regulation of nitrogen metabolism and nitrate/nitrite assimilation, this remains a significant knowledge gap for *Mab* (62,115,122,202). Recently, the GlnR ortholog in *Mab* was shown to regulate *narK3, nirBD*, *glnA* (glutamine synthetase), and *amt* (ammonium transporter) although a role in the regulation of *Mab nasN* was not reported (62). The inactivation of GlnR in *Mab* led to an inability to form biofilms resulting in drug susceptibility dependent upon glutamine and glutamate availability (62). The role of other transcription factors in the regulation of nitrogen metabolism in *Mab* remains to be investigated. Notably, there have been no reports of the identification of a NnaR ortholog or its role in the use of nitrate/nitrite as nitrogen sources or detoxification of nitrite.

NnaR was first identified in *Streptomyces coelicolor* (*S. coelicolor*) as a GlnR target and co-activator with GlnR of nitrite reductase (*nirB*), nitrate transporter (*narK*) and nitrate reductase (*nasA*) (116). In the absence of NnaR, *S. coelicolor* displayed diminished capacity to reduce nitrite to ammonium resulting in a growth defect when nitrate or nitrite were used as sole nitrogen sources. However, nitrate was reduced to nitrite suggesting $NnaR_{Sc}$ is not a regulator of nitrate reductase (116). Similar to *S. coelicolor*, *Msm* NnaR regulates key nitrogen assimilation genes and is required for use of nitrate and nitrite as sole nitrogen sources (119). Subsequent research by Tan et al., determined $GlnR_{Msm}$ is responsible for regulation of the assimilatory nitrate reductase NasN, confirming regulation of nitrate assimilation in *Msm* involves both GlnR (nitrate>nitrite) and NnaR (nitrite > ammonium) (121). The distinct roles for these two transcription factors in regulating different steps of nitrate assimilation were affirmed by EMSA data showing binding of NnaR to the

nirBD promoter and GlnR binding upstream of *nasN* (119,121). An ortholog of NnaR is also encoded by *Mtb* (Rv0260c), but little is known about it beyond its induction by multiple stress conditions including hypoxia, nutrient starvation, acid pH, and stationary phase (149). The regulon and physiological role of *Mab* NnaR remains unknown, highlighting the need for further investigation of NnaR-mediated transcriptional regulation.

The goal of this study is to elucidate the previously unexplored role of *Mab* NnaR in gene regulation and nitrogen metabolism. We generated a *Mab nnaR* knockout strain ($Mab_{\Delta nnaR}$) and complement strain ($Mab_{\Delta nnaR+C}$) to further study NnaR and its function. Our work revealed that *Mab* NnaR regulates the *nark3-nirBD-nnaR-sirB* operon and *nasN* in a species-specific manner enabling nitrate and nitrite utilization. qRT-PCR analyses demonstrated that both loci were highly upregulated when nitrate or nitrite were the sole nitrogen sources, and with the exception of *sirB*, this gene induction was dependent on NnaR. The unexpected induction of *sirB* upon deletion of *nnaR,* which was restored to baseline levels in the complemented strain, suggests additional layers of regulation on this component of the operon. The inability of $Mab_{\Delta nnaR}$ to regulate nitrogen assimilation genes resulted in growth defects when nitrate, and to a lesser degree nitrite, were used as the sole nitrogen source. This study highlights novel species-specific aspects of nitrogen metabolism in *Mab* and the critical role of NnaR and its downstream regulon in nitrate/nitrite utilization and detoxification. These findings support the hypothesis that NnaR is important for host adaptation and *Mab* pathogenesis.

Methods

Plasmid And Mycobacterium Abscessus Strain Construction

Mab$_{\Delta nnaR}$ was engineered via recombineering as described by van Kessell and Hatfull in the strain *Mab* 390S obtained from the Thomas Byrd lab (41,203). In brief, an allelic exchange substrate (AES) was generated containing an apramycin resistance cassette flanked by ~600 nucleotides upstream and downstream of the *nnaR* gene (*MAB_3520c*) for homologous recombination. To construct the AES, the *nnaR* gene plus ~600 nucleotides upstream and downstream were PCR amplified and cloned into pCRBluntII-TOPO 170 vector (Thermo Fisher) followed by round-the-horn PCR to remove the *nnaR* gene retaining nucleotide overlap from genes upstream and downstream of *nnaR* (141). After removal of *nnaR* a phosphorylated apramycin resistance cassette was ligated between the upstream and downstream flanking regions. PCR amplification was then used to generate the AES consisting of the apramycin cassette flanked by upstream and downstream nucleotides. Mab::pJV53 competent cells induced with .02% acetamide for 4 hours were electroporated with 100 ng AES, recovered in 7H9 OADC media for 24 hours, and plated on 7H10 agar supplemented with apramycin 50 µg/ml. Complement strain, *Mab*$_{\Delta nnaR+C}$ containing *nnaR* and *sirB* inserted downstream of the constitutive hsp60 promoter (P_{hsp60}) in the episomal vector pVV16 was engineered using round the horn PCR of the vector (141) and blunt ligation of the phosphorylated insert (204). The *sirB* gene downstream of *nnaR* was included due to anticipated polar effects of inactivation of *nnaR.* This construct was introduced by electroporation into *Mab*$_{\Delta nnaR}$, followed by recovery in 7H9 OADC media for 24 hours and plating on 7H10 agar supplemented with kanamycin 50 µg/ml.

Mycobacterial Protein Fragment Complementation (M-PFC) constructs were generated in the background plasmids pUAB100, pUAB200, and pUAB400 (142) using round the horn cloning and ligation. *Mycobacterium smegmatis* competent cells were electroporated with 100ng of each pUAB100:*dosS*/pUAB400:*dosR*, pUAB100:*dosS*/pUAB200:*nnaR* or pUAB100:*dosS*/pUAB400:*nnaR* at the same time and recovered LB broth for 4 hours before plating on LB Agar supplemented with hygromycin B 50 µg/ml and kanamycin 50 µg/ml. Primers, strains and plasmids used in this study are listed in Table 8 & 9 in the appendix.

Bacterial Growth Conditions And Nitrogen Supplementation

Mab cultures were grown in 7H9 OADC+.05% tyloxapol from glycerol stocks and incubated at 37°C while shaking at 100 rpm. Growth kinetic studies under nitrogen limitation were carried out in Sauton's nitrogen free minimal media (0.05% KH_2PO_4, 0.05% $MgSO_4$, 0.2% citric acid, .005% ferric citrate, 0.2% glycerol, 0.0001% $ZnSO_4$, 0.015% tyloxapol) supplemented with 2.5 mM sodium nitrate, 0.5 mM sodium nitrite or 2.5 mM ammonium sulfate as previously described (119,120). Briefly, cultures were grown to mid-log phase in 7H9 OADC+.05% tyloxapol, washed twice with Sauton's minimal media, and then diluted to 0.2 OD followed by nitrogen supplementation. On days 0-5 cultures were serially diluted and spot plated on LB Agar for CFU enumeration.

RNA Extraction And QRT-PCR And Operon Validation

RNA was extracted as described by Rohde et., al (144) in triplicate from cultures grown in 7H9 OADC+.05% tyloxapol or Sauton's nitrogen free minimal media supplemented with nitrogen sources. Cultures were pelleted at 4300 rpm for 10 minutes, resuspended in guanidine thiocyanate buffer, pelleted again at 12,000 rpm for 5 min, and stored at -80º C until processing.

Thawed pellets were resuspended in 65º C Trizol then lysed using 0.1mM silicon beads in a BeadBeater at max speed for 1 minute 2x followed by cooling on ice for 1 minute between bead beating. Isolation of total RNA from Trizol lysates was performed using chloroform extraction and Qiagen RNeasy column purification. Total RNA was treated with Turbo DNase (Invitrogen) to eliminate DNA contamination. 50 ng/µl of total RNA was used to generate cDNA using iScriptTM cDNA synthesis kit (Bio-Rad) for qRT-PCR and RT-PCR. qRT-PCR reactions were carried out in a QuantStudio7 thermocycler using SYBR green as readout. Primers used for qRT-PCR are listed in Table 10 in the appendix. To confirm whether genes in the putative *nark3-sirB* operon were transcribed as a single transcript, 400ng cDNA generated from RNA as described above was PCR amplified using primers that went across gene junctions (primers are listed in Table 9) and analyzed by agarose gel electrophoresis.

Mycobacterial Protein Fragment Complementation Assays (M-PFC)

Mycobacterium smegmatis containing M-PFC constructs grown to mid-log phase in LB + 0.05% Tween 80 supplemented with hygromycin B 50 µg/ml and kanamycin 50 µg/ml were then diluted to 0.0005 OD in same media. Cultures were then incubated in a 96-well plate for 48 hours with 2-fold serial dilutions of trimethoprim ranging from 200-3.125 µg/ml. After 48 hours, 0.01% resazurin was added to wells and left to incubate for 4 hours. Data was collected using a Synergy 4 plate reader with fluorescence set to 530 nm excitation and 590 nm emission (142).

Nitrogen Utilization Assay

The ability for Mab to utilize nitrite was analyzed via colorimetric Griess reagent assay as described by Yang et., with minor modifications (206). On days 2 and 4, 50 µl of supernatant was added to a 96 well plate with 100 µl Griess Reagent (Thermo Fisher Scientific # 328670500)

consisting of 1% sulphanillic acid in 5% phosphoric acid and .1% naphthylethylenediamine dihydrochloride. After plate was incubated at 37º C for 10 minutes absorbance was read at 535 nm on a Synergy 4 Plate reader. A standard curve with known nitrite concentrations was used to calculate concentrations of nitrite in supernatant.

Results

Identification And Bioinformatic Analysis Of Mab Orphan Response Regulator NnaR

Our previous study investigating *Mab* transcriptional modulation during hypoxic adaptation revealed dramatic down-regulation of a gene locus containing an uncharacterized transcriptional regulator (*MAB_3520c*) that appeared to be an orphan response regulator (ORR) downstream of nitrogen assimilation genes (*MAB_3523c*, *MAB_3522c*, *MAB_3521C*) (114). The down-regulation of these genes in response to hypoxia contrasts with reported transcriptional adaptations of *Mtb* hypoxia (99,107,108) prompting our interest in the role of this ORR and nitrogen assimilation in *Mab*. Bioinformatic analysis of *MAB_3520c* using UniProt and Alphafold structural modeling revealed a C-terminal OmpR/PhoB-type winged helix DNA binding domain commonly found in response regulators of two-component systems (Figure. 13A). However, lack of an adjacent histidine kinase gene and an unusual N terminal domain containing a HemD domain rather than a receiver domain with aspartate phosphorylation sites indicates a unique ORR (Fig. 13A). This atypical ORR is orthologous to the NnaR response regulator of *S. coelicolor*, *Msm* and *Mtb* with 58%, 55%, and 54% sequence identity, respectively. Alignments between these organisms display homology between the C-terminal DNA binding domain of helix 3 and the unique HemD domain residues (Figure 13B). Due to homology within the DNA binding domain between organisms and published data documenting *S. coelicolor, Msm,* and *Mtb* NnaR binding motifs we were able to justify using these orthologous motifs to identify *Mab* NnaR promoter binding sites (116,119).

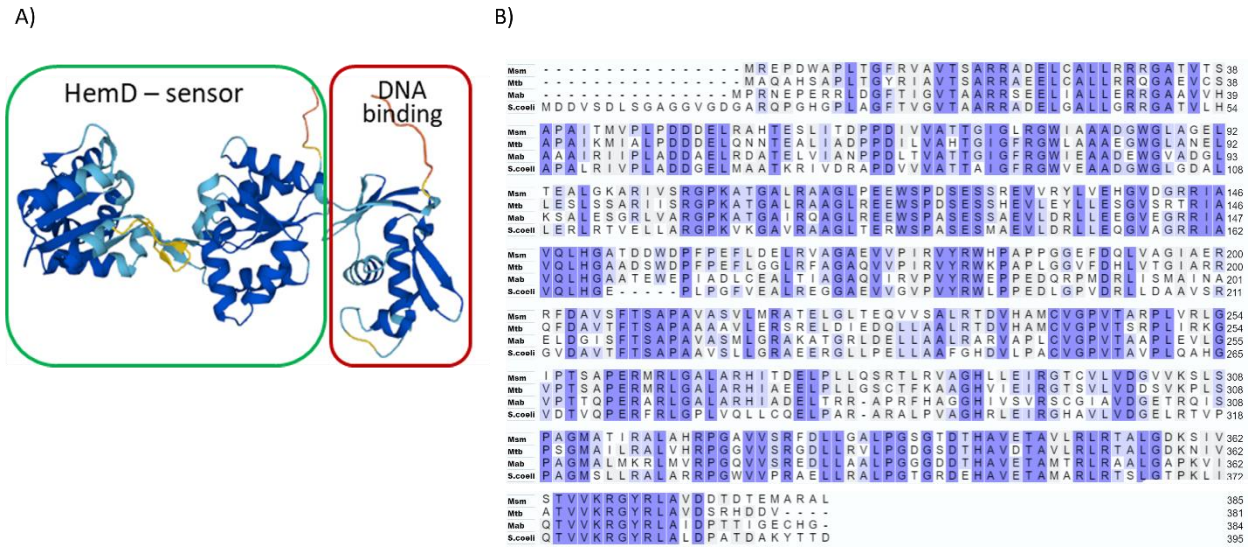

Figure 13: Bioinformatic analysis of NnaR domain structure and sequence alignment

Uniprot Bioanalysis Online Tool was used to generate the **A)** Alpha-fold model of 3-D structure of Mab NnaR HemD-ORR protein. and B) sequence alignment of *Mab nnaR* (*MAB_3520c*) compared to *Msm nnaR* (*MSMEG_0432*), *Mtb* (*Rv0260c*) and *S. coelicolor nnaR* (SCO2958). Sequences for *Mab*, *Msm* and *Mtb* were obtained from the online data base Mycobrowser. *S. coelicolor* sequence was obtained from the online KEGG data base.

The Genomic And Transcriptional Organization Of The NnaR Regulon In Mab

Initially, we sought to leverage previously published NnaR binding sites from *S. coelicolor* to define a putative NnaR regulon in *Mab* via *in silico* analysis of the *Mab* ATCC_19977 genome using the DNA Pattern Find Tool (116). Using either the motif (CTCAC[A/C][Cg]..$_{[13\text{-}16bp]}$..GTGAG[CG][GA] based on predicted *S. coelicolor* and *Mtb* promoters or (CTCAC[A/C]..$_{16bp}$..[T/GGTGAG) reported by Antczak *et al.* for *Msm* (119), only two predicted binding sites for *Mab* NnaR were identified. These NnaR promoters were positioned 63 bp and 66 bp upstream of the translational start sites of *narK3* and *MAB_2438*, respectively. *MAB_2438* encodes a previously uncharacterized protein annotated as a possible oxidoreductase (Figure 15A). Subsequent bioinformatic analysis of *MAB_2438* revealed 61% identity (71% similarity) with the recently described NADPH-dependent assimilatory NR *Msm* NasN encoded by *MSMEG_4206*, which had been erroneously annotated as a pseudogene due to an unconfirmed frame-shift mutation (121). Based on this observation, we will refer to the product of *MAB_2438* as NasN, which we noted was significantly shorter than its ortholog in *Msm* (MSMEG_4206 = 1351aa, *MAB_2438* =1257aa). Primary amino acid sequence alignments of the two NasN orthologs (Figure 14) revealed two reasons for this difference: 1) *MSMEG_4206* contains a ~75aa longer linker between the N-terminal nitrate reduction catalytic domain and C-terminal diflavin reductase domain (121), and 2) the annotated start codon for *MAB_2438* is incorrect. We predict that NasN$_{Mab}$ contains an additional 25 aa on the N-terminus based on homology with NasN$_{Msm}$ and the presence of a critical [4Fe-4S] binding site. NnaR-mediated regulation of nitrate assimilation would be unique to *Mab* given the absence of NnaR binding sites upstream of *Msm nasN* as previously mentioned (121). We next sought to verify whether genes *nark3-nirBD-nnaR-sirB* are co-transcribed as an operon via RT-PCR using intergenic primers amplifying the 3' end of one gene and the 5' end of the next gene (Figure. 15B). Amplification of junctions between

nark3-nirB, *nirB-nirD*, *nirD-nnaR* and *nnar-sirB* all yielded the expected bands in the DNA (positive control) and cDNA lanes, with no bands present in the RNA (no RT negative controls) lanes (Figure. 15B). This data confirms that the five-gene *narK3-sirB* locus positioned downstream of a predicted NnaR binding site is expressed as a single mRNA transcript. This represents a species-specific organization of genes involved in nitrate/nitrite assimilation, compared to *Mtb* or *Msm* in which these genes are not arranged in a single operon (Figure 15A & 16).

We next investigated transcription of the *nark3-sirB* operon and *nasN* in the presence of nitrate or nitrite as sole nitrogen sources via qRT-PCR (Figure 15C&D). *Mab390S* cultures were supplemented with either 2.5 mM ammonium sulfate (AS) (control), 2.5mM of sodium nitrate, or 0.5 mM of sodium nitrite in Sauton's minimal media for 4 hours prior to RNA extraction. Sodium nitrite was used at a lower concentration due to toxicity at concentrations equivalent to AS and sodium nitrate (Figure. 17A-C). qRT-PCR confirmed a 1-2 log induction of all genes within the *nark3-sirB* operon and *nasN* in the presence of nitrate (Figure 15C) and nitrite (Figure 15D) compared to the AS control, which bypasses the first two-steps of nitrate assimilation. These studies demonstrated the coordinated induction of the predicted NnaR regulon, including the *nark3-sirB* operon as well as *nasN*, specifically when nitrate or nitrite (but not ammonium sulfate) are utilized as sole nitrogen sources.

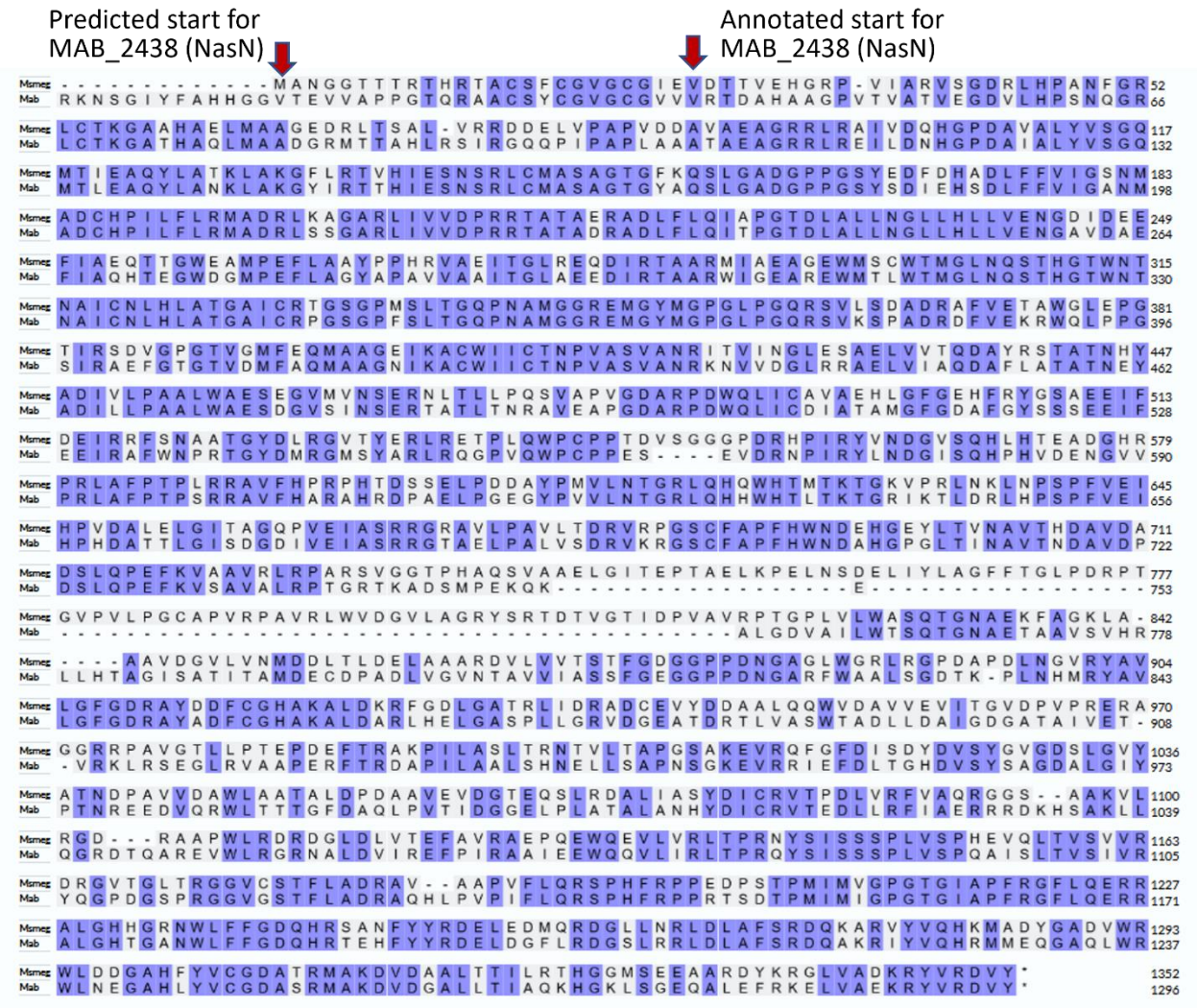

Figure 14: NasN sequence alignment

Uniprot sequence amino acid sequence alignment of NasN orthologs MSMEG_4206 and MAB_2438

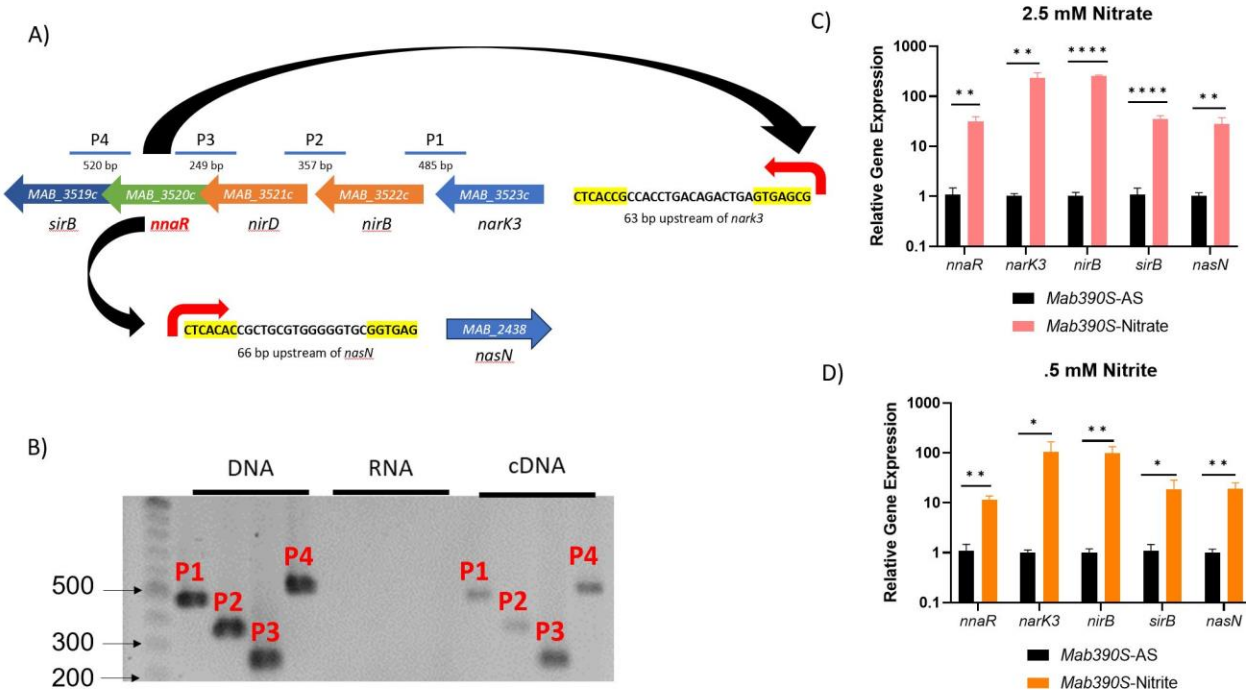

Figure 15: The nnaR regulon is induced when nitrate or nitrite are the sole sources of nitrogen

A) Schematic depicting nitrogen assimilation gene arrangement and nnaR binding sites discovered using DNA Pattern Find. Yellow highlighted nucleotides coincide with motifs used to find promoter region. **B)** RT-PCR and agarose gel analysis of operon structure of *MAB_3523c-3519c*, demonstrating transcriptional linkage. DNA and RNA (no RT) controls were included to affirm amplicons derived from mRNA. P1-P4 refers to schematic for intergenic amplicon within the operon as shown in panel A. qRT-PCR was performed to evaluate induction of nnaR regulon when nitrate **C)** or nitrite **D)** is the sole source nitrogen. *Mab*390S supplemented with 2.5 mM ammonium sulfate (AS) (black bars), 2.5 mM nitrate (pink bars) and .5mM nitrite (orange bars). Transcript levels in WT *Mab390S* in AS were normalized to 1 and serve as reference for relative gene expression ratios. qRT-PCR data is representative of 3 experiments performed in duplicate. P values were calculated via t-test using GraphPad. *P-value <.05, **P-value <.01 ****P-value <.0001.

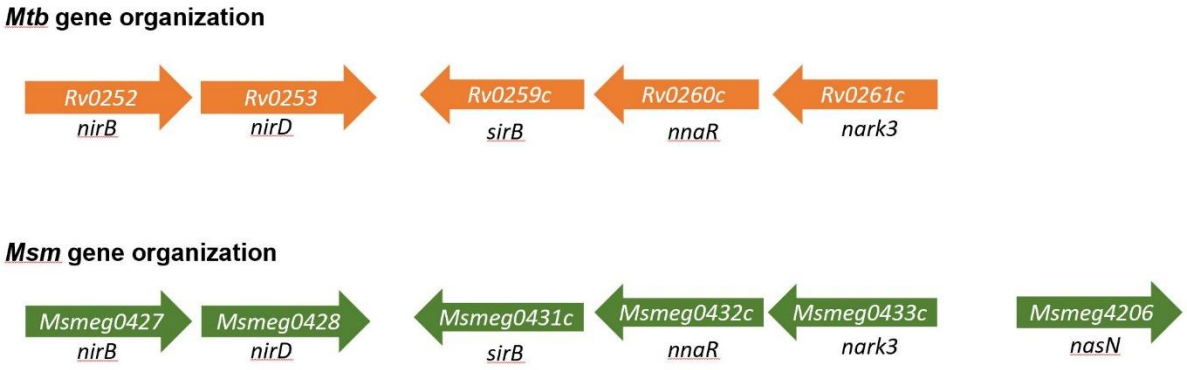

Figure 16: Nitrate assimilation gene organization in Mtb and Msm

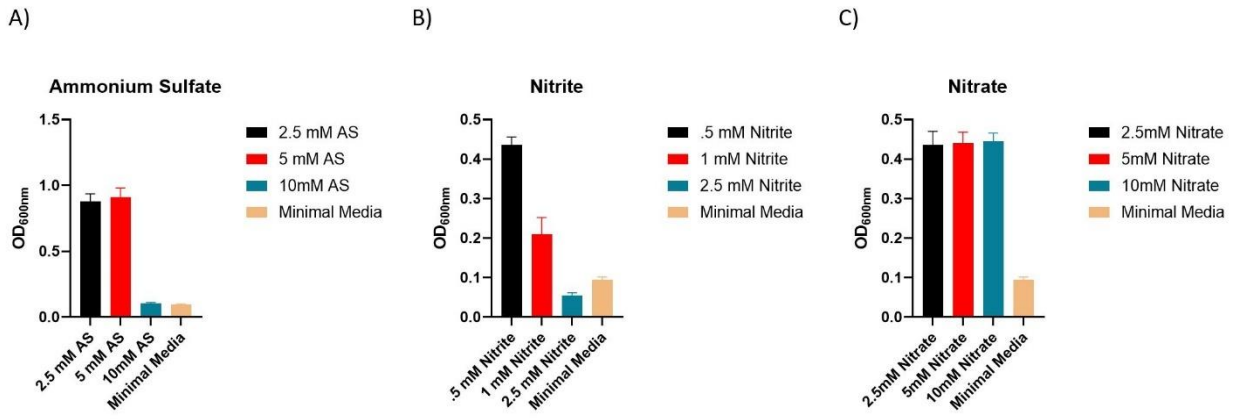

Figure 17: Growth analysis of Mab390S at different concentrations of inorganic nitrogen sources.

Growth kinetics were measured by OD_{600nm} on day 4 of growth in minimal media supplemented with **A)** 2.5 mM, 5 mM, and 10 mM ammonium sulfate **B)** .5 mM, 1 mM, 2.5 mM sodium nitrite **C)** 2.5 mM, 5 mM, and 10 mM sodium nitrate.

NnaR-Dependent Expression Of The NarK3-SirB Operon And NasN

To further investigate the role of NnaR, a *Mab nnaR* knockout strain (*Mab*$_{\Delta nnaR}$) was generated via recombineering (139). Anticipating polar effects, a corresponding complement strain (*Mab*$_{\Delta nnaR+C}$) containing both *nnaR* and *sirB* constitutively expressed from the *hsp60* promoter in the episomal vector pVV16 was constructed (203,204). qRT-PCR was used to confirm the knockout and complement via expression levels of *nnaR* and the effect on genes within the predicted *nnaR* regulon (Figure 18A). Data from log-phase cultures in 7H9 media confirmed *nnaR* transcripts were not detectable in *Mab*$_{\Delta nnaR}$ with restoration to WT levels in *Mab*$_{\Delta nnaR+C}$. Consistent with the predicted role for NnaR as an activator of its own operon plus *nasN,* we expected loss of NnaR to lead to downregulation of its regulon. Surprisingly, gene expression levels for *narK3*, *nirBD and nasN* in all three strains grown in 7H9 media were unaltered in the absence of NnaR, despite the presence of a NnaR binding site upstream *nark3* and *nasN*. Closer analysis of qRT-PCR raw data showed high C_t values for all genes, indicating minimal expression of these genes under nitrogen replete conditions. This observation is consistent with *Msm* NnaR studies which found no difference in the expression levels of *narK* and *nirB* in the absence of NnaR when grown in nitrogen replete media (119). In contrast to WT levels of *nark3*, *nirB* and *nasN*, *sirB* exhibited significant ~3-log up-regulation in the *nnaR* mutant strain, which was restored to WT levels in the complement strain. Thus, our data indicate that the basal expression of *nnaR* and associated nitrate/nitrite assimilation genes is low in WT *Mab* under nitrogen replete conditions such that the absence of NnaR had little effect on gene expression. The unusual expression pattern of *sirB*, which appears to be cotranscribed with the *narK3-sirB* operon but suppressed by NnaR, points to the possibility of additional internal promoters and/or additional layers of regulation acting on *sirB*.

Since the absence of NnaR had no effect on gene expression levels in nitrogen rich media, we evaluated gene expression between *Mab390S* and $Mab_{\Delta nnaR}$ under inducing conditions with nitrate or nitrite as the sole nitrogen sources. Briefly, cultures were incubated in minimal media supplemented with 2.5 mM AS, 2.5 mM sodium nitrate or 0.5 mM sodium nitrite for 4hr prior to RNA isolation and qRT-PCR analysis. During growth on defined inorganic nitrogen sources, the absence of NnaR resulted in a significant down-regulation (≥ 1 log) or lack of induction of *nark3*, *nirB* and *nasN,* with restoration to wild-type levels in $Mab_{\Delta nnaR+C}$ (Figure 18B&C). Consistent with our observations in 7H9 media, *sirB* transcript levels in $Mab_{\Delta nnaR}$ remained elevated in nitrate or nitrite supplemented cultures, with restoration to WT levels in $Mab_{\Delta nnaR+C}$. As noted above, this lack of correlation between the transcription profiles of *sirB* and upstream genes appears inconsistent with their co-transcription as part of an operon. Decreased transcription of *nark3*, *nirBD*, and *nasN* in the mutant strain under inducing conditions affirms that NnaR mediates upregulation of its regulon in response to nitrate and nitrite. Induction of a putative assimilatory nitrate reductase *nasN* represents a species-specific role for $NnaR_{Mab}$ since $NnaR_{Msm}$ does not appear to regulate *nasN* (121). This data provides the first insights regarding regulation of nitrogen assimilation for *Mab* outside of what has been previously published for GlnR (62).

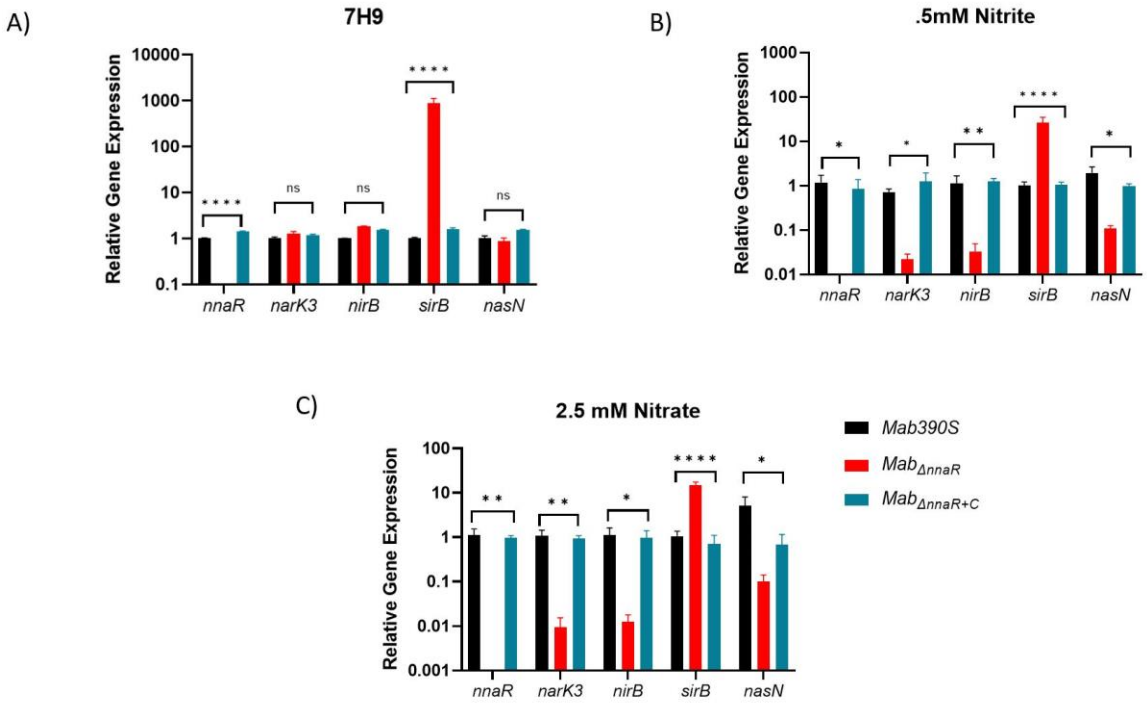

Figure 18: NnaR-dependent expression of the nark3-sirB operon and nasN

qRT-PCR was performed to confirm the deletion and restoration of *nnaR* in $Mab_{\Delta nnaR}$ and $Mab_{\Delta nnaR+C}$, respectively, and effect of *nnaR* inactivation on predicted regulon in 7H9 media (**A)**, or minimal media supplemented with nitrite (**B)** or nitrate **(C).** *Mab 390S* (black), $Mab_{\Delta nnaR}$ (red) and $Mab_{\Delta nnaR+C}$ (blue). Relative gene expression is compared to *Mab390S* in 7H9 media in panel A, or *Mab390S* with nitrite (Panel B) or nitrate (Panel C). Data is representative of 3 experiments performed in duplicate. *P* values were calculated via one -way ANOVA using GraphPad. Red stars indicate C_t values were not detected for *Mab dosR* nor *dosS* in the mutant strain. **P*-value <.05, ***P*-value <.01 *****P*-value <.0001.

NnaR Is Required For Survival On Nitrate Or Nitrite

Based on our data revealing NnaR-dependent upregulation of genes linked to nitrogen metabolism, we next investigated whether the absence of NnaR affects growth when nitrate or nitrite are the sole sources of nitrogen. Cultures of *Mab390S*, $Mab_{\Delta nnaR}$, $Mab_{\Delta nnaR+C}$ were grown in minimal media or minimal media supplemented with 2.5mM AS, 2.5 mM sodium nitrate or 0.5mM sodium nitrite, with CFUs enumerated daily through day 4 (Figure 19A-C). The slight initial increase in CFU of *Mab390S* cultures supplemented with AS which was sustained until day 4, in contrast to the ~4-log decline in CFU observed in minimal media alone (Figure 19A), affirms that *Mab* can utilize AS as a sole nitrogen source. Notably, the growth of $Mab_{\Delta nnaR}$ in AS was indistinguishable from WT (Fig 19A) indicating that NnaR is not required when the first two-steps of nitrate assimilation (nitrate>nitrite>ammonium) are bypassed by providing ammonium as the sole nitrogen source (194). When supplemented with nitrate or nitrite, on the other hand, the WT and complement either maintained a steady number of CFU (nitrate) or decreased slightly (nitrite) (Figure 19B & C). We suspect the slight decline in CFU for nitrite supplemented cultures of strains expressing NnaR is due to nitrite toxicity resulting in growth inhibition, a phenomenon also observed in *Mtb* (55). As predicted, the survival of $Mab_{\Delta nnaR}$ was severely impaired when nitrate was the only nitrogen source, with a final CFU difference of ~3 logs on day 4 (Figure. 19B). This verified the importance of NnaR in nitrate assimilation. The dramatic $Mab_{\Delta nnaR}$ phenotype observed on day 4 with nitrate supplementation (Figure 19B) was less pronounced with nitrite supplementation (Figure 19C). However, a log difference was observed on day 2 and 3 when comparing $Mab_{\Delta nnaR}$ to WT and complement with nitrite as the sole nitrogen source (Figure 19C). Due to decreased CFU from day 3 to day 4 in WT and complement in nitrite and a plateau in growth of $Mab_{\Delta nnaR}$ during the same period, there was only a difference of 0.5 log in CFU by the end of the assay (Figure 19C). Although the reason why loss of NnaR had a less deleterious effect

on growth/survival of *Mab*$_{\Delta nnaR}$ on nitrite versus nitrate is unclear, it is evident that NnaR plays a critical role in nitrogen assimilation and/or nitrite detoxication when nitrite is the sole nitrogen source available. To biochemically validate the role of NnaR in nitrite utilization, we compared the ability of WT, *Mab*$_{\Delta nnaR}$, and *Mab*$_{\Delta nnaR+C}$ to use nitrite as a nitrogen source via Griess assay. Briefly, nitrite concentrations in supernatants taken from the growth kinetic study were measured on day 2 and day 4 to gauge nitrite utilization by *Mab* strains. Nitrite concentrations in the supernatant of *Mab*$_{\Delta nnaR}$ were significantly higher than WT and complement at both day 2 and 4 (Figure. 19D), affirming a reduction in the ability to metabolize nitrite in the absence of NnaR.

In summary, we have identified an orphan response regulator designated NnaR based on homology with recently characterized ortholog in *Msm*, its unusual domain structure (fusion of HemD domain with DNA binding domain), and critical role in Nitrate/Nitrite Assimilation Regulation (NnaR). It is encoded in a species-specific operon that is downregulated by hypoxia (123) but highly induced by inorganic nitrogen sources, specifically nitrate and nitrite. Our data indicated that NnaR$_{Mab}$ activates transcription of a six gene regulon responsible for reduction of nitrate to nitrite (NasN) and nitrite to ammonia (NirBD), transport of nitrate and/or nitrite (NarK3), and synthesis of the siroheme cofactor for nitrite reductase. Finally, NnaR is required for the utilization of nitrate and nitrite as sole nitrogen sources and detoxification of nitrite, suggesting an important role for this transcription factor in *Mab* host adaptation and pathogenesis.

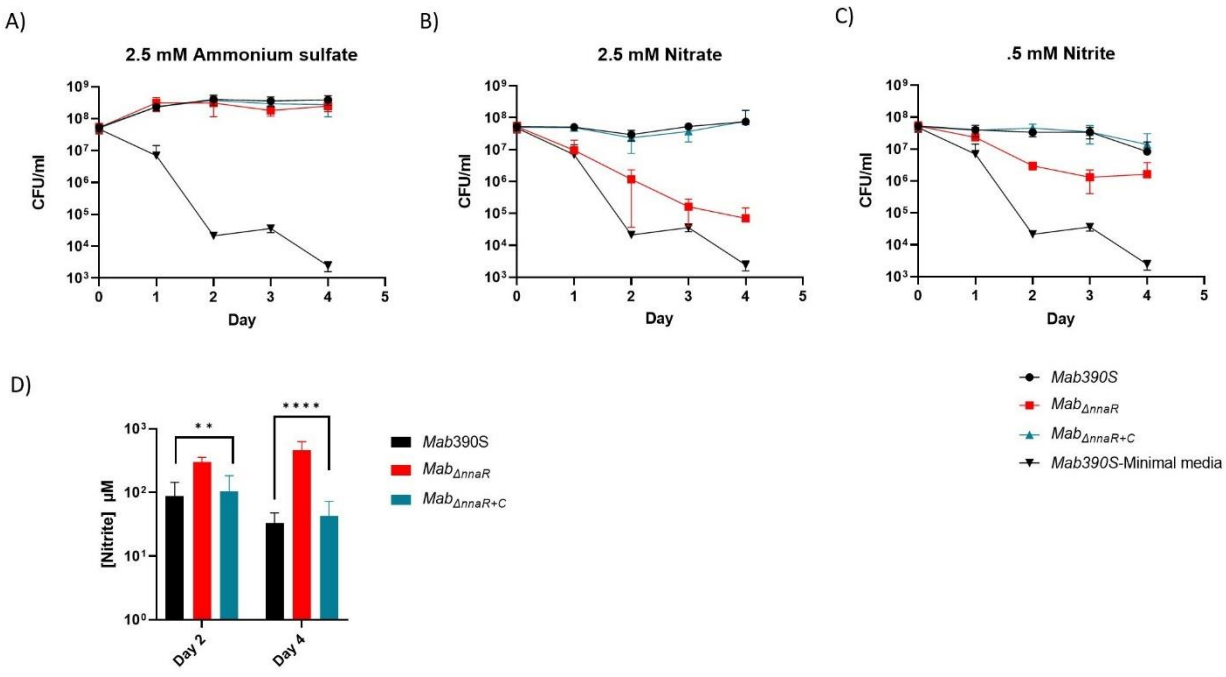

Figure 19: nnaR is responsible for nitrite utilization and growth when nitrate and nitrite are sole sources of nitrogen

Growth kinetics **(A-C)** in minimal media supplemented with various nitrogen sources was assessed *via* serial dilutions, spot plating and enumeration of CFU/ml on days 0-4. Growth kinetics supplemented with **(A)** ammonium sulfate, **(B)** nitrite or **(C)** nitrate. Griess assay **(D)** was performed to measure nitrite utilization on day 2 and 4. *Mab 390S* (black), *Mab$_{\Delta nnaR}$* (red) and *Mab$_{\Delta nnaR+C}$* (blue). Data reflects 3 independent experiments performed in triplicate.

NnaR and DosS Do Not Display Interaction In An M-PFC Assay

Signaling mechanisms activating *Mab* NnaR are currently unknown and no known signaling mechanisms have been identified for *S. coelicolor* or *Msm* NnaR. However, *Mtb* NnaR (*Rv0260c*) was identified in an M-PFC-based screen for proteins that interact with Mtb DosS, although this interaction has not been validated by alternative methods nor is the role of this putative interaction known (207). To test whether an interaction between *Mab* NnaR and *Mab* DosS exists we engineered M-PFC constructs as previously described by Singh *et al*., (142). The positive control for M-PFC, $GCN4_{(F1,2)}$:$GCN4_{(F3)}$ displayed growth in TRIM at all concentrations whereas the negative control (empty vector) did not display growth at any concentration validating the M-PFC Alamar Blue Assay (Figure 20). $DosS_{(F1,2)}$ was confirmed to be functional as the strains harboring $DosS_{(F1,2)}$:$DosR_{(F3)}$ displayed interactions via growth in TRIM at low concentrations (Figure 20). To account for possible inhibition of binding caused by the location of $mDHFR_{(F3)}$ domain, NnaR was fused to either the N terminus or the C terminus. Strains harboring $DosS_{(F1,2)}$:$NnaR_{(F3)}$ were not able to grow in the presence of TRIM even at the lowest concentration (Figure 20). Based on these data it appears that, unlike *Mtb*, the *Mab* NnaR ortholog does not interact directly with the DosS sensor kinase.

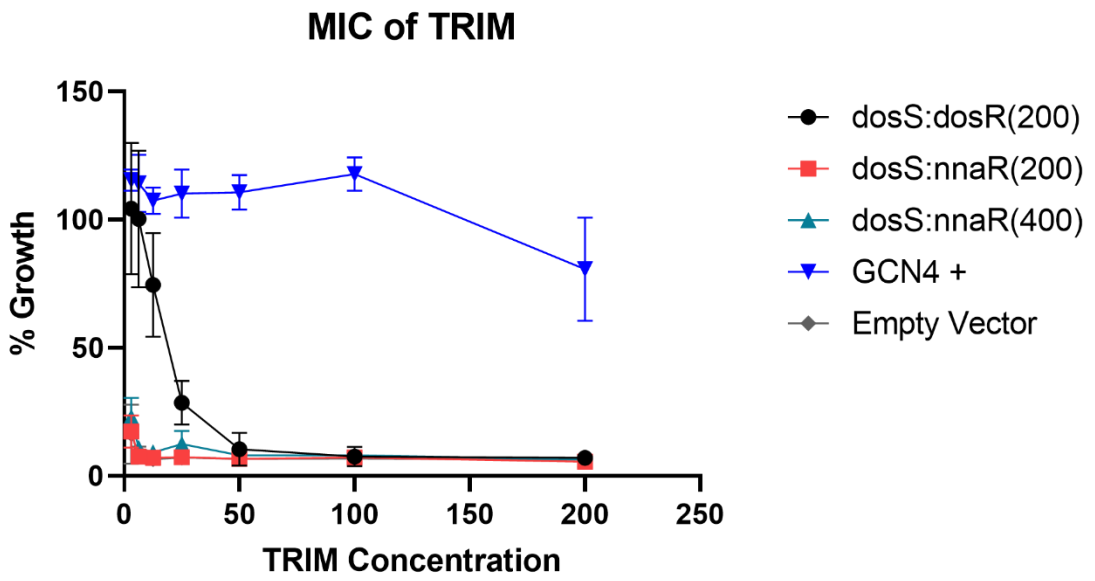

Figure 20: M-PFC assay displays lack of interaction between NnaR and DosS

Minimum inhibitory concentration of trimethoprim (TRIM) was analyzed to measure interaction of $DHFR_{1,2}$ and $DHFR_3$. **Black circle)** pUAB100-*dosS*-($DHFR_{1,2}$ on C-term):pUAB200-*dosR*-($DHFR_3$ on C-term) **Red square)** pUAB100-*dosS*-($DHFR_{1,2}$ on C-term):pUAB200-*nnaR*-($DHFR_3$ on C-term) **Turquoise triangle)** pUAB100-*dosS*-($DHFR_{1,2}$ on C-term):pUAB400-*nnaR*-($DHFR_3$ on N-term) **Blue triangle)** pUAB300-GCN4-($DHFR_{1,2}$ on C-term):pUAB400-GCN4-($DHFR_3$ on N-term) **Gray Diamond**) empty vector

Discussion

Mab persistence within the hostile niches of macrophage phagosomes, granulomas, and mucus-laden CF lung requires intricate gene regulation to combat low oxygen tension, reactive nitrogen intermediates (RNI), nutrient depletion, and exposure to excess nitrate and nitrite. Given the capacity of *Mtb* to adapt to similar niches and presence of many orthologous virulence factors and transcriptional regulators, it is tempting to extrapolate from available *Mtb* data to understand *Mab* gene regulation and function. However, emerging data from our lab and others highlights significant species-specific differences in transcriptional regulatory networks and strategies of adapting to *in vivo* conditions that urge caution when doing this. Unique strategies of *Mab* host adaptation and persistence stem from its distinct repertoire of genes compared to *Mtb* (112), variable genomic arrangements of the same genes, as well as shared orthologous transcription factors that control species-specific regulons (61,84,111,123).

In *Mtb*, the overlap and integration of genes involved in adaptation to hypoxia and nitrate metabolism, not only as a means of alternative respiration but also to defend against host generated RNI, are well-documented (107,109,122,149,169). On the other hand, relatively little is known about mechanisms used by *Mab* to coordinate responses to these two intertwined host cues. Our interest in nitrate assimilation in *Mab* and the interplay with hypoxia was sparked by our recent observation that genes implicated in nitrate assimilation are downregulated under hypoxic conditions (123). These data contrast with the response of *Mtb* to hypoxia, including upregulation of *narK2* and *nirBD* (107,109,122,169), which facilitates utilization of nitrate as a terminal electron acceptor via reduction by the constitutively expressed *narGHIJ,* which acts as both a respiratory and assimilatory nitrate reductase (NR) (108,109,122). The resulting nitrite produced by NR could then be extruded by the putative nitrite transporter NarK2 to avoid toxicity

or be further reduced to ammonium via the nitrite reductase *nirBD* under nitrogen-limited conditions (109,122). This strategy is not an option for *Mab,* due to the conspicuous lack of a NarGHJI-like respiratory NR. Our recently reported RNAseq analysis of *Mab* hypoxia adaption showed down-regulation of two response regulators implicated in nitrate assimilation, *MAB_0744* (*glnR*) and *MAB_3520c* (*nnaR*), in addition to the five additional genes of the NnaR regulon (this study), which may serve to reduce protein synthesis and aid transition to slowed growth under stressful conditions (114).

In addition to species-specific regulation of the nitrate metabolism apparatus under hypoxic conditions, the genomic organization of genes predicted to be involved in this process is unique in *Mab.* The genes encoding proteins required for nitrate/nitrite transport (NarK3), reduction of nitrite to ammonia (NirBD), an ORR associated with nitrate assimilation (NnaR), and synthesis of the siroheme cofactor for NirBD (SirB) are clustered in *MAB_3523c-MAB_3519c* locus, with the *nasN* NiR gene located elsewhere. The overlap between open reading frames of *nirB-nnaR* and *nnaR-sirB* suggest close translational coupling of these components (208). All five genes appear to be transcribed as a single unit, as evidenced by our RT-PCR analysis and tight co-regulation under hypoxia and nitrate/nitrite supported growth (Figure 15B-D). However, we cannot rule out the possibility of additional transcripts of subsets of genes from internal promoters. While *narK3, nnaR,* and *sirB* are arranged contiguously in *Mtb* and *Msm,* the *nirBD* operon is upstream and oriented divergently and nitrate reductases (*narGHJI-Mtb* and *nasN-Msm*) are located elsewhere (Figure 16). Following identification of an uncharacterized orphan response regulator designated NnaR embedded within this operon, our focal point became elucidating its role in *Mab* gene regulation and nitrate assimilation.

In silico analyses identified only 2 putative NnaR binding sites in the *Mab* genome - upstream of *nark3-sirB* operon and *nasN* (Figure 15A) – suggesting a small regulon of genes with focused roles on nitrate and nitrite metabolism. This is comparable to the small repertoire of genes reportedly controlled by the *S. coelicolor* ortholog shown to regulate *narK, nirAB* (NiR), and *nasA* (assimilatory NR) (116). In *Msm*, NnaR controls a slightly larger gene set comprised of seven mRNA transcripts (four single genes, 3 operons), however only 3 target loci (*narK3, nirBD, nasN*) have corresponding orthologs in *Mab* (119). The coordinated induction of the *nark3-sirB* operon and *nasN* during growth on inorganic nitrogen sources is consistent with regulation by the same transcription factor, NnaR. It is also worth noting that the dramatic ~20- to 200-fold induction of the NnaR regulon (Figure 15C&D) is in reference to equimolar concentrations of nitrogen in the form of ammonium sulfate. This would suggest that NnaR-mediated transcriptional activation is not in response to low nitrogen levels overall but is somehow specific to nitrate and nitrite. Based on these observations, the lack of induction of *nasN, nark3*, and *nirBD* in $Mab_{\Delta nnaR}$ during growth on nitrate or nitrite was not surprising. However, the upregulation of *sirB* in the absence of *nnaR* in both nitrogen replete and deplete conditions was unexpected (Figure 18A-C). This is inconsistent with *sirB* being expressed only by NnaR-activated co-transcription with the four upstream genes. An initial hypothesis we considered was upregulation due to read-through from the promoter of the apramycin^R cassette used to inactivate *nnaR*. However, restoration of *sirB* to wild-type levels when both *nnaR* and *sirB* were constitutively expressed in trans argues against this. If anything, an additional copy of *sirB* on the complement construct (included because we anticipated a polar negative effect) was expected to boost *sirB* expression in the complement, not restore levels to normal. It is possible that deletion of *nnaR* disrupts the proposed translational coupling with *sirB* (despite care taken not to delete the overlapped 5' end of *sirB*) such that diminished SirB activity triggers compensatory upregulation of *sirB.* Recall that SirB is a

ferrochelatase responsible for catalyzing the last step of siroheme synthesis, a cofactor required for the activity of nitrite reductase (NirBD) and sulfite reductases (209-211). This would require a second internal promoter able to drive expression of *sirB* alone (or with additional upstream genes since putative promoter cannot be within *nnaR)* activated by a transcription factor that is induced by NnaR. More research will be needed to understand this unexpected regulation of *sirB* and the role of NnaR.

The mechanism by which NnaR senses nitrate and nitrate, either directly or indirectly, and becomes activated to promote transcription of its regulon remains a mystery. No studies of the better characterized orthologs in *S. coelicolor*, *Msm*, or *Mtb* have addressed this question. We initially hypothesized that NnaR activation may be mediated by DosS, the sensor histidine kinase (HK) partner of the response regulator (RR) DosR, known to sense hypoxia, NO, and CO in *Mtb* (76,92,93,95,212). This was based on a report by Gautam *et al.* of potential protein-protein interactions (PPI) between DosS and the *Mtb* NnaR ortholog Rv0260 (207). Using the same M-PFC (Mycobacterial Protein Fragment Complementation) method (142), we were able to detect *Mab* DosS-DosR PPI, but were unable to detect an interaction between *Mab* DosS and NnaR (Figure 20). This is perhaps not surprising given the other species-specific differences we have noted between *Mtb* and *Mab* in their responses to hypoxia and nitrogen limitation. Further *in silico* analysis also failed to identify a receiver domain with aspartate residues likely to serve as phosphorylation sites (data not shown) suggesting NnaR is not likely to be activated by a non-cognate HK. Alternative hypotheses include NnaR activation by serine/threonine kinases as observed with the ORR GlnR (196,197,213), or self-activation via the unique HemD domain. The domain architecture of NnaR consisting of an N-terminal HemD domain (also known as a uroporphyrinogen III synthase) fused to a C-terminal OmpR DNA binding domain is restricted to Actinomycetes (116). Uroporphyrinogen III synthase is responsible for the cyclization of

hydroxymethylbilane (HMB) which forms uroporphyrinogen III (UroPIII), a precursor for vitamin B12 and siroheme. It is worth noting that the HemD domain of NnaR in *S. coelicolor* is catalytically inactive (116,209,210,214). The role of the NnaR HemD domain remains unclear but it is plausible it acts as a sensing domain for HMB or UroPIII and self-activates resulting in conformational changes in the DNA-binding domain as evidenced by the self-modulating RRs, JadR1 and RedZ of streptomyces (80).

This study provides clear evidence that *Mab* utilizes species-specific strategies of nitrogen assimilation when nitrate or nitrite are the only sources of nitrogen and employs the ORR NnaR in distinct ways compared to *Msm* and *Mtb*. This is illustrated by confirmation of a unique operon containing genes *narK3-nirBD-nnaR-sirB*, regulation of this operon and *nasN* by NnaR, and the importance of NnaR for survival when nitrate or nitrite are the sole sources of nitrogen. There are still unanswered questions regarding the regulation of nitrogen metabolism in *Mab*, and the role of NnaR in particular, that remain to be addressed. One key knowledge gap is the degree of regulatory overlap and interaction with GlnR, which typically controls larger regulons involved in nitrogen metabolism and many other processes. Although Fan *et al.* did report that *Mab* GlnR regulates 8 genes associated with nitrogen metabolism, they only queried 9 promoters by ChIP-qPCR (62). The full extent of the GlnR regulon in *Mab* remains to be determined. Other relevant questions include how hypoxia triggers down-regulation of the NnaR regulon, what is the function of the HemD domain, what underlies the unusual regulation of *sirB*, and what signaling mechanisms contribute to NnaR activation. These data revealing a species-specific role for *Mab* NnaR and its significance in nitrate assimilation establishes a premise for future studies exploring a role in persistence within host environments such as macrophage phagosomes, granulomas, and mucus-laden airways affected by CF.

CHAPTER FOUR: UNPUBLISHED ANIMAL EXPERIMENTS

Abstract

The focus of this chapter is the documentation of the animal work performed during my time in the Rohde lab. A universal *in vivo* infection model for *Mab* has not been established hindering studies exploring the interplay of transcriptional regulation and pathogenesis, and *in vivo* drug efficacy. We aimed to establish an *in vivo* model mimicking the pathology of the CF lung to study *Mab* transcriptional regulation and pathogenesis. Since transgenic mice with CFTR mutations are not representative of human CF pathology we explored other options to suit our needs (215,216). An ideal mouse model to establish persistent *Mab* infections is immunocompetent and harbors similar pathologies to the human CF lung particularly hypoxia so we can further study the role of *Mab* DosRS and other transcriptional modulators relating to hypoxic adaptation. Mice with intact immune systems clear *Mab* infections however, immunocompromised mice capable of developing a persistent infection have little utility due to the CF lung being immunocompetent (217,218). We sought to develop a mouse model fulfilling the criteria specific to our needs. Our search in the literature led us to the discovery of βENaC mice. These mice were promising as an *in vivo* model for our research due to similar pathology of the human CF lung. βENaC are not a true CF model due to an intact CFTR gene however, these mice over-express the β subunit of the epithelial sodium channel in a tissue specific manner within the lung resulting in dysregulation of a sodium channel resulting in similar lung physiology to CF (219). Prior to our animal work we found one *Mab* study that successfully utilized βENaC mice for infection validating our pursuit of this model for infection. Previous work fulfilling dissertation requirements by Vongtongsalee, determined multi-dose *Mab* infection on consecutive days enabled a persistent infection in βENaC mice despite an intact immune system helping us to set the stage for our own mouse work (220).

Attempts at establishing a persistent infection in βENaC mice via intranasal administration on 4 consecutive days didn't yield the results we expected. Our first βENaC study yielded a ~3 log decrease by day 28 compared to day 0 and *Mab* was not recovered from the lungs of all mice. The Vongtongasalee study, not only used a different delivery method but also infected mice with a rough strain of *Mab* which, is associated with virulence *in vivo* (220). We next attempted intranasal infection with a rough lab strain, *Mab390R,* and 2 rough clinical isolates. Infection with rough strains resulted in decreased CFU by the last time point however, we used 1x intranasal infection verse 4x. Since we struggled to infect all the mice in our previous studies and observed a decline in CFU we next explored the utility of a neutropenic mouse model to establish infection (221). This model was also unsuccessful in yielding a persistent infection and we were unable to recover *Mab* from the lungs in many of the mice. The Rohde lab is committed to developing a mice model and efforts are on-going in the hopes we will establish a persistent *Mab* infection to allowing persistent infection for the study of transcriptional regulation and its affect on pathogenesis.

Introduction

Current animal models for the study of *Mab* lack a universal/common *in vivo* model therefore development of a model fitting the criteria previously mentioned is imperative for continued progress in understanding *Mab* pathogenesis. The Rohde lab is committed to the development of an *in vivo* mouse model mimicking CF lung pathology, is immunocompetent, and able to maintain a persistent *Mab* infection for the study of gene regulation. Additionally, to continue studying *Mab* DosR and its effect on non-replicating persistence, an *in vivo* model must also have the ability to form hypoxic granulomas or at least develop hypoxic mucus such as observed in the CF lung. Previous *in vivo Mtb* DosRS/T studies have shown variable results dependent upon

whether the model develops hypoxic granulomas (the hallmark pathology of an infected lung) within the lung during infection (89,100,137,138,207). These models include guinea pigs, rabbits, rhesus macaques and C3HeB/FeJ Mice (Kramnik mice) (88,137,138). Although the Kramnik mice are appealing for the study of *Mab* DosR due to the hypoxic lung and granuloma formation, a previous study assessing the utility of mouse models for *Mab* to test *in vivo* drug susceptibility determined Kramnik mice cleared the infection (217). In this same study the only mice that were able to retain an infection were MyD88 -/-, GKO -/-, nude, SCID and GMCSF -/- mice all of which are immunocompromised and lack the capability of developing hypoxic granulomas (217). A subsequent study assessing the utility of Kramnik mice for *Mab* infections was able to generate a sustained infection via administration of daily corticosteroid injections 1 week prior to infection and then daily for 3 consecutive weeks (218). This piqued our interest due to the recovery of the immune system after cessation of corticosteroids. However, daily cortisone injections over a 4-week period prompted us to keep investigating other mouse models.

We found three promising transgenic (*Tg*) mouse models of interest mimicking the pathology of the CF lung in the literature: 1) $CFTR^{tm1UNC}$/ $CFTR^{tm1UNC}$, 2) $CFTR^{tm1UNCTgN(FABPCFTR)}$, and 3) βENaC. All three transgenic mice are immunocompetent however, only the βENaC displays hypoxic mucus plugs (216,219,222). Upon further comparison we ruled out the utility of $CFTR^{tm1UNC}$/ $CFTR^{tm1UNC}$ due to the high rate of mortality caused by the absence of the CFTR channel in the intestine (216,222). Zhou et al., were able to develop a gut corrected CFTR transgenic mouse ($CFTR^{tm1UNCTgN(FABPCFTR)}$) however the lung pathology of this strain and the uncorrected strain did not develop the same pathology exhibited in humans. Neither of the CFTR *Tg* mice displayed reduced mucociliary clearance, mucus plugging, or increased mucus

concentration all of which are salient features necessary for mimicking *Mab* infections in CF lung environment (219).

Although the βENaC mouse model is not a true CF mouse model due to a functioning CFTR channel the lung pathology of this mouse model is more comparable to the human CF lung. One of the characteristics of the human CF lung is dysfunctional ion transport due to increased Na^+ absorption mediated by the ENaC transporter (epithelial sodium channel) (223). Zhou et al., generated a mouse model overexpressing ENaC activity to more accurately mimic CF lung pathology. The ENaC protein is a heterotrimeric protein consisting of αβγ subunits however it was found the overexpression of the β subunit was sufficient to establish an overexpressing phenotype. Clara cell secretory protein promoter element upstream of the β subunit was used to generate tissue specific overexpression of the β subunit constructs. These constructs were used to generate βENaC *Tg* mice via pronuclear injection of oocytes (C3H x C57BL/6 background) (219).

The βENaC *Tg* mouse model created by Zhou et al., exhibits many of the features observed in human CF pathology. Most notably, increased Na+ transport led to decreased airway surface liquid (ASL) resulting in decreased mucociliary clearance and accumulation of mucus. In addition to these pertinent features in an *in vivo* model, airway inflammation was also present which is a common characteristic of the human CF lung due to accumulation of neutrophils and eosinophils (219). Due to the comparable human like CF lung pathology of the βENaC mouse model our lab has chosen this *in vivo* model to study *Mab* persistence and transcriptional regulation.

Methods

βENaC Breeding

A single βENaC mouse was purchased from University of North Carolina Chapel Hill and sent to Texas A&M University (TAMU) for *in vitro* fertilization in C57BL/6N mice purchased from Taconic. Tail snips from mice bred by (TAMU) were genotyped via DNA extraction followed by PCR amplification to identify βENaC positive mice (primers are listed in Table 11). After receiving βENaC positive mice from TAMU all future breeding was conducted at the University of Central Florida Lake Nona Vivarium.

Mab Culture Preparation For Infection

Cultures were grown in 7H9-OADC+.05% tyloxapol from glycerol stocks at 37˚C while shaking unless otherwise noted. Infection inoculum was prepared from log phase cultures by washing 3x in PBS, resuspended in PBS, syringed with tuberculin needle to break up clumps and diluted to a final OD of .5 ~10^6 CFUs. An aliquot of inoculum was taken for CFU enumeration, 10-fold serial dilutions in PBS + .05% Tween 80 ranging from 10^0 to 10^-7 were plated on 7H10-OADC plus 100 ug/ml of cycloheximide quad plates. Colonies were counted between 3-5 days post plating.

Animal Infection

Different *Mab* strains were used throughout the animal study to investigate an infection model, to assess differences between smooth and rough strains, and clinical isolates verse lab strains. These strains are as follows, *Mab390S* (smooth lab strain isolated from an ileal granuloma), *Mab390R* (rough lab strain isolated from an ileal granuloma), *Msm CF17* (rough clinical isolate

gifted from National Jewish Laboratories) and *Mab CF22* (rough clinical isolate gifted from National Jewish Laboratories). Animals between 8-12 weeks old were intranasally infected either 1x or 4x (infection daily over 4 days) with 20 µl of .5 OD inoculum. Mice were sacrififed to harvest lungs at varying time points. Lungs were homogenized with 1 mm silicon carbide beads in bead beater. Homogenate was Bserially diluted ranging from 10^0 to 10^-7 in PBS +.05% Tween 80 and plated on 7H10-OADC plus 100 ug/ml of cycloheximide quad plates. Colonies were counted between 3-5 days post plating.

Cyclophosphamide Administration

Cyclophosphamide was resuspended in PBS at 150 mg/kg. Four days prior and one day prior to infection mice were administered cyclophosphamide via intraperitoneal (IP) injection as described by Wu et al.,(224). 52 total mice (26 each of C57BL/6N and βENaC) were administered cyclophosphamide to test the efficacy of the neutropenic mouse model.

Results

Pilot Study Utilizing C57BL/6N Mice

Previous research by Vongtongsalee in fulfillment of a thesis project reported a multi-dose infection of *Mab* yielded ~ 2 log increase in CFU at D30 in βENaC mice compared to a single infection prompted our lab to verify if the same was true in our hands (220). Since breeding of βENaC mice with C57BL/6N mice yields less than 50% transgenic mice we utilized C57BL/6N in a preliminary multi-dose study to optimize the protocol in case changes were needed and to utilize the C57BL/6N mice for technical development such as handling and practice of intranasal infection. C57BL/6N mice (6 per group) were intranasally infected either 1x or 4x (24 hours apart

on 4 consecutive days) with *Mab390S* or *Mab*$_{\Delta dosRS}$ (this strain was only used in the 4x time experiment and only on D0 and D10 due to limited number of mice available). On D0 (immediately after infection), D5, D10 and D20 lungs were harvested to measure bacterial burden via CFU/lung and reported in (Figure 21). Our results suggest on D0, *Mab390S* 4x infection group was not successfully infected due to only 3/6 mice having countable colonies after plating. Overtime we observed a steady decline in CFU for the 1x *Mab390S* infection and 4 x *Mab*$_{\Delta dosRS}$ infection which was not surprising due to a competent immune system and functional lung. However, the 4x *Mab390S* infection bacterial burden on D20 remained similar to D0 average with 6/6 mice infected. Due to the inconsistent data on D0 with only 3/6 animals infected in the 4x *Mab390S* group it is hard to draw conclusions on data collected. However, the increased CFU in the 4x *Mab390S* infected group from D10 to D20 is promising and will hopefully garner results in the βENaC mouse model.

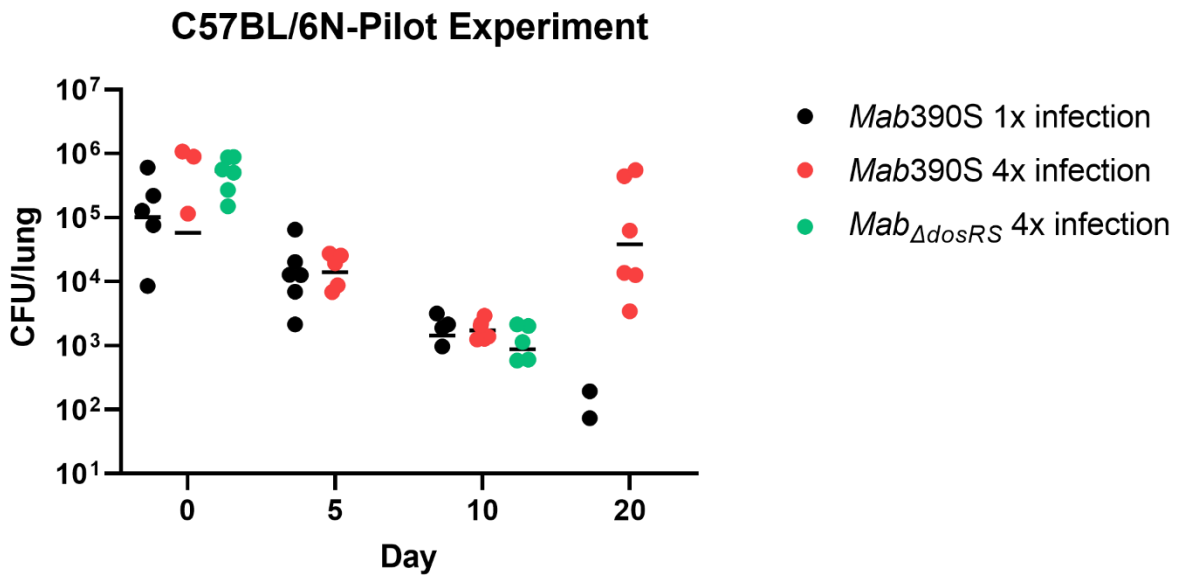

Figure 21: Multi-dose infection yields sustained infection over time in C57BL/6N mice

C57BL/6N mice were infected with Mab390S 1x (black), *Mab390S* 4x (red) or $Mab_{\Delta dosRS}$ *(green).* 6 mice per infection group per time point were infected with the exception of $Mab_{\Delta dosRS}$. Two time points, day 5 and 10 were chosen for $Mab_{\Delta dosRS}$ infection with 6 mice used in each group. CFU/lung were enumerated on day 0, 5, 10 and 20.

βENaC Multi-dose Infection

The same multi-dose infection model used with the C57BL/6N mice was administered to βENaC mice for infection. 8-10 week-old mice were intranasally infected 1x or 4x (24 hours apart) with

Mab390S or 4x $Mab_{\Delta dosRS}$ (6 mice per group per time point). Lungs were harvested at D0 (immediately after infection), D5, D14 and D28 to measure bacterial burden via CFU/lung and reported in (Figure 22). On D0 5/6 mice for both 1x and 4x infections of *Mab390S* were infected and 6/6 for 4x $Mab_{\Delta dosRS}$. Despite ≥ 83% of βENaC mice infected on D0, by D28 only 3/6 1x *Mab390S* mice were infected, 4/6 4x *Mab390S* mice were infected and 2/6 4x $Mab_{\Delta dosRS}$ were infected. Bacterial burden steadily decreased over time however, on D14 the 3 groups had detectable CFU ranging from $10^{2.5}$ to 10^{3}. We had expected higher CFU on D14 based on the work performed by Vongtongsalee in the range of ~10^{5} by D15 (220). However, there are 2 differences in our study:1) delivery method of *Mab* and 2) strains used for infection. Our study used 20 µl of inoculum via intranasal route whereas 35 µl of inoculum was used for intratracheal infection with a microsprayer by Vongtongsalee (220) which may contribute to the variability in results between the labs/experiments. Additionally, the strains used in the infection model for βENaC mice could also account for variability across the two studies. Our lab uses *Mab390S* which is a smooth strain previously recovered from an ileal granuloma for our *in vitro* and *in vivo* research. The Vongtongsalee study utilized the hyper virulent strain *Mycobacterium abscessus sp. masilience* OM194 that they and others have documented as an outbreak clinical isolate with a rough colony morphology (220,225).

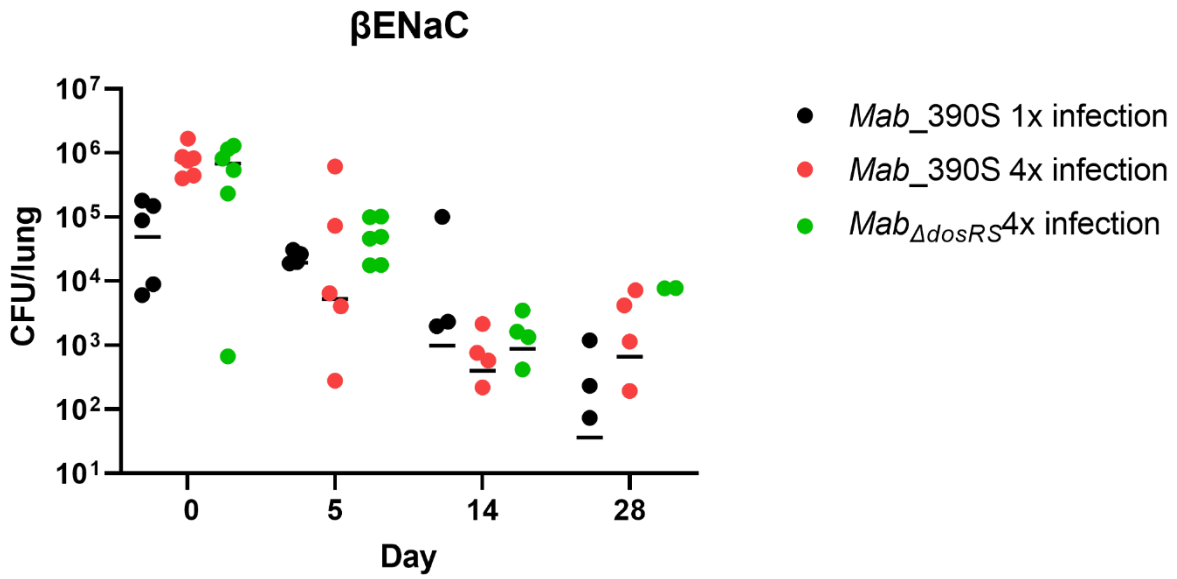

Figure 22: βENac multi-dose infection model

βENaC mice were infected with Mab390S 1x (black), *Mab390S* 4x (red) or *Mab*$_{\Delta dosRS}$ 4x *(green).* CFU/lung were enumerated on day 0, 5, 14 and 28 post infection.

Smooth, Rough And Clinical Isolate Infection Model

Since we were concerned with maintaining persistent lung infection using *Mab390S* due to its isolation from an ileal granuloma rather than the lung and it being a smooth strain rather than a rough strain (41) we compared *Mab390S* (smooth) against *Mab390R* (rough) and compared 2 rough clinical isolates from the National Jewish Laboratory, *MsmCF17 (M. abscessus sp. massiliense)* and *MabCF22* (*M. abscessus*) (Figure 23& 24). Inoculum was prepared as described above except for the syringe step (to break-up clumps) for the rough strains. This step was excluded due to the culture of the rough strains sticking to the inside of the syringe which resulted in lower OD when preparing the inoculum. βENaC mice (4 per group) were infected 1x with ~10^6 CFU in 20 ul of *Mab390S* or *Mab390R.* CFU was assessed on day 0 and day 14, for each time point and each strain only 3/4 mice were infected (Figure 23). CFU on day 0 for *Mab390R* was a log lower than *Mab390S* suggesting the mice were not infected with the same CFU across both strains. The difference in CFU on day 0 may be attributed to the hydrophobicity of the R strain. The R strain was difficult to work with due to its adherence to conical tubes and pipette tips preventing delivery of the full infectious dose. Despite discrepancies in the initial CFU, day 14 displayed similar CFU between both strains.

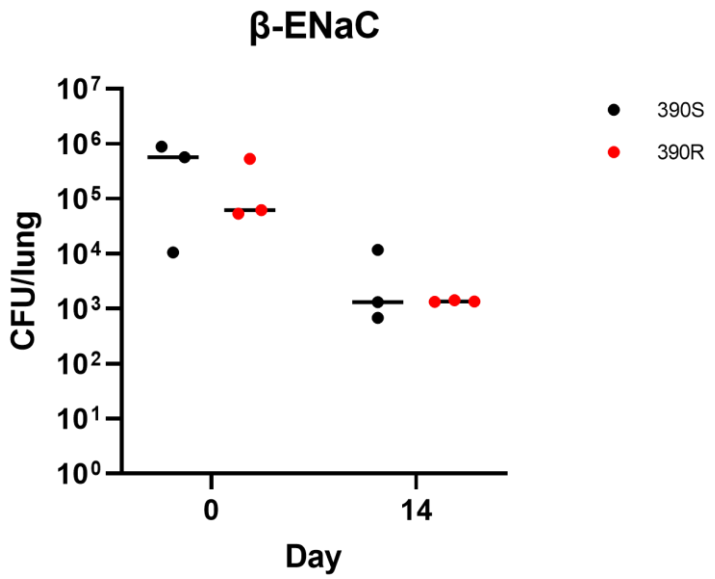

Figure 23: βENaC smooth and rough strain infection

βENaC mice were infected 1x with *Mab390S* (black) or *Mab390R* (red). CFU/lung were enumerated on day 0 and day 14 post infection.

We next tested whether clinical strains recovered from the lungs of CF patients allowed for a persistent infection. Five β*ENaC* mice per group were infected with a single dose of clinical isolates *MsmCF17* or *MabCF22* with 10^6 CFU in 20 ul of PBS (Figure 24). CFU was enumerated on day 0 (immediately after infection) and on day 21 to determine if we were able to establish a persistent infection over a longer time course with clinical isolates. On day 0, 5/5 mice were infected with *MsmCF17* and 4/5 mice were infected with *MabCF22.* By day 21 only 3/5 mice in each group were infected with an average loss of 10^2 and 10^4 in *MabCF22* and *MsmCF17*, respectively compared to D0 (Figure 24). We had anticipated higher bacterial burden with all animals remaining infected by day 21 due to utilizing clinical isolates recovered CF lungs.

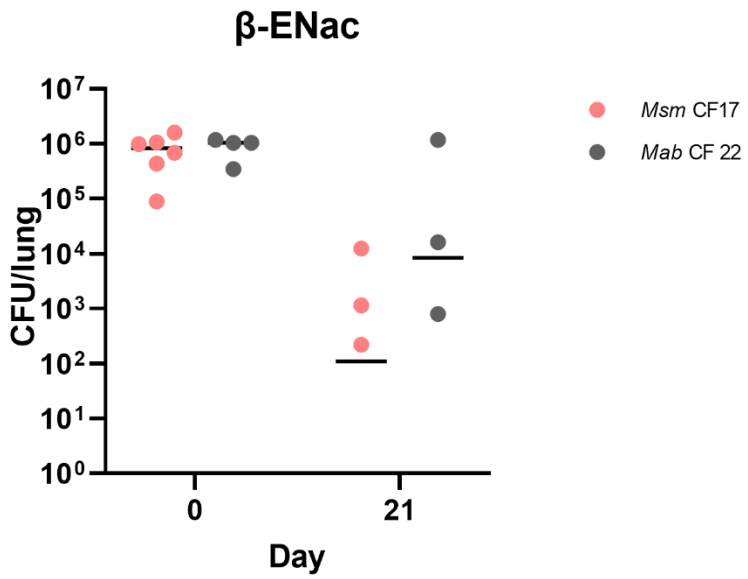

Figure 24: Clinical isolate infection of βENaC mice

βENaC mice were infected 1x with clinical isolates *Msm* CF17 (pink) and *Mab* CF22 (gray). CFU/lung were enumerated on day 0 and day 21 post infection.

Neutropenic Mouse Model

Due to lower bacterial burden than anticipated throughout our *in vivo* studies we further investigated animal models. We explored the literature for methods used to temporarily suppress the innate immune system in mice without having to use the laborious corticosteroid method previously described (218). Zuluaga *et al*., used a neutropenic mouse model to investigate infection models with various pathogens which resulted in a persistent and severe infection (221). In brief, mice administered cyclophosphamide become neutropenic within 4 days with restoration of neutrophils by day 11 allowing examination of intrinsic drug activity independent of immune activity. Cyclophosphamide was administered via intraperitoneal injection (IP) 4 days and 1 day prior to infection allowing time for neutrophil depletion. A subsequent study performed by Wu *et al*., used this method prior to intranasally infecting BALB/c mice with 10^7 CFU of *Mab* clinical isolate CIP 108297 (224). Their work resulted in a ~2-log CFU increase by day 14 compared to day 3 (initial time point) with all animals remaining infected (224). This methodology was appealing as it could allow successful establishment of infection using temporary immunosuppression with only having to administer cyclophosphamide twice.

We used both C57BL/6N and βENaC mice to test the efficacy of the neutropenic mouse model previously established. Mice were administered 150mg/kg in PBS via IP injection 4 days and 1 day prior to intranasal infection (1x infection) with *Mab*390S, *Mab*390R or $Mab_{\Delta dosRS}$ (10^6 CFU). For *Mab*390S and *Mab*390R 5 mice each of C57BL/6N and βENaC per time point per (day 3 and 14) were used whereas only 3 mice total were infected with $Mab_{\Delta dosRS}$ due to number of mice available. CFU/lung was enumerated 3 days and 14 days post infection for *Mab*390S and *Mab*390R and on day 14 only for mice infected with $Mab_{\Delta dosRS}$ again due to number of mice available.

The neutropenic mouse model of infection did not yield the persistent infection we had anticipated (Figure 25). On day 3 only 1/5 C57BL/6N and 2/5 βENaC mice had countable colonies for *Mab*390S and *Mab*390R infected mice. Day 14 yielded slightly better results however countable colonies were only present in 3/5 *Mab390S*, 2/5 *Mab390R*, 2/3 $Mab_{\Delta dosRS}$ with bacterial burden of ~$10^{2.5}$ CFU/lung for C57BL/6N infected mice. Similarly, βENaC mice displayed ~$10^{2.5}$ CFU/lung for strains *Mab390S* and *Mab390R* with 4/5 and 3/5 mice infected, respectively. No countable colonies were observed for βENaC mice infected with $Mab_{\Delta dosRS}$ whether this is a DosRS phenotype or inefficient administration of inoculum is unknown.

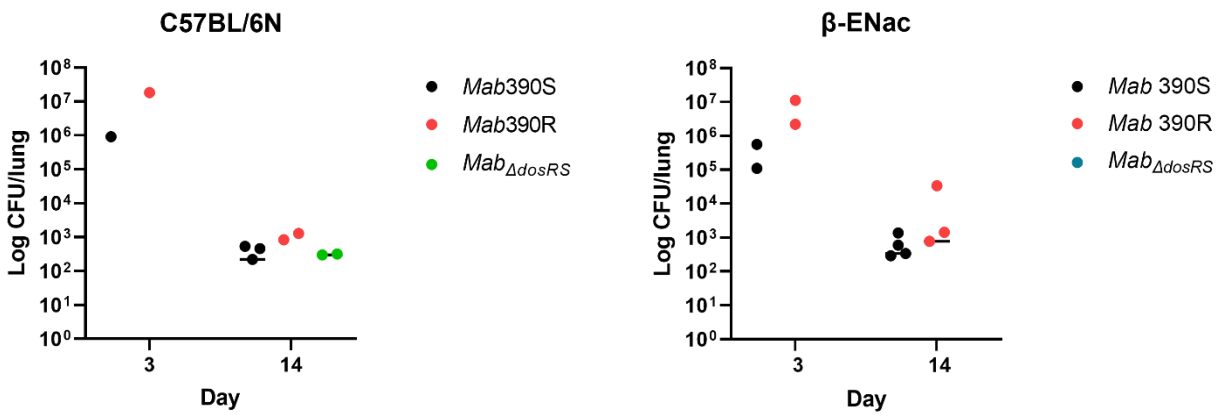

Figure 25: Cyclophosphamide treated mice

Cyclophosphamide was administered to C57BL/6N and βENaC mice 4 days and 1 day prior to infection with *Mab390S* (black), *Mab390R* (red) or *Mab$_{\Delta dosRS}$* (green). CFU/lung were enumerated on day 3 and 14 post infection.

Discussion

Current mouse models used to study *Mab* are lacking in utility due to the inability of immunocompetent mice to sustain a persistent *Mab* infection and lack of transgenic mice representative of CF pathology (216,217,219,222). Immunosuppressed mice are not representative of the host response and immune pressures within the CF lung limiting their utility as an *in vivo* model. It's imperative for a mouse model to have an intact immune system and characteristics of the CF lung such as hypoxic mucus, increased sodium absorption, and increased nitrate, nitrite and nitric oxide levels due to increased neutrophils to study the transcriptional regulation required for *Mab* persistence (216,219,222,226). Transgenic CFTR mice exist, however these mice don't represent the characteristics of the human CF lung *e.g.*, decreased mucociliary clearance, increased sodium absorption and mucus plugs (216,219,222). Development of a universal mouse model mimicking the CF lung and capable of maintaining a persistent *Mab* infection in an immunocompetent mouse is a top priority in the Rohde lab.

Our literature review led us to βENaC mice, a promising mouse model matching our criteria of human-like CF lung pathology and immunocompetent. Zhou et al., developed a tissue specific over expressor of the β subunit of epithelial sodium channel in the lung resulting in pathology mimicking the human CF lung despite an intact and functional CFTR gene. Previous research by Vongtongsalee, utilized these mice for a multi-dose *Mab* infection yielding promising results. The multi-dose infection model resulted in a ~2 -log higher CFU on day 30 compared to day 5 suggesting this model will allow us to study transcriptional regulation during a persistent *Mab* infection.

Our pilot experiment utilizing the multi-dose infection model with C57BL/6N WT mice didn't yield successful infection for all animals in the study (Figure 21). However, we were able observe a difference in CFU by day 20 between 1x and 4x infected mice providing validation for use of the multi-dose infection model for βENaC studies. Even though we observed inconsistent results in our ability to administer inoculum to all animals the purpose of this study was the development technical skills required for successful administration of innoculum prior to the start of animal experiments utilizing βENaC mice.

The multi-dose infection model using βENaC mice didn't garner the results we had anticipated. We observed ~ 3-log decline in CFU on day 28 compared to day 0 (Figure 22) contrasting with the Vongtongsalee study where an increase in CFU was observed on day 30 compared to their initial time point (220). Differences in delivery method of inoculum and strains used may account for contrasting results between our study and the Vongtongsalee study (220). Difference between our smooth lab strain recovered from an ileal granuloma rather than the lungs used in our study verses a rough clinical isolate known to be hypervirulent in the Vongtongsalee study made us question the utility of our strain for establishing an infection (220). This led us to investigate a βENaC infection model using the rough lab strain *Mab390R* and rough clinical isolates recovered from CF lung patients, *Msm* CF17 and *Mab* CF22, acquired from National Jewish Laboratory.

Infection of βENaC mice with a single dose of *Mab390R*, *Msm CF17* or *Mab CF 22* didn't yield a persistent infection overtime and not all mice had recoverable CFU (Figure. 23&24). This could be attributed to the difficulty of working with rough strains of *Mab* which are hydrophobic causing adherence of bacteria to conical tubes and pipette tips resulting in decreased CFU delivered to lungs compared to the smooth strain. An additional issue that may have led to the decreased

CFU observed in mouse lungs was the use of single dose infection vs multi-dose (Figure 23&24). Validating this theory is the marked difference in CFU between single and multi-dose infection observed in C57BL/6N WT mice and βENaC (Figure. 21&22). In hindsight, a multi-dose infection should have been performed to validate the efficacy of using rough strains to establish a persistent infection.

Due to βENaC mice having an intact immune system which, has been known to inhibit successful *Mab* infection we sought to temporarily deplete neutrophils via IP injection of cyclophosphamide in βENaC mice. This model of infection has previously been used by Wu *et al*., to establish *Mab* infections in BALB/c mice using a 1x infection dose resulting in a ~2-log increase of CFU by day 14 (224). To investigate the utility of this infection model we used the same schedule and concentration of cyclophosphamide in βENaC mice and harvested lungs for CFU enumeration at the same points, 3 days and 14 days post infection. In our hands this method of infection yielded very poor results, only 1/4 C57BL/6N mice and 2/4 βENaC mice infected with *Mab390S* or *Mab390R* displayed CFU on day 3 (Figure 25). By day 14 there was ~3-log decrease in CFU in mice with recoverable CFU compared to starting inoculum (Figure 25). Differences between our cyclophosphamide study and the study performed by Wu et al., may contribute to discrepancies in our results. These differences include mouse models used (BALB/c versus βENaC) and *Mab* strains used (*Mab* CIP 108297 versus our strains of *Mab 390S* and *Mab390R*).

Due to difficulties recovering *Mab* from the lung immediately after infection in our initial studies or on day 3 for the cyclophosphamide treated mice, we were unable to establish a persistent infection or attribute the observed clearance of *Mab* to host pressures. Inconsistent infections at the initial time point led us to re-evaluate our method of infection. We later learned a larger

inoculum volume with the same CFU previously used allowed for a more consistent infection. A CRISPRi project not included in this dissertation yielded 100% *Mab* infection in C57BL/6N mice using 40 µl of inoculum verse 20 µl we had been using earlier. A manuscript detailing *Mab* CRISPRi work is underway however, it is not included in this dissertation as this is a collaborative project with Dr. Rashmi Gupta and not part of my graduate thesis work. Despite our many efforts pursuing a persistent *Mab* infection in βENaC mice the results were disappointing. Efforts to establish an *in vivo* model utilizing the βENaC mice are ongoing and a top priority moving forward.

CHAPTER FIVE: UNPUBLISHED PROTEIN WORK

The purpose of this chapter is the documentation of our attempts to perform EMSA assays to affirm DosR binding to promoter regions of genes we determined to be DosR regulated in Chapter 2. We set out to assess DosR binding to promoter regions upstream of *dosR*, the gene *MAB_2489* that we showed was down-regulated via RNAseq, qRT-PCR, and lux reporter assays in the *dosRS* mutant, and the two genes displaying the greatest DGE via RNAseq in the *dosRS* mutant, *MAB_3937* and *MAB_3354*. The DosR protein proved difficult to work with due to insolubility and supplementation with acetyl phosphate for phosphorylation. DosR binding of *dosR*, *2489*, *3937* and *3354* promoters was affirmed in one EMSA assay but was not reproducible.

Methods

Cloning Of DosR Into pET28b

The *Mab dosR* gene was cloned into the protein expression vector pET28b via round the horn cloning and fast cloning (140,141). In brief, the pET28b vector (containing kanamycin resistant cassette and histidine tag) was linearized and the amplified *dosR* PCR product was ligated via overlapping bp that complemented the vector (140,141). The pET28b-*dosR* vector was transformed into chemically competent *E.coli* 10- β cells and plated on LB agar supplemented with 50 µg/ml of kanamycin. Positive clones were confirmed via agarose gel and sequencing. The vector was extracted via mini-preparation and transformed via electroporation into *E.coli* Rosetta2 cells. Transformations were plated on LB agar supplemented with 50 µg/ml of kanamycin and 34 µg/ml of Chloramphenicol.

Protein Purification

Positive clones for pET28b-*dosR* in Rosetta2 cells were cultured in LB broth supplemented with 50µg/ml of kanamycin and 34 µg/ml of Chloramphenicol at 37ºC while shaking. Cultures were grown to log phase and supplemented with 1mM IPTG for 3 hours to induce protein expression at 37ºC while shaking. Cultures were pelleted for 30 minutes at 4300 rpm at 4 ºC. Supernatant and pellet fractions were run on SDS-PAGE to confirm which fraction the protein resided. Western blot was used to confirm the DosR protein using rabbit anti-his antibody The DosR protein was found in the pellet fraction so additional steps were required for purification. Briefly, the pellet was resuspended in 0.5% Triton X, followed by centrifugation at 4300 rpm for 20 minutes at 4 ºC. After centrifugation the pellet was resuspended in binding buffer (20mM Tris-HCl and 500mM NaCl) with 6M guanidine HCl and pelleted again at 4300 rpm for 20 minutes at 4 ºC. Supernatant was removed after centrifugation and purified using Talon Metal Affinity Beads. Protein fractions were run on SDS-PAGE to confirm purified protein. Fractions containing the protein were dialyzed to remove guanidine HCl, the isoelectric point for DosR is 5.36 therefore the protein was dialyzed in buffer pH 7. Primers used in this chapter are in Table 12&13 in the appendix.

Electromobility Shift Assay

A non-radiolabeled EMSA was used to identify protein-DNA interaction as described by Jing *et al*., Briefly, DosR-protein (range from 65 ng-1000ng) and promoter sequences (50 ng) amplified from genomic DNA were incubated for 20 minutes in EMSA binding buffer (10 mM Tris-HCl, 150 mM KCl, 0.1 mM DTT, and 0.1 mM EDTA) (227). Incubated products were run on a 12% Native PAGE at 200 V for ~45 minutes. Gel was stained with SYBR green and visualized on Bio-Rad gel doc (227).

DosR Phosphorylation

Previous research demonstrated the requirement of *Mtb* DosR phosphorylation for promoter binding (228). DosR was phosphorylated using lithium acetyl phosphate as a phosphodonor as described by Chauhan *et al*. DosR was incubated with 50 mM lithium acetyl phosphate, 40 mM Tris-HCl (pH 8.0) and 5mM $MgCl_2$. For 30 minutes at 30 ºC in a thermocycler.

Results

DosR Protein Resides In The Insoluble Fraction

The *dosR* gene was amplified into the protein expression vector pET28B containing a histidine-tag for purification (Figure 26A). Prior to column purification supernatant and pellet fractions were run on SDS-PAGE followed by western blot to confirm which fraction to column purify (Figure 26B&C). The molecular weight of the DosR protein including the histidine tag was 26.3 kDa. SDS-PAGE and western blot confirmed DosR resided in the insoluble fraction (Figure 26B&C). The insoluble fraction was column purified using TALON Metal Affinity beads and yielded bands on an SDS-PAGE in multiple lanes (Figure 26D).

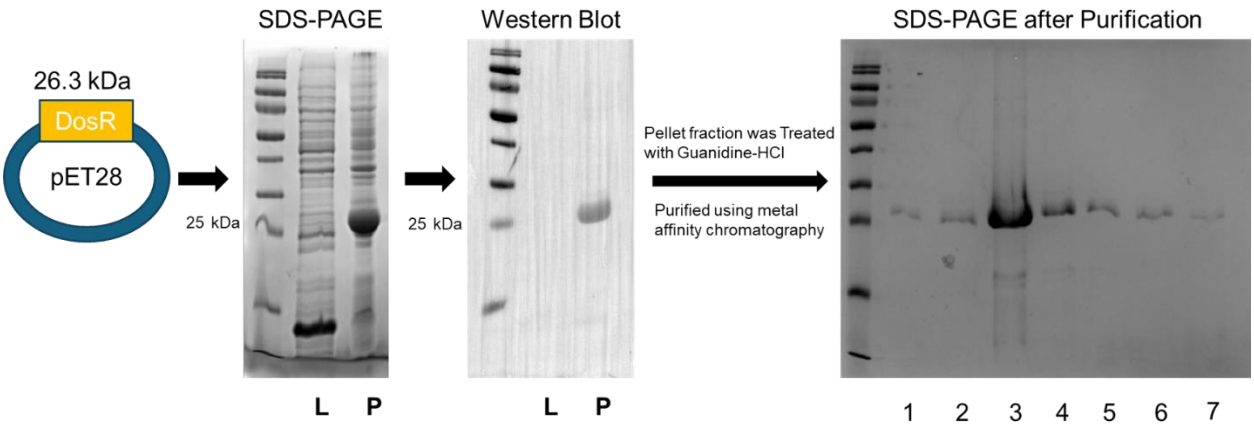

Figure 26: Protein workflow

DosR protein (26.3 kDa) resides in the insoluble fraction **A)** schematic of *dosR* cloning into pET28B vector **B)** SDS-PAGE of lysate (L) and pellet (P) fractions prior to column purification **C)** Western Blot of SDS-PAGE using rabbit anti-his antibodies **D)** SDS-PAGE of purified fractions after column purification with TALON Metal Affinity Beads. Lanes labeled 1-7 represent elution fractions.

Phosphorylated DosR Interacts With Predicted Promoter Sites

To assess DosR promoter binding with putative DosR regulated genes electromobility shift assays were performed. Dr. Shawn Li's lab provided predicted sequences for *MAB_2489*, and *MAB_3354* (Figure 27A&B). Predicted promoters of *MAB_2489* and *MAB_3354* and a 200bp region upstream of *MAB_3937* were amplified from genomic DNA using PCR. 50 ng of PCR product was incubated with 65 ng, 130, 260 ng, 520 ng, or 780 ng of purified DosR protein in binding buffer. The DNA-protein binding reaction was resolved on a native page gel and stained with SYBR green to detect shifts of DNA bands (Figure 27A-C) The native gel did not display shifts in DNA bands at any protein concentration (Figure 27A-C).

Since the DosR ortholog of *Mtb* requires phosphorylation for DNA promoter binding to occur we utilized that tactic to verify if the same was true in our hands (228). Prior to setting up the incubation for protein-DNA binding DosR was phosphorylated with lithium acetyl phosphate. Immediately after phosphorylation 1000ng of DosR was incubated with 50 ng of DNA in binding buffer. Phosphorylated DosR displayed binding with *dosR*, *MAB_2489*, *MAB_3354* and *MAB_3937* promoter sequences (Figure 28). Shifts in DNA were observed with bright bands in the lanes for *dosR*, *2489*, and *3354* however *3937* displayed a very faint band that is not easily discernible on the gel. Since this band is faint and bioinformatics performed by Dr. Shawn Li didn't yield a promoter sequence for this gene it is possible DosR doesn't have a strong affinity for this gene despite this gene displaying DGE in the *dosRS* mutant strain (Figure10). Unfortunately, this data was not reproducible in other EMSA experiments. After many failed attempts we decided to temporarily move on to other work. Whether these failed attempts arose from solubility issues or from inefficient DosR phosphorylation or a combination of the two needs to be resolved to affirm protein-DNA interactions. Future work will include cloning *dosR* into the pET43.1 vector (kindly

given to us by Dr. Mollie Jewett) which contains an N-utilization substance A (NusA) fusion to the protein of interest. NusA is a highly soluble protein from *E.coli* which has been shown to aid in solubilizing inclusion bodies during protein expression (229). We are hopeful this next strategy will yield reproducible results and provide more insight into DosR regulation.

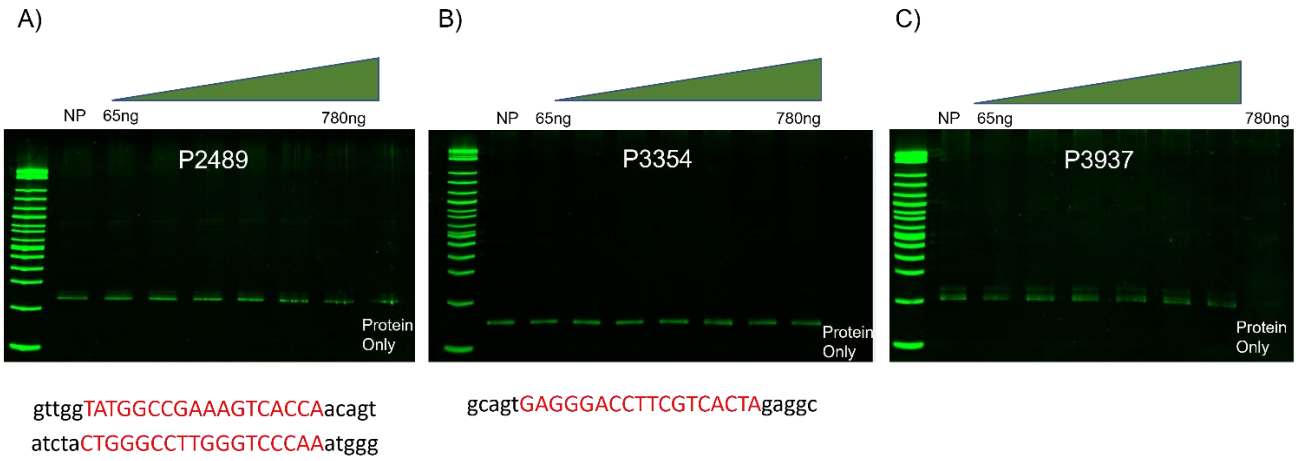

Figure 27: Unphosphorylated DosR EMSA assay

EMSA assays were performed with unphosphorylated DosR at 65 ng, 130 ng. 260ng, 400ng, 520 ng, or 780ng incubated with 50 ng of promoter **A)** *MAB_2489*, **B)** *MAB_3354* and **C)** *MAB_3937.* Promoter sequences displayed below A & B are the predicted promoter regions from Dr. Shawn Li. ~200 bp of upstream DNA regions were amplified to ensure promoter sequences were included in PCR product.

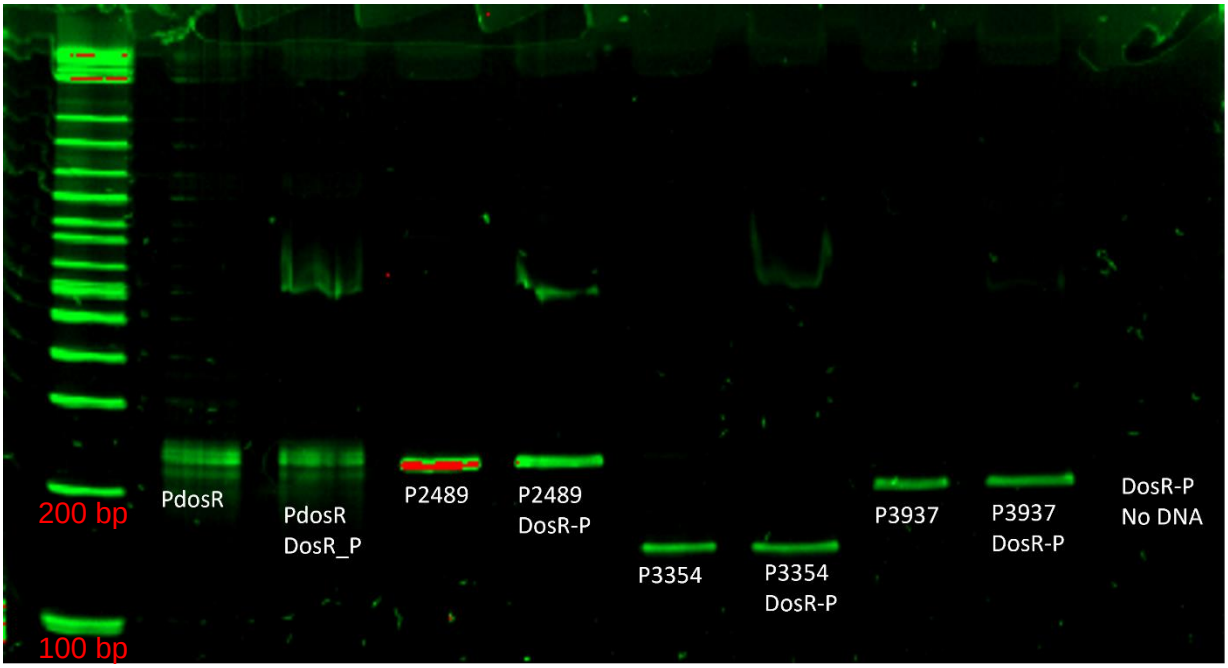

Figure 28 Phosphorylated DosR displays binding interaction with promoters

EMSA assays were performed with phosphorylated DosR at a single concentration of 1 µg incubated with 50 ng of promoters *dosR* (250 bp), *MAB_2489* (212 bp), *MAB_3354* (188 bp) or *MAB_3937* (200 bp). PdosR, P2489, P3354, and P3937 indicate lanes only containing DNA. Lanes containing promoters and phosphorylated DosR are denoted with DosR-P underneath specific promoter name. Note-P3937-DosR-P has a faint band that is hard see when not visualizing in image lab software.

CHAPTER SIX: DISCUSSION

The prevalence of nontuberculous mycobacteria (NTM) infections has been rising at an alarming rate surpassing the occurrence of *Mtb* in the United States (10) . Centers for Disease Control and Prevention last reported 2.5 per 100,000 people infected with *Mtb* compared to 4.73 per 100,000 infected with NTM however, NTM prevalence was seen as high as 91 per 100,000 people dependent on geographical region and climate (230-232). The rates of NTM disease are increasing at a rate between 4.1-7.5% per year causing concern among the immunocompromised and persons with pre-existing lung conditions such as Cystic Fibrosis (CF) (231,233,234). The incidence of NTM among CF patients is ~13-20% however there is a strong likelihood this number will continue to increase due to the possibility of person to person spread within CF treatment centers (28,52). Patients suffering from CF are particularly vulnerable to bacterial infection due to the inability to clear infections from the lung as a result of the thick viscous mucus that accumulates in the airways and dysregulated innate immune responses (50,51). *Mycobacterium abscessus* (*Mab*) is the most common NTM recovered from the lungs of CF patients accounting for ~56% of recovered NTM species (28). The prognosis for CF patients infected with *Mab* is poor due to limited treatment strategies arising from *Mab's* inherent and acquired drug resistance (14,23,24). Current treatment for *Mab* pulmonary infections consists of a multi-drug cocktail lasting one year or longer (Fig. 1) with poor results ranging from 30-50% cure rates (14,235,236). *Mab's* increased occurrence, possible person to person spread, and low cure rates are a cause of concern among CF patients warranting further research in the hopes of eradicating this pathogen (235).

Similar to *Mtb*, *Mab* is able to reside within macrophages and granulomas which limits drug accessibility and promotes persistence (29,53,54,124). For *Mab* to successfully establish an

infection transcriptional remodeling must occur to counteract the hypoxic environments associated with macrophages, granulomas and the thick mucus that accumulates within the CF lung. In addition to these hypoxic environments with a pO_2 measuring ~1%, *Mab* must also thwart elevated reactive nitrogen intermediates and be able to utilize the increased levels of nitrate and nitrite within the CF lung (55-59,138). Despite *Mab's* discovery over 70 years ago studies examining the genetic alterations required for adaptation to host-like stresses encountered *in vivo* are extremely limited. Lack of depth in this area of research prompted our investigation of the transcriptional regulation required for *Mab's* ability to adapt to hypoxia and elevated nitrate and nitrite.

Two-component signaling (TCS) is a mechanism utilized by prokaryotes for adaptation in response to a wide range of environmental cues via alterations in gene expression (63,64,67,69-75) Briefly, TCS consists of a sensor kinase (SK) responsible for recognizing stimuli resulting in autophosphorylation which then activates a cognate response regulator via phosphoryl transfer (63,69). The activated RR forms a homodimer and binds a DNA binding site specific to the RR resulting in genetic alterations (63,69). Although SKs and RRs are genetically linked, signaling mechanisms allowing alterations in gene expression can arise from non-cognate mechanism/interactions. Crosstalk among non-cognate SKs and RRs can occur resulting in fine tuning of responses via additional layers of regulation. (63,68-70,79).

Mab shares 11 of the 12 well-documented *Mtb* TCS orthologs (Fig 2) however, biochemical exploration of the *Mab* orthologs is severely lacking (60,61,84,111,123). Of interest to our lab is the role of the previously uncharacterized *Mab* DosRS TCS in hypoxic adaptation, the *Mtb* ortholog is responsible and necessary for hypoxic adaptation *in vitr*o and *in vivo*

(75,89,100,137,138,176,207). *Mtb* DosR regulon consists of ~50 genes responsible for intracellular survival within macrophages and granulomas where the pO_2 is ~ 1% and in *in vitro* hypoxia experiments resulting in a non-replicating dormant like state (75,89,95,137,138,207). Hypoxic adaptation and nitrate assimilation are strongly linked in *Mtb* via the upregulation of the nitrate symporter *narK2* resulting in the import of nitrate for the use as a terminal electron acceptor (93,108,191). Intracellular nitrate is reduced by the constitutively expressed respiratory nitrate *narGHIJ* to allow respiration when oxygen is limited for hypoxic adaptation (107,108,191). NarGHIJ reduces nitrate to nitrite which can then be extruded or further reduced to ammonium by the nitrite reductase (nirBD) for entry into the glutamate/glutamine cycle (109,122). In addition to a link between hypoxia adaptation and nitrate assimilation via DosR dependent *narK2* induction, hypoxic adaptation is also linked to the co-regulation of DosR with the RR PhoP for the transition from aerobic respiration to hypoxia (70,78,106). The cooperative regulation by *Mtb* DosR and PhoP for hypoxic adaptation demonstrates the convergence of TCS driving alterations in gene expression (70,106). *Mtb* requires regulation by numerous transcription factors and converging pathways for successful hypoxic adaptation with DosR being the primary TCS employed (70,93,106,135,149).

Prior to the initiation of this research very few publications existed investigating the role of *Mab* DosRS in hypoxic adaptation or other TCS (60,84). The two publications available at the time were a bioinformatics study and an RNAseq study investigating differential gene expression (DGE) during *in vitro* stress associated with the CF lung (61,111). A much smaller DosR regulon than documented for *Mtb* was predicted using bioinformatics via comparisons of known DosR promoters from other mycobacterial species (111). The putative *Mab* DosR regulon consisted of 6 genes, *Mab dosR* and *dosS,* and 4 universal stress proteins (111). RNAseq performed by

Miranda-CasoLuengo et al., demonstrated these 6 genes plus 50 others were induced when supplemented with nitric oxide for 40 minutes to induce a hypoxic-like environment however, whether gene induction was due to DosRS was not determined. A more in-depth investigation of *Mab* DosRS is required to identify genes regulated by *Mab* DosR and to determine if *Mab* DosRS is responsible for adaptation to hypoxia. We propose the *Mab* DosR regulon contains more genes than predicted due to *Mab* having a larger genome than *Mtb* and the ability to survive within the host and the environment and plays a key role in adaptation to hypoxia prompting our investigation of this TCS. It should be noted that while working towards determining the role of *Mab* DosRS during adaptation to hypoxia another group examining *Mab* DosR published their findings first (60). A comparison of our data sets/ results are detailed later in this chapter.

Our *Mab* DosR research identified for the first time global transcriptional alterations due to hypoxia, a species-specific regulon controlled by DosR, a *dosRS* phenotype including morphological changes due to hypoxia. Analysis of DGE due to hypoxia revealed key differences in transcriptional alterations for *Mab* compared to *Mtb* such as genes involved in nitrate assimilation (107,108,149) which are upregulated in *Mtb* to allow the use of nitrate as a terminal electron acceptor at low oxygen tension. We observed DosR independent downregulation of *Mab* nitrate assimilation genes *narK3*, *nirBD*, an *ORR nnaR*, *sirB* and *nasN* in hypoxia suggesting the interplay between hypoxia and nitrate assimilation is different in *Mab* compared to *Mtb*. The role of the *Mab* ORR NnaR has not been characterized, leading us to investigate this further. We identified a NnaR regulon with unique gene arrangement compared to other actinobacteria and determined *Mab* NnaR is necessary for successful nitrate assimilation. These results affirm species specific regulation for adaptation to hypoxia and nitrate assimilation driven by DosR and NnaR, respectively. Findings contributing to this assessment are detailed below and demonstrate

TCS ortholog modeling from other species is a good point of reference but differences exist and experimental studies must be performed to fully assess the roles of TCS for adaptation among species.

To better understand the role of *Mab* DosR in hypoxic adaptation global gene expression was analyzed via RNAseq comparing WT *Mab* in 1% O_2 verse 20% O_2 and $Mab_{\Delta dosRS}$ verse WT *Mab* in 1% O_2. Hypoxia induced 1,190 genes in WT *Mab* of which 127 were downregulated in $Mab_{\Delta dosRS}$ affirming DosR dependency (Figure 5A&10). Among these 127 genes were the previously predicted genes (*MAB_3902, MAB_3904, MAB_2489*) (111), an MCE operon, 57 hypothetical proteins, 9 transcription factors, species-specific genes, and two genes displaying the greatest DGE, *MAB_3937* (hypothetical protein) and *MAB_3354* (*desA1*) among others. The roles of the predicted genes have not been determined and are annotated as hypothetical proteins in the Mycobrowser data base however these genes displayed some the largest DGE in the *dosRS* mutant signifying the importance of these genes for hypoxic adaptation. Notably, two genes with the largest DGE in the *dosRS* mutant *MAB_3937* and *MAB_3354* are not regulated by DosR in *Mtb*. *MAB_3937* is annotated as a hypothetical protein with no known ortholog. *MAB_3354* is classified as a desaturase enzyme and although the *Mtb* ortholog is upregulated in hypoxia it is not DosR dependent (111). Data collected from this experiment emphasizes the differences between the DosR regulon between *Mab* and *Mtb*. This set of 127 genes differentially expressed in $Mab_{\Delta dosRS}$ is deemed the *Mab* DosR putative regulon displaying differences from the *Mtb* DosR regulon.

Unexpectedly, when comparing the genes of the *Mtb* and *Mab* DosR regulons there was only an overlap of 7 genes including the 6 genes previously predicted by Gerasimova *et al*., (111). Absent

from the *Mab* DosR regulon are orthologs of *Mtb tgs1 (*triacylglycerol synthase) and *narK2*, which are induced in hypoxia and important features of *in vitro* dormancy signifying lipid accumulation and utilization, and a transition to nitrate respiration, respectively (95,107,108,175). Not only is the *Mab tgs1* (*MAB_3551c*) ortholog not DosR dependent it was not upregulated in hypoxia implying lipid accumulation is specific to *Mtb* for hypoxic adaptation which is an important characteristic of *Mtb* dormancy. *Mtb narK2* is required for nitrate importation and the initiation of nitrate respiration at low oxygen tension (108,191). *narK2* is absent from the *Mab* genome suggesting, nitrate importation occurs by a different means with the possibility that nitrate respiration at low oxygen tension doesn't occur in *Mab* due to its absence and the absence of a respiratory nitrate reductase ortholog to *narGHIJ*. Absence of these key features in *Mab* that are hallmarks of in vitro dormancy for *Mtb* implies *Mab* respiration and energy utilization in hypoxia requires different tactics. DGE of $Mab_{\Delta dosRS}$ in hypoxia demonstrates a larger DosR regulon than observed in *Mtb* with very little overlap between the 2 regulons emphasizing a species-specific strategy for *Mab* hypoxic adaptation.

The importance of *Mab* DosR for hypoxic adaptation is evident from our growth kinetic assays. In the absence of DosR, *Mab* was unable to grow at the same rate as WT in 1% O_2 or resuscitate in 20% O_2 after prolonged hypoxic exposure (Figure 7&9), features also observed with *Mtb* (75). A critical aspect associated with the transition of *Mtb* infection from a dormant to active state is the ability to resuscitate in response to an increase in O_2 levels (75,170). This implies the importance of DosR for hypoxic adaptation in both species despite differences between regulons. Results from growth kinetic assays also identified morphological changes in the absence of DosR after 20 and 30 days in hypoxia (Figure 8). A switch from a smooth to rough morphology was observed in the *dosRS* mutant only in hypoxia suggesting a hypoxia dependent morphotype.

Genetic alterations contributing to this morphotype have not been identified in this study and more work will need to be done to assess contributing factors responsible for this morphological switch. Mechanisms contributing to morphological switching range from SNPs and idels in the *gpl* locus and DGE of the *gpl* locus including genes responsible for glycosylation (44-46). Due to the presence and recovery of the rough variants within the CF lung and association with hypervirulence further study of this morphological switch may give insight into *Mab's* pathogenesis. Identification of a *Mab* DosRS phenotype in hypoxia *in vitro* may translate to an *in vivo* phenotype and establish the importance of *Mab* DosR in virulence particularly within the context of the CF lung where pO2 is measured at 1% (59).

As mentioned previously, during the time we were working to determine the role of *Mab* DosR another group aiming to identify *Mab* DosR inhibitors published a predicted DosR regulon with some commonalities and differences to our findings (60). Belardinelli *et al*., reported down-regulation of 180 genes in microaerophilic conditions in their $Mab_{\Delta dosRS}$ strain (60). Comparison of our *Mab* DosR regulon with the Belardinelli group's DosR regulon revealed an overlap of 45 genes of which 38 had DosR motifs (60). These differences can be attributed to the use of different *Mab* strains, different time points, different hypoxic models, different media between the two studies, and different criteria for establishing DGE (60,114). Despite the differences observed between our putative DosR regulons both studies demonstrated a *dosRS* phenotype in hypoxia however a hypoxia dependent morphotype was not reported by Belardinelli *et al*. Unique to our study was the assessment of genome wide transcriptional changes in hypoxia for WT *Mab* allowing us to assess hypoxia induced DosR dependent and independent genes.

Strikingly, we detected minimal contribution from other TCS during hypoxia as evidenced by DosRS being the only TCS upregulated by >$\log_2$FC of 2 (Figure 5B). *Mtb* DosR has been shown to cooperatively interact with non-cognate RRs to facilitate hypoxic adaptation such as PhoP and NarL (70,78,105,106). Previously, Gonzalo-Asensio *et al*., established an overlap of genes regulated by *Mtb* DosR and PhoP including *dosRS* implying these pathways converge during hypoxic adaptation (70). It should be distinguished that *Mtb dosR* is regulated by PhoP and DosR but *Mtb phoP* is not regulated by DosR signifying induction of the DosR regulon requires an additional layer of regulation for hypoxic adaptation in *Mtb* (70,85,93,95). The minimal induction of other TCS besides DosRS in our RNAseq study doesn't confirm they are dispensable for hypoxic adaptation perhaps induction of other TCS occurred at a different time point. However, unlike the study performed by Gonzalo-Asensio *et al*., we did not observe DGE of *dosR* in our unpublished RNAseq study comparing a *Mab phoPR* knockout mutant to *Mab* WT (data not shown) (70). Further validating independent roles and activation of *Mab* PhoP and DosR is a transcriptional study examining DGE in macrophages and amoeba. This study observed regulation of *dosR* and *phoP* in opposite directions within macrophage (dosR induction, phoP down) and amoeba (phoP up, dosR down) implying these systems in *Mab* are unlinked (127). *Mtb* NarL and DosR are also documented as interacting partners and NarL is observed to regulate *dosR* in aerobic conditions in the presence of nitrate but not in hypoxia signifying an additional level of regulation for basal expression of DosR (105). To affirm DosR interaction with other RR protein-protein interaction assays will need to be performed to assess possible binding partners and co-regulation of DosR regulated genes. Notably, dramatic down-regulation of an ORR, *MAB_3520c*, occurred (Figure 5B). The orthologs of *MAB_3520c* in actinobacteria are annotated as nitrate/nitrite regulators (*nnaR*) and implicated in nitrate assimilation (116,119). Genes adjacent to *MAB_3520c* are identified as putative nitrate transporters (*MAB_3523c*) and nitrite

reductases (MAB_3522c) which are also downregulated in hypoxia (Table S1). Down-regulation of *Mab nnaR* and adjacent nitrate assimilation genes in hypoxia reveals different tactics for adaptation compared to *Mtb*. A recent study examining *Mtb* in hypoxia displayed upregulation of the *Mtb nnaR* ortholog and nitrite reductases affirming differences between *Mab* and *Mtb* in hypoxia (149). Our study determined little contribution by other TCS for hypoxic adaptation on day 5 however, earlier time points or prolonged hypoxia may present additional contributions from other TCS. This assertion is supported by a study examining the enduring hypoxic response of *Mtb* which documents a transition from DosR dependent hypoxia adaptation to induction of a set of genes independent of DosR (176). However, it's important to note based on our lux reporter data *Mab* DosR is still expressed after 20 days in hypoxia (Figure 12C) signifying its importance for enduring hypoxia unlike *Mtb* (176).

DosR independent gene induction in hypoxia consisted of >1,000 genes in *Mab* (Table S1), a much higher number of genes than is observed in *Mtb* in similar models of hypoxia (87,149). The upregulation of these DosR independent genes is attributed to the 80 transcription factors (TF) we observed to be upregulated in response to hypoxia (Table S1). The majority of these TF are not characterized in *Mab* however some of the most highly induced TF belong to the TetR, GntR and IclR families. Regardless of how individual TFs impact transcriptional remodeling in this study it is evident hypoxic adaptation requires regulation of a large repertoire of genes. Among these DosR independent hypoxia induced genes are genes implicated in energetic pathways, cell wall remodeling, and pathogenesis along with 520 genes annotated as hypothetical proteins (Table S1).

Contrary to what is documented with *Mtb* in hypoxia, *Mab* displayed upregulation of *nuoA-N* and ATPases (Table S1) (149,166). *nuoA-N* are subunits of a NADH dehydrogenase type 1 proton pump which shuttles electrons to menaquinone in the ETC to generate a PMF in an energy conserving manner (163). Differences in gene expression of *nuoA-N* and ATPases between *Mab* and *Mtb* point to different mechanisms utilized for energy during hypoxic adaptation. In addition to *nuoA-N* and ATPases, genes involved in β-oxidation were also employed signifying a transition to fatty acid metabolism. Upregulation of 5 out of 7 *Mab mce* operons were observed, *Mtb* contains 4 mce operons implying the importance of these genes for *Mab* during hypoxic adaptation. *Mtb* orthologs *mce2* and *mce3* are upregulated in hypoxia but the roles have not been experimentally determined. *mce1* and mce4 have been identified as fatty acid and cholesterol transporters however induction in hypoxia is not documented for *mce1 and mce4* hypoxic induction is seen after 15 and 20 days in hypoxia (158-160). Fatty acid and cholesterol metabolism are features of *Mtb* observed in hypoxia, and within granulomas and is crucial to pathogenesis (157,158). Induction of *Mab mce* operons in hypoxia points to a transition to fatty acid and cholesterol metabolism. Induction of *mce* operons, *nuoA-N*, ATPases and β-oxidation genes implies a shift in metabolism occurs during hypoxia that is unique to *Mab*.

Expectedly, genes associated with slowed growth and halted protein synthesis like alternative sigma factors, ribosomal proteins, and TF were down-regulated along with hypothetical proteins (Table S1&S2). This data along with growth kinetic data displaying inhibition of growth due to hypoxia suggests *Mab* adaptation relies upon the ability of growth cessation for survival (Figure 4). As previously mentioned, one of the genes displaying the most downregulation in hypoxia is the ORR *MAB_3520c* known as *nnaR*. This gene is located within a locus containing *narK3* (nitrate symporter, *MAB_3523c*), *nirBD* (nitrite reductase, *MAB_3522c* and *MAB_3521c*) and *sirB*

(a ferrochetalase responsible for the last step of siroheme synthesis, *MAB_3519c*). The NnaR orthologs found *S. coelicolor* and *Msm* are implicated in nitrate metabolism however, the role for *Mab* has not been experimentally determined. Interestingly, not only is *Mtb nnaR* and *nirBD* upregulated in hypoxia, *Mtb* is able to utilize nitrate as a final electron acceptor via the respiratory nitrate reductase *narGHIJ* (107-109,149). The absence of a *narGHIJ* ortholog within the *Mab* genome and downregulation of *nnaR*, *narK3*, *nirBD*, and *sirB* (TableS1) in hypoxia suggest the interplay between hypoxic adaptation and nitrate utilization is different from *Mtb.* These differences led to our interest in examining the role of NnaR for nitrate utilization in *Mab*.

Until recently, regulation of nitrogen metabolism genes in *Mab* had not been explored. Fan *et al*., demonstrated GlnR regulation of nitrogen metabolism genes *narK3*, *nirBD*, *glnA* (glutamine synthetase) and *amt* (ammonium transporter) but lacked phenotypic studies for the ability to utilize nitrate and nitrite. *Streptomyces* and *Msm* require coordination of GlnR with other response regulators such as NnaR to regulate nitrogen metabolism genes. However, there are no documented studies on the role of NnaR in *Mab* or *Mtb*, studies have focused on NnaR orthologs in *S. coelicolor* and *Msm*. The architecture of NnaR is unique and restricted to actinobacteria consisting of a of a N-terminal HemD (uroporphyrinogen synthase III) domain fused to a C-terminal OmpR DNA binding domain (116). We performed a NnaR protein sequence alignment comparing *Mab* to *S. coelicolor*, *Msm* and *Mtb* to determine if structural homology exists (Figure 13B). Our results yielded 58%, 55%, and 54% identity in *S. coelicolor*, *Msm* and *Mtb* , respectively with strong homology in the HemD and DNA binding domains. Due to homology in the DNA binding domain of NnaR, documented NnaR binding motifs from *S. coelicolor* and *Mtb* were used to identify motifs in *Mab* using DNA Pattern Find. Two binding motifs were found upstream of translational start sites for *narK3* and *MAB_2438* (annotated as an oxidoreductase) (Figure 15A).

Sequence alignment for *MAB_2438* displayed 61% identity with MSMEG_4206 (NasN, an assimilatory nitrate reductase) (Figure 14). *Msm* NasN is a unique nitrate reductase due to the ability to utilize NADPH as an electron donor via a heterotrimeric electron transfer domain consisting of FMN, FAD, and NAD subunits which has not been previously reported in prokaryotes (121). This peculiar NADPH dependent nitrate reductase is documented as restricted to RGM underscoring distinctive mechanisms of nitrate metabolism between RGM and SGM (121). Interestingly, despite similarities in NasN structure among *Mab* and *Msm* it appears different regulators drive transcription in these species. *In silico* analysis of *Mab* NnaR motifs yielded a binding site upstream of *Mab nasN*, however research affirms *Msm nasN* is regulated by GlnR (121).

Gene organization of nitrate assimilation genes in *Mab* is different compared to *Mtb* and *Msm* suggesting the possibility of different regulatory mechanisms. *Mab narK3* is located upstream of *nirBD*, *nnaR*, and *sirB* in a predicted operon with *nasN* located in a different locus (Figure 15A). We determined *narK3*, *nirBD*, *nnaR*, and *sirB* comprise an operon via RT-PCR which was not previously determined and is specific to *Mab (*Figure 15B*)*. This unique *Mab* gene organization implies NnaR drives transcription of *narK3*, *nirBD*, *nnaR*, *sirB*, and *nasN* a feature not observed in *S. coelicolor* or *Msm* (116,119,121). qRT-PCR analysis affirmed our prediction of *Mab* NnaR regulation of the *nark3-sirB* operon and *nasN* (Figure 18B&C). All genes except *sirB* were shown to be downregulated in the absence of NnaR ($Mab_{\Delta nnaR}$) when nitrate or nitrite were the sole sources of nitrogen (Figure 18B&C). No difference was observed in gene regulation in the mutant except for *sirB* when cultures were grown in 7H9 due to low basal expression in nitrogen replete conditions (Figure 18A). Elevated expression of *sirB* in the mutant strain was unexpected and requires more work to determine why this occurred. Our first thoughts on why *sirB* might be

elevated in the mutant strain was due to read through from the apramycin cassette directly upstream of *sirB* however, complement restored activity to WT levels. If read through from apramycin cassette was the culprit, complement would not have restored activity but shown higher levels as *sirB* was complemented with *nnaR* to prevent possible polar effects. Other possibilities such as degenerate NnaR binding sites upstream of *nnaR* or feedback loops will have to be experimentally tested to identify *sirB* regulation in the absence of NnaR. DGE of *nark3-sirB* operon and *nasN* in a NnaR dependent manner highlights the importance of this ORR in regulation of nitrate assimilation genes.

NnaR regulation of *nasN* is unique to *Mab* as *S. coelicolor* and *Msm* nitrate reductase are governed by GlnR for regulation (116,117,119,121). Neither *S. coelicolor* or *Msm* are able to utilize nitrate or nitrite as sole nitrogen sources in the absence of NnaR however, this is attributed to the inability to reduce nitrite ammonium (116,119). *nnaR* mutants in both organisms were able to reduce nitrate to nitrite (the first step of nitrate assimilation) revealing nitrate reductase regulation is controlled by a different transcription factor other than NnaR. EMSA data affirmed GlnR and NnaRcontribute to regulation of nitrogen metabolism genes in both species in a similar way, GlnR-NnaR co-regulate nitrite reductase, but nitrate reductase is only regulated by GlnR (116,119,121). This data reveals for the first time NnaR regulation by *Mab* is distinct from both *S. coelicolor* and *Msm*.

The significance of *Mab* NnaR was revealed in growth kinetic assays utilizing nitrate or nitrite as sole nitrogen sources. Growth defects were observed in $Mab_{\Delta nnaR}$ compared to WT when grown in nitrate or nitrite with growth restored in the complement strain (Figure 19B&C). A larger growth deficit occurred between $Mab_{\Delta nnaR,}$ and WT and complement in nitrate than in nitrite (Figure

19B&C). Differences in growth deficits between nitrate and nitrite can be attributed to nitrite toxicity which is reported in *Mtb* and also observed in this study when comparing concentrations of ammonium sulfate, nitrate and nitrite to determine experimental concentrations (Figure 17A-C) (55). No growth defects were observed in the *nnaR* mutant when the first 2 steps of nitrate assimilation were bypassed (Nitrate>nitrite>ammonium) using AS as the sole source of nitrogen (Figure 19A). This data affirms NnaR is required for nitrate assimilation genes but not required for ammonium assimilation.

Fan *et al*., demonstrated *Mab* GlnR regulation of *narK3*, *nirBD*, and ammonium assimilation genes such as *glnA* and *amt* via qRT-PCR and ChIP-qPCR (62). Putative GlnR binding sites were found upstream of ammonium assimilation genes, *narK3*, and *nirD* but no mention was made of a GlnR binding site upstream of *nasN* (62). Clearly, both NnaR and GlnR are implicated in regulating *nark3* and *nirBD* as evidenced by downregulation of these genes in individual knockout strains of NnaR (from our study) and GlnR (62). This is further affirmed by the presence of NnaR (Figure 15A) and GlnR putative binding motifs upstream of *narK3* (62). To gain better insight into the regulatory network required for nitrogen metabolism in *Mab* further work will need to be completed to verify whether NnaR and GlnR co-regulate nitrogen metabolism genes and possible signaling mechanisms for activation.

Our study on the *Mab* ORR NnaR identified for the first time its role as a regulator of nitrogen metabolism genes, *narK3-sirB* and *nasN,* and its necessity for utilization of nitrate and nitrite as sole nitrogen sources. NnaR regulation of *nasN* has not been documented in other organisms highlighting the distinct regulation of nitrate assimilation in *Mab*. Work is ongoing in the Rohde lab to identify possible signaling mechanisms activating NnaR which is also absent from studies in

other organisms such as *S. coelicolor* and *Msm*. The NnaR ortholog in *Mtb* was reported to interact with DosS via protein-protein interaction in an M-PFC assay however, we did not observe this when we performed a similar assay with *Mab* DosS and NnaR (Figure 20). Possible signaling mechanisms activating *Mab* NnaR are serine/threonine kinases or self-activation (via the HemD domain) which have been confirmed for the ORR GlnR and in self-modulating RR found in streptomyces, respectively (196,197,237). Identifying signaling mechanisms responsible for activating NnaR will shed light on possible cues driving *Mab* pathogenesis. In addition to resolving possible signaling mechanisms for NnaR it's also necessary to confirm NnaR promoter binding to the predicted motifs we established via *in silico* analysis. This will provide further evidence of NnaR regulation and experimentally confirm the predicted binding sites.

The work in this dissertation provides evidence that *Mab* utilizes the DosRS TCS and the ORR NnaR for regulation in a species-specific manner. DGE comparing WT *Mab* to the $Mab_{\Delta dosRS}$ displayed a large and unique DosR regulon consisting of a large number of species-specific genes that is not observed in *Mtb* during hypoxic adaptation. Regulation of DosR dependent genes was crucial for maximal growth in hypoxia, resuscitation, and maintenance of smooth colony morphology. DosRS was the most highly induced TCS in hypoxia suggesting this is the main TCS employed during hypoxic adaptation. A large number of DosR independent genes were induced during hypoxic adaptation affirming hypoxic regulation is multi-faceted and also driven by the numerous transcription factors we observed to be upregulated. DosR independent transcriptional modulation in hypoxia consisted of a larger set of genes than observed in *Mtb* with differences in the direction (+/-) of expression in genes involved in energy pathways and nitrate assimilation. In contrast with *Mtb* we observed down-regulation of nitrate assimilation genes including an ortholog to the ORR NnaR of *S. coelicolor*, *Msm* and *Mtb*. Our work uncovered a distinctive role for NnaR

in regulation of nitrate assimilation genes. qRT-PCR demonstrated NnaR regulation of the *narK3-sirB* operon and the nitrate reductase *nasN* in nitrogen limiting conditions. *NnaR* regulation of nitrate reductases has not been observed in other organisms nor has an upstream promoter site been identified making this a distinctive feature in *Mab*. We also affirmed *narK3*, *nirBD*, *nnaR* and *sirB* are within an operon. These genes are organized differently in other organisms affirming the distinguishes NnaR regulation in *Mab* from other actinobacteria. NnaR regulation of nitrate assimilation is required for optimal growth in nitrogen limiting conditions highlighting the importance of this regulator in environments where nitrogen metabolism is necessary for survival. *In vivo* assessment of DosR and NnaR is crucial to understanding the roles of these response regulators for pathogenesis. Ongoing mouse work is being performed to develop a relevant mouse model for infection as detailed in Chapter 4. It is our hope to establish a mouse model of infection as few studies have been performed assessing transcription factors or TCS in *Mab in vivo*. A recent study examining the role of the RR PhoP *in vivo* determined a *Mab* phoP mutant was hypervirulent which contrasts with *Mtb* studies (84,238) Data collected from the *Mab phoP* study reflects the importance of experimental studies to distinguish the roles and impacts of TCS among species (238). Analysis for both DosR and NnaR *in vivo* and *in vitro* is ongoing with the goal of addressing their roles in pathogenesis. This collective work of DosRS and NnaR studies confirms species-specific regulation for hypoxic adaptation and nitrate assimilation underscoring the necessity of experimental studies for assigning roles of TCS orthologs.

APPENDIX
PRIMER, PLASMID AND STRAIN TABLES

Table 1; Strains used in Chapter 2

Name	Description	Resource
Strains		
Mab _390S	WT strain used to generate knockouts	Howard et., 2006
Mab _ΔdosRS	*Mab* _390S with dosRS knocked out (dbl k/o)	This study
Mab _ΔdosRS+C	*Mab* _ΔdosRS complemented with pUAB400_dosRS_complement	This study
E.coli 10-β	Used for cloning	
Mab _390S-hsp-lux	*Mab* _390S with pMV306hsp+LuxG13	This study
Mab _ΔdosRS-hsp-lux	*Mab* _ ΔdosRS with pMV306hsp+LuxG13	This study
Mab _390S-dosR-lux	*Mab*_ 390S with pMV306dosR+LuxG13	This study
Mab _ΔdosRS-dosR-lux	*Mab* _ ΔdosRS with pMV306dosR+LuxG13	This study
Mab _390S-2489-lux	*Mab*_ 390S with pMV306_2489+LuxG13	This study
Mab _ΔdosRS-2489-lux	*Mab* _ ΔdosRS with pMV306_2489+LuxG13	This study

Table 2; Plasmids used in Chapter 2

Name	Description	Resource
Plasmids		
pMV306_hsp+LuxG13	integrating lux reporter with constituitive hsp promoter	Andreu et al., 2010
pMV306_dosR+LuxG13	integrating lux reporter with hsp promoter replaced with dosR promoter	This study
pMV306_2489+LuxG13	integrating lux reporter with hsp promoter replaced with 2489 promoter	This study
pMV306_3902c+LuxG13	integrating lux reporter with hsp promoter replaced with 3902c promoter	This study
pUAB400	integrating mycobacterial *E.coli* shuttle plasmid	Singh et al., 2006
pUAB400_dosRS_complement	integrating mycobacterial *E.coli* shuttle plasmid containg dosRS with native promoter	This study
pTOPO Zero Blunt	used for cloning Mab_dosRS knockout contruct	

Table 3; Primers used to Construct dosRS Mutant

Construction of *Mab* _ΔdosRS		
Mab_DosRSko_R	AGGTCCTGGCTCCGCAGTT	Amplification of Mab DosRS plus flanking region to be cloned into pTOPO Zero Blunt
Mab_DosRSko_R	CGGCCTGCAGCGTTTG	
Mab_DosRSko_fcF	CCGCGACTCGTTCAGGT	Removal of dosRS gene in pTOPO via RTH cloning
Mab_DosRSko_fcR	GTCCGTTTTCCTTCCACCC	
Mab_DosRSko_ApramF	GGGTGGAAGGAAAACGGACTTCATGTGCAGCTCCATCAG	Amplification of apramycin resistance cassette to be cloned in place of dosRS gene via fast cloning
Mab_DosRSko_ApramR	ACCTGAACGAGTCGCGGCTCCAACGTCATCTCGTTCTCC	

Table 4; Primers used to Construct dosRS Complement

Construction of *Mab* _ΔdosRS+C		
pUAB300F	AAGCTTATCGATGTCGACGT	Linearization of integrating vector pUAB400 for fast cloning of *Mab dosRS*
pUAB400_FC_R3.2	TTTCTGGCGGGAACGGC	
Mab_promoter_3890c-3891c_F	CCGTTCCCGCCAGAAAGAGGCGAGAGCCCTCATC	Amplification of *Mab dosRS* including native promoter for fast cloning into pUAB400
Mab_promoter_3890c-3891c_R	ACGTCGACATCGATAAGCTTACCTGAACGAGTCGCGG	

Table 5; Primers used to Construct Lux reporters

Lux reporter construct primers		
Lux_hsp60_FC_F	GGCCAAGACAATTGCGG	Linearize pMV306hsp+G13
Lux_hsp60_FC_R	GCGTCGTTGTGGTCACCT	
Mab_dosr-prom_lux_F	AGGTGACCACAACGACGCGAGGCGAGAGCCCTCATC	Amplification of dosR promoter with overhangs for fast cloning into linearized pMV306hsp+G13
Mab_dosr-prom_lux_R	CCGCAATTGTCTTGGCCGTCCGTTTTCCTTCCA	
Mab_2489-prom_lux_F.2	AGGTGACCACAACGACGCCCTTAGACTTGCTATCTACTGGGCC	Amplification of 2489 promoter with overhangs for fast cloning into linearized pMV306hsp+G13
Mab_2489-prom_lux_R.2	CCGCAATTGTCTTGGCCAGCTCCTCCGATGTGCG	

Table 6; Primers used for qRT-PCR in Chapter 2

qRT-PCR Primers	
Mab_sigA.rt.F2	TCCGAGAAAGACAAGGCTTC
Mab_sigA.rt.r2	CCAGCTCAACTTCCTCTTCG
Mab_3891rtF3	CTGCGTTGATGAACAGGTTG
Mab_3891rtR3	GTGAGCAGACGCGAGACATA
MAB_2489_rtR	ATAGCTCGACAAGGACGG
MAB_2489_rtF	GTTCACGTCATCGACCAC
MAB_3902c_rtR	TAGCTGTCCTGCGAGATG
MAB_3902c_rtF	TACGGTCGACCTTAAGCC
MAB_3903_rtR	TATGCGAGTCATCCACCC
MAB_3903_rtF	TCCAGACCGCTATCCAAC
MAB_3904_rtR	CGCTGATACCGATTGCTC
MAB_3904_rtF	CTGAGTTCAGCGACGAAC
Mab_3890c_rt.F	CTGAACGACAAGCTGATTCC
Mab_3890c_rt.R	CCATATCGAGCTGTTCCTCA
Mab_3937_rt.F	ACAACGGCTCACGGTGTCG
Mab_3937_rt.F	CCAAGGAAGAGATCAGCACC
Mab_3354_rt.F	GCTGCTCAAACACATCTCCA
Mab_3354_rt.F	TGTCTACGACCCACAACTGC

Table 7; rRNA Depletion Probes used in Chapter 2

Pool name	Sequence
Supplemental Probe Pool	GTCCCAGACCACTTCCGCTAATCACGACACTTTTTTACTGTCCGCCGGCC
Supplemental Probe Pool	CTGGCCCAGGAACCCTTGGTCATTCGGCGGGCAAGTTTCTCACTTGCCTG
Supplemental Probe Pool	ATTACCCCACCAACAAGCTGATAGGCCGCGGGCTCATCCCACACCGCAAA
Supplemental Probe Pool	TTGTAGCATGTGTGAAGCCCTGGACATAAGGGGCATGATGACTTGACGTC
Supplemental Probe Pool	TAGGTTTCCCGCTTAGATGCTTTCAGCGGTTATCCTGTCCGAACGTAGCT
Supplemental Probe Pool	GTCTATGGTTGAGACAGTTGAGAAGTCGTTACGCCATTCGTGCAGGTCGG
Supplemental Probe Pool	TCAGCTCACGGAGCAAGTCCGGTCACCAAGCGAGGTCCCCCTTCTCCCGA
Supplemental Probe Pool	TCAGCCTGTTATCCCCGGGGTACCTTTTATCCGTTGAGCGACACCCCTTC
Supplemental Probe Pool	GAGTATTTAGGCTTACCGGGTGGTCCCGGCAGATTCACAGCAGATTCCAC
Supplemental Probe Pool	GCATTCTCACTCCCGCACCCTCCACTGCTGAATTACTTCGCAGCTTCGCT
Supplemental Probe Pool	CGTGCTGGGTTTCCCCATTCGGAGATCCTCGGATCAAAGCTCGGTTGGCA
Supplemental Probe Pool	AAGGGTGGCTGCTTCTAAGCCAACCTCCTGGTTGTCTTCGCGACTGCACA
Supplemental Probe Pool	ATTAGTAAGTTTTCGGTCGATTAGTGCCAGTTCCCTGAACGTATTACTAC
Supplemental Probe Pool	CCAGGATGCGACGAGCCGACATCGAGGTGCCAAACCATCCCGTCGATATG
Supplemental Probe Pool	CATTTCGGGGAGAACCAGCTATCACGGAGTTTGATTGGCCTTTCACCCCT
Supplemental Probe Pool	CCGCCGTCTCACTGCCGCGCTCTAACTTATTGGCATTCGGAGTTTGGCTG
Supplemental Probe Pool	TAGGGCCCATCGGCCATCCAGTAGCTCTACCTCCAACAAGAAACACGCGA
Supplemental Probe Pool	CCTTTTGGGTGGTTAGTACCGATGATTCATCATGGGCGCGCACACACGGG
Supplemental Probe Pool	CTACGGGCTTGCTCCGGTATAACCACTAACCGGTACAGCTACCTTCCTGC
Supplemental Probe Pool	GACTACTACCACCGAAGGTCCCACGCAGCGGGTTCACGTCGCACTCCGAA
Supplemental Probe Pool	AGTTTTAGTCTTGCGACCGTACTCCCCAGGCGGGGTACTTAATGCGTTAG
Supplemental Probe Pool	TTCGCCTCAATCGGCTATGCGTCACCTCTCAGACGTATGACATCCGGATT
Supplemental Probe Pool	CGCTACGGCTACCCCACACGGGTTAACCTCGCGACGTGTCCCTGACTCGC
Supplemental Probe Pool	CCTCAGTCTTCAACCTAAGTGGGTTCGGGCCTCCACGGCGTCTTACCGCC
Supplemental Probe Pool	GTTCCTCCTGATATCTGCGCATTCCACCGCTACACCAGGAATTCCAGTCT
Supplemental Probe Pool	ACCATGAAGTGTGTGGTCCTATCCGGTATTAGACCCAGTTTCCCAGGCTT
Supplemental Probe Pool	CACAGGCCACAAGGGAATACCTATCTCTAGGTACGTCCTGTGCATGTCAA
Supplemental Probe Pool	CGAACTGAGACCAGCTTTAAGGGATTCGCTCCACCTTACGGCTTCGCAGC
Supplemental Probe Pool	TCACTCCCCTCCCGGGGTACTTTTCACCATTCCCTCACGGTACTAATCCG
Supplemental Probe Pool	GCAGATCACCCACGTGTTACTCACCCGTTCGCCACTCGAGTACCCCGAAG
Supplemental Probe Pool	GCTTCACAGTCTCCCACCTATCCTACACAAACCGAACCAAACGCCAATAC
Supplemental Probe Pool	AGGTGATCCAGCCGCACCTTCCGGTACGGCTACCTTGTTACGACTTCGTC
Supplemental Probe Pool	CGAGTTGACCCCGGCAGTCTCCTACGAGTCCCCGGCATTACCCGCTGGCA

Pool name	Sequence
Supplemental Probe Pool	GCTTCACAGTCTCCCACCTATCCTACACAAACCGAACCAAACGCCAATAC
Supplemental Probe Pool	AGGTGATCCAGCCGCACCTTCCGGTACGGCTACCTTGTTACGACTTCGTC
Supplemental Probe Pool	CGAGTTGACCCCGGCAGTCTCCTACGAGTCCCCGGCATTACCCGCTGGCA
Supplemental Probe Pool	AGGTTAGAGGTTCAATACGATCAGAGTGGTATTTCAACGATGACTCCACA
Supplemental Probe Pool	TGGTGGAACAACTGGTACACCAGAGGTTCGTCCGTCCCGGTCCTCTCGTA
Supplemental Probe Pool	CCGTTGTCCATCGACTACGCCTGTCGGCCTCGCCTTAGGTCCCGACTTAC
Supplemental Probe Pool	CGGGATGAAGTACGAGACAGGTGTCGGATTTTCGCGTACCGGACTCTCAC
Supplemental Probe Pool	GTACAACTCCCACAACCCCGCACACACAACCCCTACCAGGTATCACATGC
Supplemental Probe Pool	CAGCGTTGCTGATCTGCGATTACTAGCGACTCCGACTTCATGGGGTCGAG
Supplemental Probe Pool	TTGCCGAGTTCCTTAACCATAGTTATCTCGTACGCCTTAGTATTCTCTAC
Supplemental Probe Pool	AGTCTGCCCGTATCGCCCGCACGCCCACAGTTAAGCTGTGAGTTTTCACG
Supplemental Probe Pool	CTATTGAACCCATAGTCTGTGGGTGACCTTATCCCTCTAAAAGGGTAAGA
Supplemental Probe Pool	CACTTGCACTCAACACCTGATTGCCGTCCAGGTTGAGGGAACCTTTGGGC
Supplemental Probe Pool	GAATTTCGCTACCTTAGGATGGTTATAGTTACCACCGCCGTTTACTGGGG
Supplemental Probe Pool	CTCAAGTTTCTGACGCGCGCGGCGGATAGAGACCGAACTGTCTCACGACG
Supplemental Probe Pool	TACACGCTTAGGGGCCTTAGCCGGCGATCTGGGCTGTTTCCCTCTCGACG
Supplemental Probe Pool	TTCGCTACCCACGCTTTCGCTCCTCAGCGTCAGTTACTGCCCAGAGACCC
Supplemental Probe Pool	GGTTTGGGGTACGGGCCGTGTGTGAACTCACTAGAGGCTTTTCTTGGCAG
Supplemental Probe Pool	TCGCAGCCTCCTACGTCCTTCTTCGGCTTCTAGTGCCAAGGCATTCACCA
Supplemental Probe Pool	ACCTTCGACAGCTCCCTCCAAAAGGTTAGGCCACTGGCTTCGGGTGTTAC
Supplemental Probe Pool	TACTTGAGCCCCGCTACATTGTCGGCGCACAATCACTTGACCAGTGAGCT
Supplemental Probe Pool	CTTCCGCTTTCGCTCGCCACTACTCACGGAATCACGGTTGTTTTCTCTTC
Supplemental Probe Pool	TGGGAGGCAACCGCCCCAGTTAAACTACCCACCAGGCACTGTCCCTGGAC
Supplemental Probe Pool	AAGGCACGCCATCACCCCACGAGGAGGCTTTGACGGATTGTAGGCACATG
Supplemental Probe Pool	TGTTTCACTTCCCCGCGTTTCCTCCCAAAGCCTATATATTCAGCAGTGGG
Supplemental Probe Pool	GCTGGCACGTAGTTGGCCGGTCCTTCTTCTGTAGGTACCGTCACTTTCGC
Supplemental Probe Pool	CCCTACCCATCCATGCCACTGCCCCGAAGGGAATGTATTGCATGAATGCC
Supplemental Probe Pool	TGCGACTTCGCACGGACCTGTGTTTTTAGTAAACAGTCGCTTCTCACTGG
Supplemental Probe Pool	GTCCCGGGGTCTTTTCGTCCTGCCGCGCGTAACGAGCATCTTTACTCGTA
Supplemental Probe Pool	CACCTACGAGCTCTTTACGCCCAGTAATTCCGGACAACGCTCGGACCCTA
Supplemental Probe Pool	TATCTCAGTCCCAGTGTGGCCGGTCACCCTCTCAGGCCGGCTACCCGTCG
Supplemental Probe Pool	TGGGTAGATCACTCCGCTTCGGGTCCAGAACACGCCACTATGGGCGCCCT

Table 8; Primers used to generate nnaR knockout and complement in Chapter 3

Primers used to generate *Mab* Δ_{nnaR}	nnaR-F	tttccttcgtcaacgcgcc	Amplification of *nnaR* plus ~600 bp flanking upstream and downstream.
	nnaR-R	atacgacgcgatgaagacc	
	nnaR-ko-F	atggctgagttcgtattggtg	Removal of *nnaR* gene in TOPO vector but retain flanking region
	nnaR-ko-R	ttacgcggcaaccgc	
	Apramycin-F	ttcatgtgcagctccatca	Amplification of apramycin resistance cassette to replace nnaR
	Apramycin-R	ctccaacgtcatctcgttctc	
Primers used to generate *Mab* Δ_{nnaR+C}	pvv16-R	catatggaagtgatcctccg	Primers used to linearize pvv16
	pvv16-F	aagcttcaccaccaccacc	
	Mab_nnaR-F	ttgccgcgtaacgagcc	Primers used to amplify *nnaR-sirB*
	Mab_sirB-R	ctacgcgacgtccgcca	
Primers used to generate MPFC constructs	pUAB100:dosS_MPFC-FC-F	ATTGCGGATCCTTCGAACgtggtcgaggatgttggtgcgc	Primers used to amplify dosS with pUAB100 overhangs for fast cloning
	pUAB100:dosS_MPFC-FC-R	CCACCGCCACCATCGATgggcagcggcgccga	
	pUAB400:nnaR-MPFC-FC-F	GTGGTGGGTCCCAATTGttgccgcgtaacgagcc	Primers used to amplify nnaR with pUAB400 overhangs for fastcloning
	pUAB400:nnaR-MPFC-FC-R	TCGACATCGATAAGCTTtcagccatgacattccccaatc	
	pUAB400:dosR-MPFC-FC-F	GTGGTGGGTCCCAATTGatgatcacagtgttcctggtcga	Primers used to amplify nnaR to go into pUAB200 overhnags for fast
	pUAB400:dosR-MPFC-FC-R	TCGACATCGATAAGCTTcagccgtgcagcccc	
	pUAB200:nnaR-MPFC-F	ttgccgcgtaacgagcc	Primers used to amplify dosR with pUAB400 using blunt end ligation
	pUAB200:nnaR-MPFC-R	tcagccatgacattccccaatc	
	*capitol letters represent overhang section for Fast Cloning		

Table 9; Operon primers used in chapter 3

nark3-nirB	nark3-nirB-operon_F	atggtcgcgcaccatgtc
	nark3-nirB-operon_R	aggtgaagtgtcaccatcggg
nirB-nirD	nirB-nirD-operon_F	gcccgattcgaccatcgc
	nirB-nirD-operon_R	accgcgtacaactccccg
nirD-nnar	nirD-nnar-operon-F	gtctcgatgatgcgtcgcg
	nirD-nnar-operon-R	gtcggccagcgggatgat
nnaR-sirB	nnaR-sirB-operon-F	cacattgccgatgaactgacca
	nnaR-sirB-operon-R	ggccggaagtaacaccgc

Table 10; qRT-PCR primers used in chapter 3

Mab_nnaR-qrT.F	cgttgatgaagcgtctgatg
Mab_nnaR-qrT.R	gtaaccccgcttgaccact
Mab_nirD-qRT.F	agttgtacgcggtcggtaac
Mab_nirD-qRT.R	ctcctgagcattccgatttc
Mab_nirB-qRT.F	ctgggctgtcagacaagtga
Mab_nirB-qRT.R	cccagcagtttgagtttggt
Mab_nark3-qRT.F	gtcgccatcaacctggtact
Mab_narK3-qRT.R	cttcgtttttggagctggag
Mab_sirB-qRT.F	tggctgagttcgtattggtg
Mab_sirB-qRT.R	gtcgtggtgcacatggtatc
Mab_nasN-qRT.F	atgagggcgcacatctttac
Mab_nasN-qRT.R	aagctttccgtgcttctgtg

Table 11; Primers used for genotyping βENaC Mice

Genotyping Primers	
βENaC694-F	CTTCCAAGAGTTCAACTACCG
βENaC694-R	TCTACCAGCTCAGCCACAGTG

Table 12; Primers used for pET28b cloning in Chapter 5

Primers for pET28b cloning	
Mab_dosR-F	accgaaaacctttacttccagggcatgatcacagtgttcctggtcgat
Mab_dosR-R	gctttgttagcagccggatctcatcagccgtgcagcccc
pET28b-F	gccctggaagtaaaggttttcggt
pET28b-R	tgagatccggctgctaacaaagc

Table 13; Primers used to amplify promoter sequences used in Chapter 5

Primers for Promoter Amplification	
Promoter_2489-F	gcgagattccgttacgtacaacg
Promoter_2489-R	tcctacccgcaacgctattgatc
Promoter_3354-F	gtacaggccacggctaacaaa
Promoter_3354-R	cggttgcgggattatctgtgt
Promoter_3937-F	agcccatccacgtgatgag
Promoter_3937-R	gccctctccttctttgcttcc
Promoter_dosR-F	gaggcgagagccctcatc
Promoter_dosR-R	gtccgttttccttccacccg

REFERENCES

1. Brosch, R., Gordon, S. V., Marmiesse, M., Brodin, P., Buchrieser, C., Eiglmeier, K., Garnier, T., Gutierrez, C., Hewinson, G., Kremer, K., Parsons, L. M., Pym, A. S., Samper, S., van Soolingen, D., and Cole, S. T. (2002) A new evolutionary scenario for the Mycobacterium tuberculosis complex. *Proc Natl Acad Sci U S A* **99**, 3684-3689
2. Porvaznik, I., Solovic, I., and Mokry, J. (2017) Non-Tuberculous Mycobacteria: Classification, Diagnostics, and Therapy. *Adv Exp Med Biol* **944**, 19-25
3. Sreevatsan, S., Pan, X., Stockbauer, K. E., Connell, N. D., Kreiswirth, B. N., Whittam, T. S., and Musser, J. M. (1997) Restricted structural gene polymorphism in the Mycobacterium tuberculosis complex indicates evolutionarily recent global dissemination. *Proc Natl Acad Sci U S A* **94**, 9869-9874
4. Zhang, H., Liu, M., Fan, W., Sun, S., and Fan, X. (2022) The impact of Mycobacterium tuberculosis complex in the environment on one health approach. *Front Public Health* **10**, 994745
5. To, K., Cao, R., Yegiazaryan, A., Owens, J., and Venketaraman, V. (2020) General Overview of Nontuberculous Mycobacteria Opportunistic Pathogens: Mycobacterium avium and Mycobacterium abscessus. *J Clin Med* **9**
6. Brown-Elliott, B. A., and Wallace, R. J., Jr. (2002) Clinical and taxonomic status of pathogenic nonpigmented or late-pigmenting rapidly growing mycobacteria. *Clin Microbiol Rev* **15**, 716-746
7. Runyon, E. H. (1959) Anonymous mycobacteria in pulmonary disease. *Med Clin North Am* **43**, 273-290
8. Lee, M. R., Sheng, W. H., Hung, C. C., Yu, C. J., Lee, L. N., and Hsueh, P. R. (2015) Mycobacterium abscessus Complex Infections in Humans. *Emerg Infect Dis* **21**, 1638-1646
9. O'Brien, R. J., Geiter, L. J., and Snider, D. E., Jr. (1987) The epidemiology of nontuberculous mycobacterial diseases in the United States. Results from a national survey. *Am Rev Respir Dis* **135**, 1007-1014
10. Winthrop, K. L., McNelley, E., Kendall, B., Marshall-Olson, A., Morris, C., Cassidy, M., Saulson, A., and Hedberg, K. (2010) Pulmonary nontuberculous mycobacterial disease prevalence and clinical features: an emerging public health disease. *Am J Respir Crit Care Med* **182**, 977-982
11. Griffith, D. E., Aksamit, T., Brown-Elliott, B. A., Catanzaro, A., Daley, C., Gordin, F., Holland, S. M., Horsburgh, R., Huitt, G., Iademarco, M. F., Iseman, M., Olivier, K., Ruoss, S., von Reyn, C. F., Wallace, R. J., Jr., Winthrop, K., Subcommittee, A. T. S. M. D., American Thoracic, S., and Infectious Disease Society of, A. (2007) An official ATS/IDSA statement: diagnosis, treatment, and prevention of nontuberculous mycobacterial diseases. *Am J Respir Crit Care Med* **175**, 367-416
12. Haworth, C. S., Banks, J., Capstick, T., Fisher, A. J., Gorsuch, T., Laurenson, I. F., Leitch, A., Loebinger, M. R., Milburn, H. J., Nightingale, M., Ormerod, P., Shingadia, D., Smith, D., Whitehead, N., Wilson, R., and Floto, R. A. (2017) British Thoracic Society Guideline for the management of non-tuberculous mycobacterial pulmonary disease (NTM-PD). *BMJ Open Respir Res* **4**, e000242
13. Moore, M., and Frerichs, J. B. (1953) An unusual acid-fast infection of the knee with subcutaneous, abscess-like lesions of the gluteal region; report of a case with a study of the organism, Mycobacterium abscessus, n. sp. *J Invest Dermatol* **20**, 133-169

14. Lopeman, R. C., Harrison, J., Desai, M., and Cox, J. A. G. (2019) Mycobacterium abscessus: Environmental Bacterium Turned Clinical Nightmare. *Microorganisms* **7**
15. Kubica, G. P., Baess, I., Gordon, R. E., Jenkins, P. A., Kwapinski, J. B., McDurmont, C., Pattyn, S. R., Saito, H., Silcox, V., Stanford, J. L., Takeya, K., and Tsukamura, M. (1972) A co-operative numerical analysis of rapidly growing mycobacteria. *J Gen Microbiol* **73**, 55-70
16. Kusunoki, S., and Ezaki, T. (1992) Proposal of Mycobacterium peregrinum sp. nov., nom. rev., and elevation of Mycobacterium chelonae subsp. abscessus (Kubica et al.) to species status: Mycobacterium abscessus comb. nov. *Int J Syst Bacteriol* **42**, 240-245
17. Adekambi, T., Reynaud-Gaubert, M., Greub, G., Gevaudan, M. J., La Scola, B., Raoult, D., and Drancourt, M. (2004) Amoebal coculture of "Mycobacterium massiliense" sp. nov. from the sputum of a patient with hemoptoic pneumonia. *J Clin Microbiol* **42**, 5493-5501
18. Adekambi, T., Berger, P., Raoult, D., and Drancourt, M. (2006) rpoB gene sequence-based characterization of emerging non-tuberculous mycobacteria with descriptions of Mycobacterium bolletii sp. nov., Mycobacterium phocaicum sp. nov. and Mycobacterium aubagnense sp. nov. *Int J Syst Evol Microbiol* **56**, 133-143
19. Adekambi, T., and Drancourt, M. (2004) Dissection of phylogenetic relationships among 19 rapidly growing Mycobacterium species by 16S rRNA, hsp65, sodA, recA and rpoB gene sequencing. *Int J Syst Evol Microbiol* **54**, 2095-2105
20. Prammananan, T., Sander, P., Brown, B. A., Frischkorn, K., Onyi, G. O., Zhang, Y., Bottger, E. C., and Wallace, R. J., Jr. (1998) A single 16S ribosomal RNA substitution is responsible for resistance to amikacin and other 2-deoxystreptamine aminoglycosides in Mycobacterium abscessus and Mycobacterium chelonae. *J Infect Dis* **177**, 1573-1581
21. Primm, T. P., Lucero, C. A., and Falkinham, J. O., 3rd. (2004) Health impacts of environmental mycobacteria. *Clin Microbiol Rev* **17**, 98-106
22. Kim, H. Y., Kim, B. J., Kook, Y., Yun, Y. J., Shin, J. H., Kim, B. J., and Kook, Y. H. (2010) Mycobacterium massiliense is differentiated from Mycobacterium abscessus and Mycobacterium bolletii by erythromycin ribosome methyltransferase gene (erm) and clarithromycin susceptibility patterns. *Microbiol Immunol* **54**, 347-353
23. Nessar, R., Cambau, E., Reyrat, J. M., Murray, A., and Gicquel, B. (2012) Mycobacterium abscessus: a new antibiotic nightmare. *J Antimicrob Chemother* **67**, 810-818
24. Story-Roller, E., Maggioncalda, E. C., Cohen, K. A., and Lamichhane, G. (2018) Mycobacterium abscessus and beta-Lactams: Emerging Insights and Potential Opportunities. *Front Microbiol* **9**, 2273
25. Koh, W. J., Kwon, O. J., and Lee, K. S. (2002) Nontuberculous mycobacterial pulmonary diseases in immunocompetent patients. *Korean J Radiol* **3**, 145-157
26. Harris, K. A., and Kenna, D. T. (2014) Mycobacterium abscessus infection in cystic fibrosis: molecular typing and clinical outcomes. *J Med Microbiol* **63**, 1241-1246
27. Olivier, K. N., Weber, D. J., Wallace, R. J., Jr., Faiz, A. R., Lee, J. H., Zhang, Y., Brown-Elliot, B. A., Handler, A., Wilson, R. W., Schechter, M. S., Edwards, L. J., Chakraborti, S., Knowles, M. R., and Nontuberculous Mycobacteria in Cystic Fibrosis Study, G. (2003) Nontuberculous mycobacteria. I: multicenter prevalence study in cystic fibrosis. *Am J Respir Crit Care Med* **167**, 828-834
28. Esther, C. R., Jr., Esserman, D. A., Gilligan, P., Kerr, A., and Noone, P. G. (2010) Chronic Mycobacterium abscessus infection and lung function decline in cystic fibrosis. *J Cyst Fibros* **9**, 117-123

29. Greendyke, R., and Byrd, T. F. (2008) Differential antibiotic susceptibility of Mycobacterium abscessus variants in biofilms and macrophages compared to that of planktonic bacteria. *Antimicrob Agents Chemother* **52**, 2019-2026
30. Rojony, R., Danelishvili, L., Campeau, A., Wozniak, J. M., Gonzalez, D. J., and Bermudez, L. E. (2020) Exposure of Mycobacterium abscessus to Environmental Stress and Clinically Used Antibiotics Reveals Common Proteome Response among Pathogenic Mycobacteria. *Microorganisms* **8**
31. Shaw, L. P., Doyle, R. M., Kavaliunaite, E., Spencer, H., Balloux, F., Dixon, G., and Harris, K. A. (2019) Children With Cystic Fibrosis Are Infected With Multiple Subpopulations of Mycobacterium abscessus With Different Antimicrobial Resistance Profiles. *Clin Infect Dis* **69**, 1678-1686
32. Gutierrez, A. V., Baron, S. A., Sardi, F. S., Saad, J., Coltey, B., Reynaud-Gaubert, M., and Drancourt, M. (2021) Beyond phenotype: The genomic heterogeneity of co-infecting Mycobacterium abscessus smooth and rough colony variants in cystic fibrosis patients. *J Cyst Fibros* **20**, 421-423
33. Ruger, K., Hampel, A., Billig, S., Rucker, N., Suerbaum, S., and Bange, F. C. (2014) Characterization of rough and smooth morphotypes of Mycobacterium abscessus isolates from clinical specimens. *J Clin Microbiol* **52**, 244-250
34. Clary, G., Sasindran, S. J., Nesbitt, N., Mason, L., Cole, S., Azad, A., McCoy, K., Schlesinger, L. S., and Hall-Stoodley, L. (2018) Mycobacterium abscessus Smooth and Rough Morphotypes Form Antimicrobial-Tolerant Biofilm Phenotypes but Are Killed by Acetic Acid. *Antimicrob Agents Chemother* **62**
35. Howard, S. T., Rhoades, E., Recht, J., Pang, X., Alsup, A., Kolter, R., Lyons, C. R., and Byrd, T. F. (2006) Spontaneous reversion of Mycobacterium abscessus from a smooth to a rough morphotype is associated with reduced expression of glycopeptidolipid and reacquisition of an invasive phenotype. *Microbiology (Reading)* **152**, 1581-1590
36. Whang, J., Back, Y. W., Lee, K. I., Fujiwara, N., Paik, S., Choi, C. H., Park, J. K., and Kim, H. J. (2017) Mycobacterium abscessus glycopeptidolipids inhibit macrophage apoptosis and bacterial spreading by targeting mitochondrial cyclophilin D. *Cell Death Dis* **8**, e3012
37. Julian, E., Roldan, M., Sanchez-Chardi, A., Astola, O., Agusti, G., and Luquin, M. (2010) Microscopic cords, a virulence-related characteristic of Mycobacterium tuberculosis, are also present in nonpathogenic mycobacteria. *J Bacteriol* **192**, 1751-1760
38. Roux, A. L., Viljoen, A., Bah, A., Simeone, R., Bernut, A., Laencina, L., Deramaudt, T., Rottman, M., Gaillard, J. L., Majlessi, L., Brosch, R., Girard-Misguich, F., Vergne, I., de Chastellier, C., Kremer, L., and Herrmann, J. L. (2016) The distinct fate of smooth and rough Mycobacterium abscessus variants inside macrophages. *Open Biol* **6**
39. Catherinot, E., Clarissou, J., Etienne, G., Ripoll, F., Emile, J. F., Daffe, M., Perronne, C., Soudais, C., Gaillard, J. L., and Rottman, M. (2007) Hypervirulence of a rough variant of the Mycobacterium abscessus type strain. *Infect Immun* **75**, 1055-1058
40. Catherinot, E., Roux, A. L., Macheras, E., Hubert, D., Matmar, M., Dannhoffer, L., Chinet, T., Morand, P., Poyart, C., Heym, B., Rottman, M., Gaillard, J. L., and Herrmann, J. L. (2009) Acute respiratory failure involving an R variant of Mycobacterium abscessus. *J Clin Microbiol* **47**, 271-274
41. Byrd, T. F., and Lyons, C. R. (1999) Preliminary characterization of a Mycobacterium abscessus mutant in human and murine models of infection. *Infect Immun* **67**, 4700-4707
42. Rhoades, E. R., Archambault, A. S., Greendyke, R., Hsu, F. F., Streeter, C., and Byrd, T. F. (2009) Mycobacterium abscessus Glycopeptidolipids mask underlying cell wall

phosphatidyl-myo-inositol mannosides blocking induction of human macrophage TNF-alpha by preventing interaction with TLR2. *J Immunol* **183**, 1997-2007
43. Roux, A. L., Ray, A., Pawlik, A., Medjahed, H., Etienne, G., Rottman, M., Catherinot, E., Coppee, J. Y., Chaoui, K., Monsarrat, B., Toubert, A., Daffe, M., Puzo, G., Gaillard, J. L., Brosch, R., Dulphy, N., Nigou, J., and Herrmann, J. L. (2011) Overexpression of proinflammatory TLR-2-signalling lipoproteins in hypervirulent mycobacterial variants. *Cell Microbiol* **13**, 692-704
44. Gutierrez, A. V., Viljoen, A., Ghigo, E., Herrmann, J. L., and Kremer, L. (2018) Glycopeptidolipids, a Double-Edged Sword of the Mycobacterium abscessus Complex. *Front Microbiol* **9**, 1145
45. Pawlik, A., Garnier, G., Orgeur, M., Tong, P., Lohan, A., Le Chevalier, F., Sapriel, G., Roux, A. L., Conlon, K., Honore, N., Dillies, M. A., Ma, L., Bouchier, C., Coppee, J. Y., Gaillard, J. L., Gordon, S. V., Loftus, B., Brosch, R., and Herrmann, J. L. (2013) Identification and characterization of the genetic changes responsible for the characteristic smooth-to-rough morphotype alterations of clinically persistent Mycobacterium abscessus. *Mol Microbiol* **90**, 612-629
46. Daher, W., Leclercq, L. D., Johansen, M. D., Hamela, C., Karam, J., Trivelli, X., Nigou, J., Guerardel, Y., and Kremer, L. (2022) Glycopeptidolipid glycosylation controls surface properties and pathogenicity in Mycobacterium abscessus. *Cell Chem Biol* **29**, 910-924 e917
47. Tsai, S. H., Lai, H. C., and Hu, S. T. (2015) Subinhibitory Doses of Aminoglycoside Antibiotics Induce Changes in the Phenotype of Mycobacterium abscessus. *Antimicrob Agents Chemother* **59**, 6161-6169
48. Hedin, W., Froberg, G., Fredman, K., Chryssanthou, E., Selmeryd, I., Gillman, A., Orsini, L., Runold, M., Jonsson, B., Schon, T., and Davies Forsman, L. (2023) A Rough Colony Morphology of Mycobacterium abscessus Is Associated With Cavitary Pulmonary Disease and Poor Clinical Outcome. *J Infect Dis* **227**, 820-827
49. Li, B., Ye, M., Zhao, L., Guo, Q., Chen, J., Xu, B., Zhan, M., Zhang, Y., Zhang, Z., and Chu, H. (2020) Glycopeptidolipid Genotype Correlates With the Severity of Mycobacterium abscessus Lung Disease. *J Infect Dis* **221**, S257-S262
50. Lyczak, J. B., Cannon, C. L., and Pier, G. B. (2002) Lung infections associated with cystic fibrosis. *Clin Microbiol Rev* **15**, 194-222
51. Chmiel, J. F., and Davis, P. B. (2003) State of the art: why do the lungs of patients with cystic fibrosis become infected and why can't they clear the infection? *Respir Res* **4**, 8
52. Bryant, J. M., Grogono, D. M., Greaves, D., Foweraker, J., Roddick, I., Inns, T., Reacher, M., Haworth, C. S., Curran, M. D., Harris, S. R., Peacock, S. J., Parkhill, J., and Floto, R. A. (2013) Whole-genome sequencing to identify transmission of Mycobacterium abscessus between patients with cystic fibrosis: a retrospective cohort study. *Lancet* **381**, 1551-1560
53. Bernut, A., Nguyen-Chi, M., Halloum, I., Herrmann, J. L., Lutfalla, G., and Kremer, L. (2016) Mycobacterium abscessus-Induced Granuloma Formation Is Strictly Dependent on TNF Signaling and Neutrophil Trafficking. *PLoS Pathog* **12**, e1005986
54. Peddireddy, V., Doddam, S. N., and Ahmed, N. (2017) Mycobacterial Dormancy Systems and Host Responses in Tuberculosis. *Front Immunol* **8**, 84
55. Cunningham-Bussel, A., Zhang, T., and Nathan, C. F. (2013) Nitrite produced by Mycobacterium tuberculosis in human macrophages in physiologic oxygen impacts bacterial ATP consumption and gene expression. *Proc Natl Acad Sci U S A* **110**, E4256-4265

56. Hudock, T. A., Foreman, T. W., Bandyopadhyay, N., Gautam, U. S., Veatch, A. V., LoBato, D. N., Gentry, K. M., Golden, N. A., Cavigli, A., Mueller, M., Hwang, S. A., Hunter, R. L., Alvarez, X., Lackner, A. A., Bader, J. S., Mehra, S., and Kaushal, D. (2017) Hypoxia Sensing and Persistence Genes Are Expressed during the Intragranulomatous Survival of Mycobacterium tuberculosis. *Am J Respir Cell Mol Biol* **56**, 637-647
57. Hassett, D. J., Cuppoletti, J., Trapnell, B., Lymar, S. V., Rowe, J. J., Yoon, S. S., Hilliard, G. M., Parvatiyar, K., Kamani, M. C., Wozniak, D. J., Hwang, S. H., McDermott, T. R., and Ochsner, U. A. (2002) Anaerobic metabolism and quorum sensing by Pseudomonas aeruginosa biofilms in chronically infected cystic fibrosis airways: rethinking antibiotic treatment strategies and drug targets. *Adv Drug Deliv Rev* **54**, 1425-1443
58. Robinson, J. L., Jaslove, J. M., Murawski, A. M., Fazen, C. H., and Brynildsen, M. P. (2017) An integrated network analysis reveals that nitric oxide reductase prevents metabolic cycling of nitric oxide by Pseudomonas aeruginosa. *Metab Eng* **41**, 67-81
59. Worlitzsch, D., Tarran, R., Ulrich, M., Schwab, U., Cekici, A., Meyer, K. C., Birrer, P., Bellon, G., Berger, J., Weiss, T., Botzenhart, K., Yankaskas, J. R., Randell, S., Boucher, R. C., and Doring, G. (2002) Effects of reduced mucus oxygen concentration in airway Pseudomonas infections of cystic fibrosis patients. *J Clin Invest* **109**, 317-325
60. Belardinelli, J. M., Verma, D., Li, W., Avanzi, C., Wiersma, C. J., Williams, J. T., Johnson, B. K., Zimmerman, M., Whittel, N., Angala, B., Wang, H., Jones, V., Dartois, V., de Moura, V. C. N., Gonzalez-Juarrero, M., Pearce, C., Schenkel, A. R., Malcolm, K. C., Nick, J. A., Charman, S. A., Wells, T. N. C., Podell, B. K., Vennerstrom, J. L., Ordway, D. J., Abramovitch, R. B., and Jackson, M. (2022) Therapeutic efficacy of antimalarial drugs targeting DosRS signaling in Mycobacterium abscessus. *Sci Transl Med* **14**, eabj3860
61. Miranda-CasoLuengo, A. A., Staunton, P. M., Dinan, A. M., Lohan, A. J., and Loftus, B. J. (2016) Functional characterization of the Mycobacterium abscessus genome coupled with condition specific transcriptomics reveals conserved molecular strategies for host adaptation and persistence. *BMC Genomics* **17**, 553
62. Fan, J., Jia, Y., He, S., Tan, Z., Li, A., Li, J., Zhang, Z., Li, B., and Chu, H. (2024) GlnR activated transcription of nitrogen metabolic pathway genes facilitates biofilm formation by mycobacterium abscessus. *Int J Antimicrob Agents* **63**, 107025
63. Zschiedrich, C. P., Keidel, V., and Szurmant, H. (2016) Molecular Mechanisms of Two-Component Signal Transduction. *J Mol Biol* **428**, 3752-3775
64. Gooderham, W. J., and Hancock, R. E. (2009) Regulation of virulence and antibiotic resistance by two-component regulatory systems in Pseudomonas aeruginosa. *FEMS Microbiol Rev* **33**, 279-294
65. Kendall, S. L., Movahedzadeh, F., Rison, S. C., Wernisch, L., Parish, T., Duncan, K., Betts, J. C., and Stoker, N. G. (2004) The Mycobacterium tuberculosis dosRS two-component system is induced by multiple stresses. *Tuberculosis (Edinb)* **84**, 247-255
66. Sultan, M., Arya, R., and Kim, K. K. (2021) Roles of Two-Component Systems in Pseudomonas aeruginosa Virulence. *Int J Mol Sci* **22**
67. Bretl, D. J., Demetriadou, C., and Zahrt, T. C. (2011) Adaptation to environmental stimuli within the host: two-component signal transduction systems of Mycobacterium tuberculosis. *Microbiol Mol Biol Rev* **75**, 566-582
68. Li, X., Lv, X., Lin, Y., Zhen, J., Ruan, C., Duan, W., Li, Y., and Xie, J. (2019) Role of two-component regulatory systems in intracellular survival of Mycobacterium tuberculosis. *J Cell Biochem*
69. Parish, T. (2014) Two-Component Regulatory Systems of Mycobacteria. *Microbiol Spectr* **2**, MGM2-0010-2013

70. Gonzalo-Asensio, J., Mostowy, S., Harders-Westerveen, J., Huygen, K., Hernandez-Pando, R., Thole, J., Behr, M., Gicquel, B., and Martin, C. (2008) PhoP: a missing piece in the intricate puzzle of Mycobacterium tuberculosis virulence. *PLoS One* **3**, e3496
71. Yarwood, J. M., McCormick, J. K., and Schlievert, P. M. (2001) Identification of a novel two-component regulatory system that acts in global regulation of virulence factors of Staphylococcus aureus. *J Bacteriol* **183**, 1113-1123
72. Walters, S. B., Dubnau, E., Kolesnikova, I., Laval, F., Daffe, M., and Smith, I. (2006) The Mycobacterium tuberculosis PhoPR two-component system regulates genes essential for virulence and complex lipid biosynthesis. *Mol Microbiol* **60**, 312-330
73. Hazelbauer, G. L., and Lai, W. C. (2010) Bacterial chemoreceptors: providing enhanced features to two-component signaling. *Curr Opin Microbiol* **13**, 124-132
74. Lee, A. I., Delgado, A., and Gunsalus, R. P. (1999) Signal-dependent phosphorylation of the membrane-bound NarX two-component sensor-transmitter protein of Escherichia coli: nitrate elicits a superior anion ligand response compared to nitrite. *J Bacteriol* **181**, 5309-5316
75. Leistikow, R. L., Morton, R. A., Bartek, I. L., Frimpong, I., Wagner, K., and Voskuil, M. I. (2010) The Mycobacterium tuberculosis DosR regulon assists in metabolic homeostasis and enables rapid recovery from nonrespiring dormancy. *J Bacteriol* **192**, 1662-1670
76. Sivaramakrishnan, S., and de Montellano, P. R. (2013) The DosS-DosT/DosR Mycobacterial Sensor System. *Biosensors (Basel)* **3**, 259-282
77. Cheung, J., and Hendrickson, W. A. (2010) Sensor domains of two-component regulatory systems. *Curr Opin Microbiol* **13**, 116-123
78. Vashist, A., Malhotra, V., Sharma, G., Tyagi, J. S., and Clark-Curtiss, J. E. (2018) Interplay of PhoP and DevR response regulators defines expression of the dormancy regulon in virulent Mycobacterium tuberculosis. *J Biol Chem* **293**, 16413-16425
79. Chao, J. D., Papavinasasundaram, K. G., Zheng, X., Chavez-Steenbock, A., Wang, X., Lee, G. Q., and Av-Gay, Y. (2010) Convergence of Ser/Thr and two-component signaling to coordinate expression of the dormancy regulon in Mycobacterium tuberculosis. *J Biol Chem* **285**, 29239-29246
80. Gao, R., Bouillet, S., and Stock, A. M. (2019) Structural Basis of Response Regulator Function. *Annu Rev Microbiol* **73**, 175-197
81. Shi, X., Wegener-Feldbrugge, S., Huntley, S., Hamann, N., Hedderich, R., and Sogaard-Andersen, L. (2008) Bioinformatics and experimental analysis of proteins of two-component systems in Myxococcus xanthus. *J Bacteriol* **190**, 613-624
82. Kundu, M. (2018) The role of two-component systems in the physiology of Mycobacterium tuberculosis. *IUBMB Life* **70**, 710-717
83. Schaller, G. E., Shiu, S. H., and Armitage, J. P. (2011) Two-component systems and their co-option for eukaryotic signal transduction. *Curr Biol* **21**, R320-330
84. Bryant, J. M., Brown, K. P., Burbaud, S., Everall, I., Belardinelli, J. M., Rodriguez-Rincon, D., Grogono, D. M., Peterson, C. M., Verma, D., Evans, I. E., Ruis, C., Weimann, A., Arora, D., Malhotra, S., Bannerman, B., Passemar, C., Templeton, K., MacGregor, G., Jiwa, K., Fisher, A. J., Blundell, T. L., Ordway, D. J., Jackson, M., Parkhill, J., and Floto, R. A. (2021) Stepwise pathogenic evolution of Mycobacterium abscessus. *Science* **372**
85. Galagan, J. E., Minch, K., Peterson, M., Lyubetskaya, A., Azizi, E., Sweet, L., Gomes, A., Rustad, T., Dolganov, G., Glotova, I., Abeel, T., Mahwinney, C., Kennedy, A. D., Allard, R., Brabant, W., Krueger, A., Jaini, S., Honda, B., Yu, W. H., Hickey, M. J., Zucker, J., Garay, C., Weiner, B., Sisk, P., Stolte, C., Winkler, J. K., Van de Peer, Y., Iazzetti, P., Camacho, D., Dreyfuss, J., Liu, Y., Dorhoi, A., Mollenkopf, H. J., Drogaris, P.,

Lamontagne, J., Zhou, Y., Piquenot, J., Park, S. T., Raman, S., Kaufmann, S. H., Mohney, R. P., Chelsky, D., Moody, D. B., Sherman, D. R., and Schoolnik, G. K. (2013) The Mycobacterium tuberculosis regulatory network and hypoxia. *Nature* **499**, 178-183

86. Rohde, K. H., Veiga, D. F., Caldwell, S., Balazsi, G., and Russell, D. G. (2012) Linking the transcriptional profiles and the physiological states of Mycobacterium tuberculosis during an extended intracellular infection. *PLoS Pathog* **8**, e1002769
87. Rustad, T. R., Sherrid, A. M., Minch, K. J., and Sherman, D. R. (2009) Hypoxia: a window into Mycobacterium tuberculosis latency. *Cell Microbiol* **11**, 1151-1159
88. Via, L. E., Lin, P. L., Ray, S. M., Carrillo, J., Allen, S. S., Eum, S. Y., Taylor, K., Klein, E., Manjunatha, U., Gonzales, J., Lee, E. G., Park, S. K., Raleigh, J. A., Cho, S. N., McMurray, D. N., Flynn, J. L., and Barry, C. E., 3rd. (2008) Tuberculous granulomas are hypoxic in guinea pigs, rabbits, and nonhuman primates. *Infect Immun* **76**, 2333-2340
89. Mehra, S., Foreman, T. W., Didier, P. J., Ahsan, M. H., Hudock, T. A., Kissee, R., Golden, N. A., Gautam, U. S., Johnson, A. M., Alvarez, X., Russell-Lodrigue, K. E., Doyle, L. A., Roy, C. J., Niu, T., Blanchard, J. L., Khader, S. A., Lackner, A. A., Sherman, D. R., and Kaushal, D. (2015) The DosR Regulon Modulates Adaptive Immunity and Is Essential for Mycobacterium tuberculosis Persistence. *Am J Respir Crit Care Med* **191**, 1185-1196
90. Cho, H. Y., Cho, H. J., Kim, Y. M., Oh, J. I., and Kang, B. S. (2009) Structural insight into the heme-based redox sensing by DosS from Mycobacterium tuberculosis. *J Biol Chem* **284**, 13057-13067
91. Honaker, R. W., Leistikow, R. L., Bartek, I. L., and Voskuil, M. I. (2009) Unique roles of DosT and DosS in DosR regulon induction and Mycobacterium tuberculosis dormancy. *Infect Immun* **77**, 3258-3263
92. Shiloh, M. U., Manzanillo, P., and Cox, J. S. (2008) Mycobacterium tuberculosis senses host-derived carbon monoxide during macrophage infection. *Cell Host Microbe* **3**, 323-330
93. Voskuil, M. I., Schnappinger, D., Visconti, K. C., Harrell, M. I., Dolganov, G. M., Sherman, D. R., and Schoolnik, G. K. (2003) Inhibition of respiration by nitric oxide induces a Mycobacterium tuberculosis dormancy program. *J Exp Med* **198**, 705-713
94. Wayne, L. G., and Hayes, L. G. (1996) An in vitro model for sequential study of shiftdown of Mycobacterium tuberculosis through two stages of nonreplicating persistence. *Infect Immun* **64**, 2062-2069
95. Voskuil, M. I., Visconti, K. C., and Schoolnik, G. K. (2004) Mycobacterium tuberculosis gene expression during adaptation to stationary phase and low-oxygen dormancy. *Tuberculosis (Edinb)* **84**, 218-227
96. Chauhan, S., Sharma, D., Singh, A., Surolia, A., and Tyagi, J. S. (2011) Comprehensive insights into Mycobacterium tuberculosis DevR (DosR) regulon activation switch. *Nucleic Acids Res* **39**, 7400-7414
97. Aguilar-Ayala, D. A., Tilleman, L., Van Nieuwerburgh, F., Deforce, D., Palomino, J. C., Vandamme, P., Gonzalez, Y. M. J. A., and Martin, A. (2017) The transcriptome of Mycobacterium tuberculosis in a lipid-rich dormancy model through RNAseq analysis. *Sci Rep* **7**, 17665
98. Daniel, J., Deb, C., Dubey, V. S., Sirakova, T. D., Abomoelak, B., Morbidoni, H. R., and Kolattukudy, P. E. (2004) Induction of a novel class of diacylglycerol acyltransferases and triacylglycerol accumulation in Mycobacterium tuberculosis as it goes into a dormancy-like state in culture. *J Bacteriol* **186**, 5017-5030
99. Wayne, L. G., and Hayes, L. G. (1998) Nitrate reduction as a marker for hypoxic shiftdown of Mycobacterium tuberculosis. *Tuber Lung Dis* **79**, 127-132

100. Converse, P. J., Karakousis, P. C., Klinkenberg, L. G., Kesavan, A. K., Ly, L. H., Allen, S. S., Grosset, J. H., Jain, S. K., Lamichhane, G., Manabe, Y. C., McMurray, D. N., Nuermberger, E. L., and Bishai, W. R. (2009) Role of the dosR-dosS two-component regulatory system in Mycobacterium tuberculosis virulence in three animal models. *Infect Immun* **77**, 1230-1237
101. Malhotra, V., Sharma, D., Ramanathan, V. D., Shakila, H., Saini, D. K., Chakravorty, S., Das, T. K., Li, Q., Silver, R. F., Narayanan, P. R., and Tyagi, J. S. (2004) Disruption of response regulator gene, devR, leads to attenuation in virulence of Mycobacterium tuberculosis. *FEMS Microbiol Lett* **231**, 237-245
102. Arroyo, L., Marin, D., Franken, K., Ottenhoff, T. H. M., and Barrera, L. F. (2018) Potential of DosR and Rpf antigens from Mycobacterium tuberculosis to discriminate between latent and active tuberculosis in a tuberculosis endemic population of Medellin Colombia. *BMC Infect Dis* **18**, 26
103. Kimuda, S. G., Nalwoga, A., Levin, J., Franken, K. L., Ottenhoff, T. H., Elliott, A. M., Cose, S., and Andia-Biraro, I. (2017) Humoral Responses to Rv1733c, Rv0081, Rv1735c, and Rv1737c DosR Regulon-Encoded Proteins of Mycobacterium tuberculosis in Individuals with Latent Tuberculosis Infection. *J Immunol Res* **2017**, 1593143
104. Shi, S. D., Hsueh, P. R., Yang, P. C., and Chou, C. C. (2020) Use of DosR Dormancy Antigens from Mycobacterium tuberculosis for Serodiagnosis of Active and Latent Tuberculosis. *ACS Infect Dis* **6**, 272-280
105. Malhotra, V., Agrawal, R., Duncan, T. R., Saini, D. K., and Clark-Curtiss, J. E. (2015) Mycobacterium tuberculosis response regulators, DevR and NarL, interact in vivo and co-regulate gene expression during aerobic nitrate metabolism. *J Biol Chem* **290**, 8294-8309
106. Singh, P. R., Vijjamarri, A. K., and Sarkar, D. (2020) Metabolic Switching of Mycobacterium tuberculosis during Hypoxia Is Controlled by the Virulence Regulator PhoP. *J Bacteriol* **202**
107. Sohaskey, C. D. (2008) Nitrate enhances the survival of Mycobacterium tuberculosis during inhibition of respiration. *J Bacteriol* **190**, 2981-2986
108. Sohaskey, C. D., and Wayne, L. G. (2003) Role of narK2X and narGHJI in hypoxic upregulation of nitrate reduction by Mycobacterium tuberculosis. *J Bacteriol* **185**, 7247-7256
109. Gouzy, A., Poquet, Y., and Neyrolles, O. (2014) Nitrogen metabolism in Mycobacterium tuberculosis physiology and virulence. *Nat Rev Microbiol* **12**, 729-737
110. Lee, J. S., Krause, R., Schreiber, J., Mollenkopf, H. J., Kowall, J., Stein, R., Jeon, B. Y., Kwak, J. Y., Song, M. K., Patron, J. P., Jorg, S., Roh, K., Cho, S. N., and Kaufmann, S. H. (2008) Mutation in the transcriptional regulator PhoP contributes to avirulence of Mycobacterium tuberculosis H37Ra strain. *Cell Host Microbe* **3**, 97-103
111. Gerasimova, A., Kazakov, A. E., Arkin, A. P., Dubchak, I., and Gelfand, M. S. (2011) Comparative genomics of the dormancy regulons in mycobacteria. *J Bacteriol* **193**, 3446-3452
112. Wee, W. Y., Dutta, A., and Choo, S. W. (2017) Comparative genome analyses of mycobacteria give better insights into their evolution. *PLoS One* **12**, e0172831
113. Malhotra, S., Vedithi, S. C., and Blundell, T. L. (2017) Decoding the similarities and differences among mycobacterial species. *PLoS Negl Trop Dis* **11**, e0005883
114. Simcox, B. S., Tomlinson, B. R., Shaw, L. N., and Rohde, K. H. (2023) Mycobacterium abscessus DosRS two-component system controls a species-specific regulon required for adaptation to hypoxia. *Front Cell Infect Microbiol* **13**, 1144210

115. Huang, Q., Abdalla, A. E., and Xie, J. (2015) Phylogenomics of Mycobacterium Nitrate Reductase Operon. *Curr Microbiol* **71**, 121-128
116. Amin, R., Reuther, J., Bera, A., Wohlleben, W., and Mast, Y. (2012) A novel GlnR target gene, nnaR, is involved in nitrate/nitrite assimilation in Streptomyces coelicolor. *Microbiology (Reading)* **158**, 1172-1182
117. Tiffert, Y., Supra, P., Wurm, R., Wohlleben, W., Wagner, R., and Reuther, J. (2008) The Streptomyces coelicolor GlnR regulon: identification of new GlnR targets and evidence for a central role of GlnR in nitrogen metabolism in actinomycetes. *Mol Microbiol* **67**, 861-880
118. Wang, J., and Zhao, G. P. (2009) GlnR positively regulates nasA transcription in Streptomyces coelicolor. *Biochem Biophys Res Commun* **386**, 77-81
119. Antczak, M., Plocinska, R., Plocinski, P., Rumijowska-Galewicz, A., Zaczek, A., Strapagiel, D., and Dziadek, J. (2018) The NnaR orphan response regulator is essential for the utilization of nitrate and nitrite as sole nitrogen sources in mycobacteria. *Scientific reports* **8**, 17552
120. Jenkins, V. A., Barton, G. R., Robertson, B. D., and Williams, K. J. (2013) Genome wide analysis of the complete GlnR nitrogen-response regulon in Mycobacterium smegmatis. *BMC Genomics* **14**, 301
121. Tan, W., Liao, T. H., Wang, J., Ye, Y., Wei, Y. C., Zhou, H. K., Xiao, Y., Zhi, X. Y., Shao, Z. H., Lyu, L. D., and Zhao, G. P. (2020) A recently evolved diflavin-containing monomeric nitrate reductase is responsible for highly efficient bacterial nitrate assimilation. *J Biol Chem* **295**, 5051-5066
122. Malm, S., Tiffert, Y., Micklinghoff, J., Schultze, S., Joost, I., Weber, I., Horst, S., Ackermann, B., Schmidt, M., Wohlleben, W., Ehlers, S., Geffers, R., Reuther, J., and Bange, F. C. (2009) The roles of the nitrate reductase NarGHJI, the nitrite reductase NirBD and the response regulator GlnR in nitrate assimilation of Mycobacterium tuberculosis. *Microbiology (Reading)* **155**, 1332-1339
123. Simcox, B. S., Tomlinson, B. R., Shaw, L. N., and Rohde, K. H. (2023) Mycobacterium abscessus DosRS two-component system controls a species-specific regulon required for adaptation to hypoxia. *Frontiers in Cellular and Infection Microbiology* **13**
124. Molina-Torres, C. A., Tamez-Pena, L., Castro-Garza, J., Ocampo-Candiani, J., and Vera-Cabrera, L. (2018) Evaluation of the intracellular activity of drugs against Mycobacterium abscessus using a THP-1 macrophage model. *J Microbiol Methods* **148**, 29-32
125. Hurst-Hess, K., Rudra, P., and Ghosh, P. (2017) Mycobacterium abscessus WhiB7 Regulates a Species-Specific Repertoire of Genes To Confer Extreme Antibiotic Resistance. *Antimicrob Agents Chemother* **61**
126. Philley, J. V., DeGroote, M. A., Honda, J. R., Chan, M. M., Kasperbauer, S., Walter, N. D., and Chan, E. D. (2016) Treatment of Non-Tuberculous Mycobacterial Lung Disease. *Curr Treat Options Infect Dis* **8**, 275-296
127. Dubois, V., Pawlik, A., Bories, A., Le Moigne, V., Sismeiro, O., Legendre, R., Varet, H., Rodriguez-Ordonez, M. D. P., Gaillard, J. L., Coppee, J. Y., Brosch, R., Herrmann, J. L., and Girard-Misguich, F. (2019) Mycobacterium abscessus virulence traits unraveled by transcriptomic profiling in amoeba and macrophages. *PLoS Pathog* **15**, e1008069
128. Salazar, M. E., and Laub, M. T. (2015) Temporal and evolutionary dynamics of two-component signaling pathways. *Curr Opin Microbiol* **24**, 7-14
129. West, A. H., and Stock, A. M. (2001) Histidine kinases and response regulator proteins in two-component signaling systems. *Trends Biochem Sci* **26**, 369-376
130. Stock, J. B., Ninfa, A. J., and Stock, A. M. (1989) Protein phosphorylation and regulation of adaptive responses in bacteria. *Microbiol Rev* **53**, 450-490

131. Mascher, T., Helmann, J. D., and Unden, G. (2006) Stimulus perception in bacterial signal-transducing histidine kinases. *Microbiol Mol Biol Rev* **70**, 910-938
132. Peterson, E. J. R., Abidi, A. A., Arrieta-Ortiz, M. L., Aguilar, B., Yurkovich, J. T., Kaur, A., Pan, M., Srinivas, V., Shmulevich, I., and Baliga, N. S. (2020) Intricate Genetic Programs Controlling Dormancy in Mycobacterium tuberculosis. *Cell Rep* **31**, 107577
133. Kundu, M., and Basu, J. (2021) Applications of Transcriptomics and Proteomics for Understanding Dormancy and Resuscitation in Mycobacterium tuberculosis. *Front Microbiol* **12**, 642487
134. Sherman, D. R., Voskuil, M., Schnappinger, D., Liao, R., Harrell, M. I., and Schoolnik, G. K. (2001) Regulation of the Mycobacterium tuberculosis hypoxic response gene encoding alpha -crystallin. *Proc Natl Acad Sci U S A* **98**, 7534-7539
135. Park, H. D., Guinn, K. M., Harrell, M. I., Liao, R., Voskuil, M. I., Tompa, M., Schoolnik, G. K., and Sherman, D. R. (2003) Rv3133c/dosR is a transcription factor that mediates the hypoxic response of Mycobacterium tuberculosis. *Mol Microbiol* **48**, 833-843
136. Roberts, D. M., Liao, R. P., Wisedchaisri, G., Hol, W. G., and Sherman, D. R. (2004) Two sensor kinases contribute to the hypoxic response of Mycobacterium tuberculosis. *J Biol Chem* **279**, 23082-23087
137. Gautam, U. S., Mehra, S., and Kaushal, D. (2015) In-Vivo Gene Signatures of Mycobacterium tuberculosis in C3HeB/FeJ Mice. *PLoS One* **10**, e0135208
138. Gautam, U. S., McGillivray, A., Mehra, S., Didier, P. J., Midkiff, C. C., Kissee, R. S., Golden, N. A., Alvarez, X., Niu, T., Rengarajan, J., Sherman, D. R., and Kaushal, D. (2015) DosS Is required for the complete virulence of mycobacterium tuberculosis in mice with classical granulomatous lesions. *Am J Respir Cell Mol Biol* **52**, 708-716
139. van Kessel, J. C., and Hatfull, G. F. (2007) Recombineering in Mycobacterium tuberculosis. *Nat Methods* **4**, 147-152
140. Moore, S. D., and Prevelige, P. E., Jr. (2002) A P22 scaffold protein mutation increases the robustness of head assembly in the presence of excess portal protein. *J Virol* **76**, 10245-10255
141. Li, C., Wen, A., Shen, B., Lu, J., Huang, Y., and Chang, Y. (2011) FastCloning: a highly simplified, purification-free, sequence- and ligation-independent PCR cloning method. *BMC biotechnology* **11**, 92
142. Singh, A., Mai, D., Kumar, A., and Steyn, A. J. (2006) Dissecting virulence pathways of Mycobacterium tuberculosis through protein-protein association. *Proc Natl Acad Sci U S A* **103**, 11346-11351
143. Andreu, N., Zelmer, A., Fletcher, T., Elkington, P. T., Ward, T. H., Ripoll, J., Parish, T., Bancroft, G. J., Schaible, U., Robertson, B. D., and Wiles, S. (2010) Optimisation of bioluminescent reporters for use with mycobacteria. *PLoS One* **5**, e10777
144. Rohde, K. H., Abramovitch, R. B., and Russell, D. G. (2007) Mycobacterium tuberculosis invasion of macrophages: linking bacterial gene expression to environmental cues. *Cell Host Microbe* **2**, 352-364
145. Tomlinson, B. R., Malof, M. E., and Shaw, L. N. (2021) A global transcriptomic analysis of Staphylococcus aureus biofilm formation across diverse clonal lineages. *Microb Genom* **7**
146. Tomlinson, B. R., Denham, G. A., Torres, N. J., Brzozowski, R. S., Allen, J. L., Jackson, J. K., Eswara, P. J., and Shaw, L. N. (2022) Assessing the Role of Cold-Shock Protein C: a Novel Regulator of Acinetobacter baumannii Biofilm Formation and Virulence. *Infect Immun* **90**, e0037622
147. Purkayastha, A., McCue, L. A., and McDonough, K. A. (2002) Identification of a Mycobacterium tuberculosis putative classical nitroreductase gene whose expression is

coregulated with that of the acr aene within macrophages, in standing versus shaking cultures, and under low oxygen conditions. *Infect Immun* **70**, 1518-1529
148. Cunningham, A. F., and Spreadbury, C. L. (1998) Mycobacterial stationary phase induced by low oxygen tension: cell wall thickening and localization of the 16-kilodalton alpha-crystallin homolog. *J Bacteriol* **180**, 801-808
149. Vilcheze, C., Yan, B., Casey, R., Hingley-Wilson, S., Ettwiller, L., and Jacobs, W. R., Jr. (2022) Commonalities of Mycobacterium tuberculosis Transcriptomes in Response to Defined Persisting Macrophage Stresses. *Front Immunol* **13**, 909904
150. Akusobi, C., Benghomari, B. S., Zhu, J., Wolf, I. D., Singhvi, S., Dulberger, C. L., Ioerger, T. R., and Rubin, E. J. (2022) Transposon mutagenesis in Mycobacterium abscessus identifies an essential penicillin-binding protein involved in septal peptidoglycan synthesis and antibiotic sensitivity. *Elife* **11**
151. Fol, M., Chauhan, A., Nair, N. K., Maloney, E., Moomey, M., Jagannath, C., Madiraju, M. V., and Rajagopalan, M. (2006) Modulation of Mycobacterium tuberculosis proliferation by MtrA, an essential two-component response regulator. *Mol Microbiol* **60**, 643-657
152. Plocinska, R., Wasik, K., Plocinski, P., Lechowicz, E., Antczak, M., Blaszczyk, E., Dziadek, B., Slomka, M., Rumijowska-Galewicz, A., and Dziadek, J. (2022) The Orphan Response Regulator Rv3143 Modulates the Activity of the NADH Dehydrogenase Complex (Nuo) in Mycobacterium tuberculosis via Protein-Protein Interactions. *Front Cell Infect Microbiol* **12**, 909507
153. Gautam, U. S., Mehra, S., Kumari, P., Alvarez, X., Niu, T., Tyagi, J. S., and Kaushal, D. (2019) Mycobacterium tuberculosis sensor kinase DosS modulates the autophagosome in a DosR-independent manner. *Commun Biol* **2**, 349
154. Zhu, C., Liu, Y., Hu, L., Yang, M., and He, Z. G. (2018) Molecular mechanism of the synergistic activity of ethambutol and isoniazid against Mycobacterium tuberculosis. *J Biol Chem* **293**, 16741-16750
155. Yousuf, S., Angara, R. K., Roy, A., Gupta, S. K., Misra, R., and Ranjan, A. (2018) Mce2R/Rv0586 of Mycobacterium tuberculosis is the functional homologue of FadR(E. coli). *Microbiology (Reading)* **164**, 1133-1145
156. Santangelo Mde, L., Blanco, F., Campos, E., Soria, M., Bianco, M. V., Klepp, L., Alito, A., Zabal, O., Cataldi, A., and Bigi, F. (2009) Mce2R from Mycobacterium tuberculosis represses the expression of the mce2 operon. *Tuberculosis (Edinb)* **89**, 22-28
157. Yang, H., Wang, F., Guo, X., Liu, F., Liu, Z., Wu, X., Zhao, M., Ma, M., Liu, H., Qin, L., Wang, L., Tang, T., Sha, W., Wang, Y., Chen, J., Huang, X., Wang, J., Peng, C., Zheng, R., Tang, F., Zhang, L., Wu, C., Oehlers, S. H., Song, Z., She, J., Feng, H., Xie, X., and Ge, B. (2021) Interception of host fatty acid metabolism by mycobacteria under hypoxia to suppress anti-TB immunity. *Cell Discov* **7**, 90
158. Wilburn, K. M., Fieweger, R. A., and VanderVen, B. C. (2018) Cholesterol and fatty acids grease the wheels of Mycobacterium tuberculosis pathogenesis. *Pathog Dis* **76**
159. Rathor, N., Garima, K., Sharma, N. K., Narang, A., Varma-Basil, M., and Bose, M. (2016) Expression profile of mce4 operon of Mycobacterium tuberculosis following environmental stress. *Int J Mycobacteriol* **5**, 328-332
160. Klepp, L. I., Sabio, Y. G. J., and FabianaBigi. (2022) Mycobacterial MCE proteins as transporters that control lipid homeostasis of the cell wall. *Tuberculosis (Edinb)* **132**, 102162
161. Amin, A. G., Goude, R., Shi, L., Zhang, J., Chatterjee, D., and Parish, T. (2008) EmbA is an essential arabinosyltransferase in Mycobacterium tuberculosis. *Microbiology (Reading)* **154**, 240-248

162. Madacki, J., Laval, F., Grzegorzewicz, A., Lemassu, A., Zahorszka, M., Arand, M., McNeil, M., Daffe, M., Jackson, M., Laneelle, M. A., and Kordulakova, J. (2018) Impact of the epoxide hydrolase EphD on the metabolism of mycolic acids in mycobacteria. *J Biol Chem* **293**, 5172-5184
163. Weinstein, E. A., Yano, T., Li, L. S., Avarbock, D., Avarbock, A., Helm, D., McColm, A. A., Duncan, K., Lonsdale, J. T., and Rubin, H. (2005) Inhibitors of type II NADH:menaquinone oxidoreductase represent a class of antitubercular drugs. *Proc Natl Acad Sci U S A* **102**, 4548-4553
164. Unden, G., and Bongaerts, J. (1997) Alternative respiratory pathways of Escherichia coli: energetics and transcriptional regulation in response to electron acceptors. *Biochim Biophys Acta* **1320**, 217-234
165. Berney, M., and Cook, G. M. (2010) Unique flexibility in energy metabolism allows mycobacteria to combat starvation and hypoxia. *PLoS One* **5**, e8614
166. Cook, G. M., Hards, K., Vilcheze, C., Hartman, T., and Berney, M. (2014) Energetics of Respiration and Oxidative Phosphorylation in Mycobacteria. *Microbiol Spectr* **2**
167. Ortega Ugalde, S., Boot, M., Commandeur, J. N. M., Jennings, P., Bitter, W., and Vos, J. C. (2019) Function, essentiality, and expression of cytochrome P450 enzymes and their cognate redox partners in Mycobacterium tuberculosis: are they drug targets? *Appl Microbiol Biotechnol* **103**, 3597-3614
168. Capyk, J. K., Kalscheuer, R., Stewart, G. R., Liu, J., Kwon, H., Zhao, R., Okamoto, S., Jacobs, W. R., Jr., Eltis, L. D., and Mohn, W. W. (2009) Mycobacterial cytochrome p450 125 (cyp125) catalyzes the terminal hydroxylation of c27 steroids. *J Biol Chem* **284**, 35534-35542
169. Akhtar, S., Khan, A., Sohaskey, C. D., Jagannath, C., and Sarkar, D. (2013) Nitrite reductase NirBD is induced and plays an important role during in vitro dormancy of Mycobacterium tuberculosis. *J Bacteriol* **195**, 4592-4599
170. Veatch, A. V., and Kaushal, D. (2018) Opening Pandora's Box: Mechanisms of Mycobacterium tuberculosis Resuscitation. *Trends Microbiol* **26**, 145-157
171. Kester, J. C., Kandror, O., Akopian, T., Chase, M. R., Zhu, J., Rubin, E. J., Goldberg, A. L., and Fortune, S. M. (2021) ClpX Is Essential and Activated by Single-Strand DNA Binding Protein in Mycobacteria. *J Bacteriol* **203**
172. Sassetti, C. M., Boyd, D. H., and Rubin, E. J. (2003) Genes required for mycobacterial growth defined by high density mutagenesis. *Mol Microbiol* **48**, 77-84
173. Bailo, R., Radhakrishnan, A., Singh, A., Nakaya, M., Fujiwara, N., and Bhatt, A. (2022) The mycobacterial desaturase DesA2 is associated with mycolic acid biosynthesis. *Sci Rep* **12**, 6943
174. Yeruva, V. C., Savanagouder, M., Khandelwal, R., Kulkarni, A., Sharma, Y., and Raghunand, T. R. (2016) The Mycobacterium tuberculosis desaturase DesA1 (Rv0824c) is a Ca(2+) binding protein. *Biochem Biophys Res Commun* **480**, 29-35
175. Deb, C., Lee, C. M., Dubey, V. S., Daniel, J., Abomoelak, B., Sirakova, T. D., Pawar, S., Rogers, L., and Kolattukudy, P. E. (2009) A novel in vitro multiple-stress dormancy model for Mycobacterium tuberculosis generates a lipid-loaded, drug-tolerant, dormant pathogen. *PLoS One* **4**, e6077
176. Rustad, T. R., Harrell, M. I., Liao, R., and Sherman, D. R. (2008) The enduring hypoxic response of Mycobacterium tuberculosis. *PLoS One* **3**, e1502
177. Joshi, H., Kandari, D., and Bhatnagar, R. (2021) Insights into the molecular determinants involved in Mycobacterium tuberculosis persistence and their therapeutic implications. *Virulence* **12**, 2721-2749

178. Boldrin, F., Provvedi, R., Cioetto Mazzabo, L., Segafreddo, G., and Manganelli, R. (2020) Tolerance and Persistence to Drugs: A Main Challenge in the Fight Against Mycobacterium tuberculosis. *Front Microbiol* **11**, 1924
179. Gold, B., and Nathan, C. (2017) Targeting Phenotypically Tolerant Mycobacterium tuberculosis. *Microbiol Spectr* **5**
180. Bacon, J., and Marsh, P. D. (2007) Transcriptional responses of Mycobacterium tuberculosis exposed to adverse conditions in vitro. *Curr Mol Med* **7**, 277-286
181. Stupar, M., Furness, J., De Voss, C. J., Tan, L., and West, N. P. (2022) Two-component sensor histidine kinases of Mycobacterium tuberculosis: Beacons for niche navigation. *Mol Microbiol* **117**, 973-985
182. Li, X., Lv, X., Lin, Y., Zhen, J., Ruan, C., Duan, W., Li, Y., and Xie, J. (2019) Role of two-component regulatory systems in intracellular survival of Mycobacterium tuberculosis. *J Cell Biochem* **120**, 12197-12207
183. Lin, M. Y., Reddy, T. B., Arend, S. M., Friggen, A. H., Franken, K. L., van Meijgaarden, K. E., Verduyn, M. J., Schoolnik, G. K., Klein, M. R., and Ottenhoff, T. H. (2009) Cross-reactive immunity to Mycobacterium tuberculosis DosR regulon-encoded antigens in individuals infected with environmental, nontuberculous mycobacteria. *Infect Immun* **77**, 5071-5079
184. Black, G. F., Thiel, B. A., Ota, M. O., Parida, S. K., Adegbola, R., Boom, W. H., Dockrell, H. M., Franken, K. L., Friggen, A. H., Hill, P. C., Klein, M. R., Lalor, M. K., Mayanja, H., Schoolnik, G., Stanley, K., Weldingh, K., Kaufmann, S. H., Walzl, G., Ottenhoff, T. H., and Consortium, G. B. f. T. (2009) Immunogenicity of novel DosR regulon-encoded candidate antigens of Mycobacterium tuberculosis in three high-burden populations in Africa. *Clin Vaccine Immunol* **16**, 1203-1212
185. Garton, N. J., Waddell, S. J., Sherratt, A. L., Lee, S. M., Smith, R. J., Senner, C., Hinds, J., Rajakumar, K., Adegbola, R. A., Besra, G. S., Butcher, P. D., and Barer, M. R. (2008) Cytological and transcript analyses reveal fat and lazy persister-like bacilli in tuberculous sputum. *PLoS Med* **5**, e75
186. Viljoen, A., Blaise, M., de Chastellier, C., and Kremer, L. (2016) MAB_3551c encodes the primary triacylglycerol synthase involved in lipid accumulation in Mycobacterium abscessus. *Mol Microbiol* **102**, 611-627
187. Singh, A., Varela, C., Bhatt, K., Veerapen, N., Lee, O. Y., Wu, H. H., Besra, G. S., Minnikin, D. E., Fujiwara, N., Teramoto, K., and Bhatt, A. (2016) Identification of a Desaturase Involved in Mycolic Acid Biosynthesis in Mycobacterium smegmatis. *PLoS One* **11**, e0164253
188. Jonsson, B. E., Gilljam, M., Lindblad, A., Ridell, M., Wold, A. E., and Welinder-Olsson, C. (2007) Molecular epidemiology of Mycobacterium abscessus, with focus on cystic fibrosis. *J Clin Microbiol* **45**, 1497-1504
189. Kelm, M. (1999) Nitric oxide metabolism and breakdown. *Biochim Biophys Acta* **1411**, 273-289
190. Lundberg, J. O., Weitzberg, E., Cole, J. A., and Benjamin, N. (2004) Nitrate, bacteria and human health. *Nat Rev Microbiol* **2**, 593-602
191. Sohaskey, C. D., and Modesti, L. (2009) Differences in nitrate reduction between Mycobacterium tuberculosis and Mycobacterium bovis are due to differential expression of both narGHJI and narK2. *FEMS Microbiol Lett* **290**, 129-134
192. Khan, A., and Sarkar, D. (2012) Nitrate reduction pathways in mycobacteria and their implications during latency. *Microbiology (Reading)* **158**, 301-307

193. Giffin, M. M., Raab, R. W., Morganstern, M., and Sohaskey, C. D. (2012) Mutational analysis of the respiratory nitrate transporter NarK2 of Mycobacterium tuberculosis. *PLoS One* **7**, e45459
194. Cardoso, N. C., Papadopoulos, A. O., and Kana, B. D. (2021) Mycobacterium smegmatis does not display functional redundancy in nitrate reductase enzymes. *PLoS One* **16**, e0245745
195. Martin, J. F., and Liras, P. (2019) The Balance Metabolism Safety Net: Integration of Stress Signals by Interacting Transcriptional Factors in Streptomyces and Related Actinobacteria. *Front Microbiol* **10**, 3120
196. Hong, E., Lee, H. M., Ko, H., Kim, D. U., Jeon, B. Y., Jung, J., Shin, J., Lee, S. A., Kim, Y., Jeon, Y. H., Cheong, C., Cho, H. S., and Lee, W. (2007) Structure of an atypical orphan response regulator protein supports a new phosphorylation-independent regulatory mechanism. *J Biol Chem* **282**, 20667-20675
197. Lin, W., Wang, Y., Han, X., Zhang, Z., Wang, C., Wang, J., Yang, H., Lu, Y., Jiang, W., Zhao, G. P., and Zhang, P. (2014) Atypical OmpR/PhoB subfamily response regulator GlnR of actinomycetes functions as a homodimer, stabilized by the unphosphorylated conserved Asp-focused charge interactions. *J Biol Chem* **289**, 15413-15425
198. He, J., Kang, X., Wu, J., Shao, Z., Zhang, Z., Wu, Y., Yuan, H., Zhao, G., and Wang, J. (2023) Transcriptional Self-Regulation of the Master Nitrogen Regulator GlnR in Mycobacteria. *J Bacteriol* **205**, e0047922
199. Zhu, Y., Zhang, P., Zhang, J., Xu, W., Wang, X., Wu, L., Sheng, D., Ma, W., Cao, G., Chen, X. L., Lu, Y., Zhang, Y. Z., and Pang, X. (2019) The developmental regulator MtrA binds GlnR boxes and represses nitrogen metabolism genes in Streptomyces coelicolor. *Mol Microbiol* **112**, 29-46
200. Rodriguez-Garcia, A., Sola-Landa, A., Apel, K., Santos-Beneit, F., and Martin, J. F. (2009) Phosphate control over nitrogen metabolism in Streptomyces coelicolor: direct and indirect negative control of glnR, glnA, glnII and amtB expression by the response regulator PhoP. *Nucleic Acids Res* **37**, 3230-3242
201. Sola-Landa, A., Rodriguez-Garcia, A., Amin, R., Wohlleben, W., and Martin, J. F. (2013) Competition between the GlnR and PhoP regulators for the glnA and amtB promoters in Streptomyces coelicolor. *Nucleic Acids Res* **41**, 1767-1782
202. Williams, K. J., Jenkins, V. A., Barton, G. R., Bryant, W. A., Krishnan, N., and Robertson, B. D. (2015) Deciphering the metabolic response of Mycobacterium tuberculosis to nitrogen stress. *Mol Microbiol* **97**, 1142-1157
203. van Kessel, J. C., Marinelli, L. J., and Hatfull, G. F. (2008) Recombineering mycobacteria and their phages. *Nat Rev Microbiol* **6**, 851-857
204. Parikh, A., Kumar, D., Chawla, Y., Kurthkoti, K., Khan, S., Varshney, U., and Nandicoori, V. K. (2013) Development of a new generation of vectors for gene expression, gene replacement, and protein-protein interaction studies in mycobacteria. *Appl Environ Microbiol* **79**, 1718-1729
205. Liu, X., Tian, J., Liu, L., Zhu, T., Yu, X., Chu, X., Yao, B., Wu, N., and Fan, Y. (2017) Identification of an operon involved in fluoride resistance in Enterobacter cloacae FRM. *Sci Rep* **7**, 6786
206. Yang, K., Wu, Y., Xie, H., Li, M., Ming, S., Li, L., Li, M., Wu, M., Gong, S., and Huang, X. (2016) Macrophage-mediated inflammatory response decreases mycobacterial survival in mouse MSCs by augmenting NO production. *Sci Rep* **6**, 27326

207. Gautam, U. S., Mehra, S., Kumari, P., Alvarez, X., Niu, T., Tyagi, J. S., and Kaushal, D. (2019) Mycobacterium tuberculosis sensor kinase DosS modulates the autophagosome in a DosR-independent manner. *Communications Biology* **2**, 349
208. Huber, M., Faure, G., Laass, S., Kolbe, E., Seitz, K., Wehrheim, C., Wolf, Y. I., Koonin, E. V., and Soppa, J. (2019) Translational coupling via termination-reinitiation in archaea and bacteria. *Nat Commun* **10**, 4006
209. Tripathy, B. C., Sherameti, I., and Oelmuller, R. (2010) Siroheme: an essential component for life on earth. *Plant Signal Behav* **5**, 14-20
210. Dailey, H. A., Dailey, T. A., Gerdes, S., Jahn, D., Jahn, M., O'Brian, M. R., and Warren, M. J. (2017) Prokaryotic Heme Biosynthesis: Multiple Pathways to a Common Essential Product. *Microbiol Mol Biol Rev* **81**
211. Pennington, J. M., Kemp, M., McGarry, L., Chen, Y., and Stroupe, M. E. (2020) Siroheme synthase orients substrates for dehydrogenase and chelatase activities in a common active site. *Nat Commun* **11**, 864
212. Zheng, H., Colvin, C. J., Johnson, B. K., Kirchhoff, P. D., Wilson, M., Jorgensen-Muga, K., Larsen, S. D., and Abramovitch, R. B. (2017) Inhibitors of Mycobacterium tuberculosis DosRST signaling and persistence. *Nat Chem Biol* **13**, 218-225
213. Amin, R., Franz-Wachtel, M., Tiffert, Y., Heberer, M., Meky, M., Ahmed, Y., Matthews, A., Krysenko, S., Jakobi, M., Hinder, M., Moore, J., Okoniewski, N., Macek, B., Wohlleben, W., and Bera, A. (2016) Post-translational Serine/Threonine Phosphorylation and Lysine Acetylation: A Novel Regulatory Aspect of the Global Nitrogen Response Regulator GlnR in S. coelicolor M145. *Front Mol Biosci* **3**, 38
214. Schubert, H. L., Phillips, J. D., Heroux, A., and Hill, C. P. (2008) Structure and mechanistic implications of a uroporphyrinogen III synthase-product complex. *Biochemistry* **47**, 8648-8655
215. Grubb, B. R., and Boucher, R. C. (1999) Pathophysiology of gene-targeted mouse models for cystic fibrosis. *Physiol Rev* **79**, S193-214
216. Wilke, M., Buijs-Offerman, R. M., Aarbiou, J., Colledge, W. H., Sheppard, D. N., Touqui, L., Bot, A., Jorna, H., de Jonge, H. R., and Scholte, B. J. (2011) Mouse models of cystic fibrosis: phenotypic analysis and research applications. *J Cyst Fibros* **10 Suppl 2**, S152-171
217. Obregon-Henao, A., Arnett, K. A., Henao-Tamayo, M., Massoudi, L., Creissen, E., Andries, K., Lenaerts, A. J., and Ordway, D. J. (2015) Susceptibility of Mycobacterium abscessus to antimycobacterial drugs in preclinical models. *Antimicrob Agents Chemother* **59**, 6904-6912
218. Maggioncalda, E. C., Story-Roller, E., Mylius, J., Illei, P., Basaraba, R. J., and Lamichhane, G. (2020) A mouse model of pulmonary Mycobacteroides abscessus infection. *Sci Rep* **10**, 3690
219. Zhou, Z., Duerr, J., Johannesson, B., Schubert, S. C., Treis, D., Harm, M., Graeber, S. Y., Dalpke, A., Schultz, C., and Mall, M. A. (2011) The ENaC-overexpressing mouse as a model of cystic fibrosis lung disease. *J Cyst Fibros* **10 Suppl 2**, S172-182
220. Vongtongsalee, K. (2019) UNDERSTANDING MYCOBACTERIUM ABSCESSUS IN CYSTIC FIBROSIS MICE. (University, C. S. ed., Colorado State University
221. Zuluaga, A. F., Salazar, B. E., Rodriguez, C. A., Zapata, A. X., Agudelo, M., and Vesga, O. (2006) Neutropenia induced in outbred mice by a simplified low-dose cyclophosphamide regimen: characterization and applicability to diverse experimental models of infectious diseases. *BMC Infect Dis* **6**, 55

222. Zhou, L., Dey, C. R., Wert, S. E., DuVall, M. D., Frizzell, R. A., and Whitsett, J. A. (1994) Correction of lethal intestinal defect in a mouse model of cystic fibrosis by human CFTR. *Science* **266**, 1705-1708
223. Gentzsch, M., and Mall, M. A. (2018) Ion Channel Modulators in Cystic Fibrosis. *Chest* **154**, 383-393
224. Wu, W., He, S., Li, A., Guo, Q., Tan, Z., Liu, S., Wang, X., Zhang, Z., Li, B., and Chu, H. (2022) A Novel Leucyl-tRNA Synthetase Inhibitor, MRX-6038, Expresses Anti-Mycobacterium abscessus Activity In Vitro and In Vivo. *Antimicrob Agents Chemother* **66**, e0060122
225. Larsen, M. H., Lacourciere, K., Parker, T. M., Kraigsley, A., Achkar, J. M., Adams, L. B., Dupnik, K. M., Hall-Stoodley, L., Hartman, T., Kanipe, C., Kurtz, S. L., Miller, M. A., Salvador, L. C. M., Spencer, J. S., and Robinson, R. T. (2020) The Many Hosts of Mycobacteria 8 (MHM8): A conference report. *Tuberculosis (Edinb)* **121**, 101914
226. Linnane, S. J., Keatings, V. M., Costello, C. M., Moynihan, J. B., O'Connor, C. M., Fitzgerald, M. X., and McLoughlin, P. (1998) Total sputum nitrate plus nitrite is raised during acute pulmonary infection in cystic fibrosis. *Am J Respir Crit Care Med* **158**, 207-212
227. Jing, D., Agnew, J., Patton, W. F., Hendrickson, J., and Beechem, J. M. (2003) A sensitive two-color electrophoretic mobility shift assay for detecting both nucleic acids and protein in gels. *Proteomics* **3**, 1172-1180
228. Chauhan, S., and Tyagi, J. S. (2008) Cooperative binding of phosphorylated DevR to upstream sites is necessary and sufficient for activation of the Rv3134c-devRS operon in Mycobacterium tuberculosis: implication in the induction of DevR target genes. *J Bacteriol* **190**, 4301-4312
229. Raran-Kurussi, S., and Waugh, D. S. (2014) Unrelated solubility-enhancing fusion partners MBP and NusA utilize a similar mode of action. *Biotechnol Bioeng* **111**, 2407-2411
230. Schildknecht, K. R., Pratt, R. H., Feng, P. I., Price, S. F., and Self, J. L. (2023) Tuberculosis - United States, 2022. *MMWR Morb Mortal Wkly Rep* **72**, 297-303
231. Winthrop, K. L., Marras, T. K., Adjemian, J., Zhang, H., Wang, P., and Zhang, Q. (2020) Incidence and Prevalence of Nontuberculous Mycobacterial Lung Disease in a Large U.S. Managed Care Health Plan, 2008-2015. *Ann Am Thorac Soc* **17**, 178-185
232. Mejia-Chew, C., Chavez, M. A., Lian, M., McKee, A., Garrett, L., Bailey, T. C., Spec, A., Agarwal, M., and Turabelidze, G. (2023) Spatial Epidemiologic Analysis and Risk Factors for Nontuberculous Mycobacteria Infections, Missouri, USA, 2008-2019. *Emerg Infect Dis* **29**, 1540-1546
233. Dahl, V. N., Molhave, M., Floe, A., van Ingen, J., Schon, T., Lillebaek, T., Andersen, A. B., and Wejse, C. (2022) Global trends of pulmonary infections with nontuberculous mycobacteria: a systematic review. *Int J Infect Dis* **125**, 120-131
234. Adjemian, J., Olivier, K. N., Seitz, A. E., Holland, S. M., and Prevots, D. R. (2012) Prevalence of nontuberculous mycobacterial lung disease in U.S. Medicare beneficiaries. *Am J Respir Crit Care Med* **185**, 881-886
235. Degiacomi, G., Sammartino, J. C., Chiarelli, L. R., Riabova, O., Makarov, V., and Pasca, M. R. (2019) Mycobacterium abscessus, an Emerging and Worrisome Pathogen among Cystic Fibrosis Patients. *Int J Mol Sci* **20**
236. Victoria, L., Gupta, A., Gomez, J. L., and Robledo, J. (2021) Mycobacterium abscessus complex: A Review of Recent Developments in an Emerging Pathogen. *Front Cell Infect Microbiol* **11**, 659997

237. Gao, R., and Stock, A. M. (2010) Molecular strategies for phosphorylation-mediated regulation of response regulator activity. *Curr Opin Microbiol* **13**, 160-167
238. Martin, C., Williams, A., Hernandez-Pando, R., Cardona, P. J., Gormley, E., Bordat, Y., Soto, C. Y., Clark, S. O., Hatch, G. J., Aguilar, D., Ausina, V., and Gicquel, B. (2006) The live Mycobacterium tuberculosis phoP mutant strain is more attenuated than BCG and confers protective immunity against tuberculosis in mice and guinea pigs. *Vaccine* **24**, 3408-3419